University of South-Eastern Norway
Faculty of Technology, Natural Sciences and Maritime Sciences

–

Master's Thesis

Study programme: Master of Science in Micro and Nano Systems Technology

Autumn /Spring2024

Bahareh Malekianarani

Evaluation and simulation of LiNbO3 (Lithium Niobate) piezocomposite ultrasound transducer with center frequency of 3MHz.

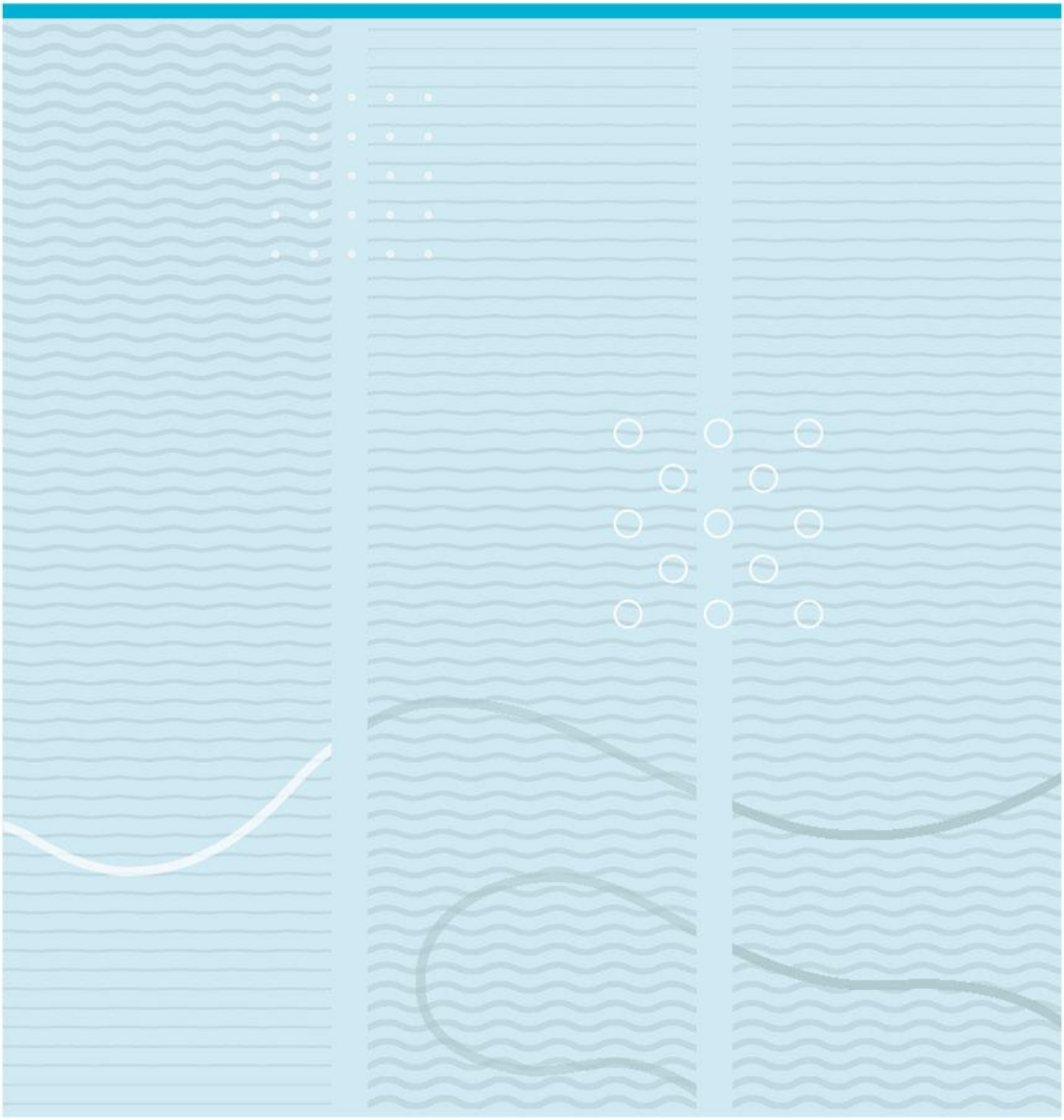

University of South-Eastern Norway
Faculty of Technology, Natural Sciences and Maritime Sciences
Department of Microsystems.
Raveien 215
NO-3184 Borre, Norway

http://www.usn.no

Summary

An ultrasound transducer is a critical and important component of any ultrasonic measurement system. Transducers convert electrical energy into acoustic energy and vice versa to transmit and receive sound waves.

The study in this thesis mainly focuses on the simulation of single element piezocomposite ultrasound transducers by using the Lithium Niobate ($LiNbO_3$) as a main material for piezocomposite and different polymer fillers such as hard, soft material and air. We compared the two different cuts of composite such as 36° / Y-cut and Z-cut.

The transducer was designed in COMSOL (Develop FEM simulation models in COMSOL Multiphysics(2D) in both 36° / Y-cut and Z-cut).

3MHz of the 36° / Y-cut $LiNbO_3$ sample was measured in the USN laboratory.

Preface

First, Having the support and guidance of my supervisor, [Professor Lars Hoff], is essential to the success of this endeavour. This journey would not have been possible without their expertise, mentorship, and support.

I am also grateful for the technical training and support of my co-supervisor, a PhD candidate Josh Hoi Yi Siu. My thesis included simulation parts, which he always taught me very useful information about.

I am deeply thankful to Associate Professor Hamed Salmani for his continuous guidance and support throughout the course of this project. His willingness to share his expertise and provide invaluable information has been invaluable to my progress and learning experience.

To my family (My parents and my lovely sister), I extend heartfelt appreciation for their encouragement, understanding and companionship. They have kept me motivated and focused by believing in my abilities and lending an ear when I doubt myself.

I also appreciate my friends who support me during this project.

Finally, I want to thank my husband for his constant love, understanding, and encouragement. His support has been a source of strength and motivation, sustaining me through the challenges of this project.

<Bakkenteigen/20.05.2024>

<Bahareh Malekianarani>

List of Symbols

A	Area	m^2
W	Width	m
L	Length	m
t	Thickness	m
ρ	Density	kg/m^3
ν	Poisson's Ratio	_
E	Young's modulus	Pa
c_l	Longitudinal wave velocity	m/s
c_S	Shear wave velocity	m/s
Z	Acoustic impedance	$MRayl$
Q_m	Mechanical quality factor	_
$\Phi_P(\omega)$	Transmission ratio	_
$C_{i,j}^E$	Elastic stiffness at constant electric Field	N/m^2
$C_{i,j}^D$	Elastic stiffness at constant displacement Field	N/m^2
D	Displacement Field	C/m^2
S	Strain	_
T	Stress	Pa
V	Voltage	V
$V.F$	Volume Fraction	_
$S_{i,j}^D$	Compliance at constant displacement Field	m^2/N
$S_{i,j}^E$	Compliance at constant electric Field	m^2/N
$d_{i,j}$	Piezoelectric strain constant	C/N
$e_{i,j}$	Piezoelectric stress constant	C/m^2
$h_{i,j}$	Piezoelectric stiffness constant	V/m
ε^S	Relative permittivity at constant strain	_
f_r	Resonance	Hz
f_a	Anti- resonance	Hz
k_t	Electromechanical coupling coefficient for thin plate	_
k_{33}	Electromechanical coupling coefficient for free rod	_

Contents

1 Introduction

1.1 Background

Ultrasound technology utilizes sound waves at frequencies beyond the human audible range. Its applications span a wide array, encompassing communication, non-destructive testing, and notably, medicine. The numerous advantages it presents have established it as a crucial diagnostic instrument across various medical fields. Among its diagnostic capabilities, ultrasound is particularly notable for Doppler measurements.

Recently, in pulse-echo medical ultrasound imaging, composite piezoelectric transducers have proven beneficial. PZT /rods and polymer composites are used to make these medical transducers. there are several requirements for the piezoelectric used in these transducers. First, the piezoelectric must be able to convert electrical energy into mechanical energy efficiently for sensitive transducers. Second, Acoustic matching of the piezoelectric device with tissue is essential for good transmission and reception of acoustic waves. Third, driving and receiving electronics must be compatible with the electric properties. The relevant properties are the electromechanical coupling constant (k_t), the specific acoustic impedance, (Z), and the dielectric constant, (ε^S), respectively. For sensitive transducers, one must also give attention to electrical (tan δ) and mechanical (Q_m) loses.

Traditional piezoelectric materials only partially fulfil these requirements. Piezoelectric ceramics like lead zirconate-titanate and modified lead titanates are the preferred options for medical ultrasonic transducers. These ceramics offer notable attributes such as high electromechanical coupling (k_t ~ 0.4-0.5), a diverse range of dielectric constants (ε^S, ranging from 100 to 2400), and minimal electrical and mechanical losses (tan δ ≤ 0.02, Q_m ranging from 10 to 1000). However, their notable drawback lies in their high acoustic impedance (Z ~ 20-30 Mrayls). To address this, an acoustic matching layer technology has been devised to connect these ceramics with tissue. This approach enables the creation of relatively broad-spectrum, sensitive transducers.

Piezoelectric polymers exhibit a distinct set of material characteristics. Their advantageous low acoustic impedance (Z ≈ 4 Mrayls) simplifies acoustic matching. However, their low electromechanical coupling ($k_t \leq 0.3$) and elevated dielectric losses (tan δ ≈ 0.15) significantly degrade sensitivity. Furthermore, their low dielectric constant

(ε^S ~ 10) imposes substantial requirements on both transmitters and receivers. Composite piezoelectric offer material properties superior both piezoceramics and piezopolymers. Their coupling constants can be notably larger (k_t ~ 0.6 to 0.75) compared to ceramics, while exhibiting significantly lower acoustic impedance (Z < 10 MRayls), nearly approaching the range of piezopolymers. Additionally, these composites offer a broad spectrum of dielectric constants (ε^S ~ 10_1000) along with minimal dielectric and mechanical losses. Demonstrations have already showcased piezocomposites with characteristics superior to those of traditional piezoceramics and piezopolymer [1].

1.2 Thesis objectives

The aim is to make a more efficient transducer by using a composite of Lithium Niobate and polymer material as a softer material that will be achieved by increasing electromechanical coupling coefficient and decreasing acoustic impedance. These two parameters are the most important to consider the efficiency of the transducer. The lower acoustic impedance will be desired as it facilitates better compatibility with biological tissues, so this reduction in acoustic impedance helps to improve the transmission of acoustic waves into biological tissues, enhancing the effectiveness of medical imaging.

Moreover, the increased electromechanical coupling coefficient achieved through this composite design enhances the conversion efficiency of electrical energy to mechanical vibration and vice versa. This leads to improved sensitivity and performance of the transducer, enabling more accurate detection and measurement of signals.

It needs to be considered both 1-3 and 2-2 piezocomposite ultrasound transducer for Z-cut and 36°/Y-cut rotation. The challenging is related to calculating the constitutive equations for piezocomposite of $LiNbO_3$ and polymer material in 36°/Y-cut that needs to be simulated in MATLAB by considering Euler angles and get the material matrices like stiffness constant, piezoelectric constant and clamped dielectric constant.

Tasks:

- Design and Model

- Design and model 1-3 and 2-2 Lithium Niobate ($LiNbO_3$) piezocomposite ultrasound transducer for both Z-cut and 36°/Y-cut with 3MHz center frequency in a Mason equivalent circuit model, using the X. Trans software for MATLAB.

It will be simulated by considering different polymer materials (EpoTek 3012 and RTV 3140) and different loads like water and steel.

- Simulate the structure in FEM, using COMSOL.
- Characterize the 36°/Y-cut plate with 3MHz center frequency in the USN lab.
- Compare measurements and calculations, comment, explain.

1.3 Thesis structure

The first chapter of thesis structure is related to background and thesis objectives. The second chapter is focused on theoretical background foundation which contains physical properties and crystal structure of $LINbO_3$, piezoelectric constitutive equation, acoustic impedance matching, different cuts of piezoelectric crystal, piezoelectric crystal (36°/ Y-cut), polymer filler and modelling of single element transducers in X. Trans and COMSOL. Chapter 3 is dedicated to methods which is listed the values of active piezoceramic and different polymer materials like EpoTek 3012 and RTV 3140.in addition it drives the constitutive equations for 1-3 and 2-2 composite in different cuts (Z-cut and 36°/ Y-cut). Also, this chapter is focused on method of simulation in finite element modelling (COMSOL).

Chapter 4 is shown the result of simulation in both X. Trans and COMSOL for Lithium niobate in Z-cut and 36°/ Y-cut. In addition, this chapter is illustrated the results for composite properties with different polymer materials (EpoTek 3012, RTV 3140 and air) in both Z-cut and 36°/ Y-cut. The last part is shown the measurement of 36°/ Y-cut lithium niobate plate in the lab at USN.

The next chapter (5^{th} chapter) is written as discussion part and discusses the result for 1-3 composite of lithium niobate and filler material in 36°/ Y-cut.

The last part of the thesis is related to the conclusion part.

2 Theoretical background

2.1 Physical properties and crystal structure of Lithium Niobate ($LiNbO_3$)

Due to its excellent optical, piezoelectric, electro-optic, elastic, photo elastic, and piezoelectric properties, ferroelectric lithium niobate ($LiNbO_3$) optics are widely used in integrated and guided wave applications.

Lithium niobate is an effective piezoelectric material for high temperature devices. There are a lot of inexpensive and widely available sources of this material, and it has a very high Curie temperature (T_c) about 1210°C. To prevent degradation and ageing, the operating temperature of the piezoelectric material should not exceed $T_c/2$. Therefore, transducers based on LiNbO3 have the potential to operate up to 600°C. In addition, at temperatures above 650°C lithium niobate experiences oxygen loss and becomes increasingly conductive. Lithium niobate has the disadvantage of relatively weak piezoelectric properties including a low electromechanical coupling coefficient, (k_t). Although not the material of choice for mainstream ultrasonic transducers, lithium niobate has been explored for specialist applications. In non-destructive testing (NDT) it has been used for high-temperature applications, it has also been used for high-frequency transducers for biomedical imaging as it can be layered very thin [5]. In compared to PZT (Lead zirconate titanate) that has superior coupling coefficients but low mechanical quality factors at high frequencies, $LiNbO_3$ has higher quality factors, smoother surfaces, and higher ultimate strength.

Lithium Niobate is a synthetic crystal in class (3m) that because of combination of optical, piezoelectric, ferroelectric, and elastic properties, it is attracted much interest.

2.2 Piezoelectric Constitutive Equation

A piezoelectric effect occurs when a material changes its physical dimensions when an electrical field is applied (the conversion mechanism from mechanical energy to electrical energy and vice versa). A direct piezoelectric effect occurs when an electrode is subjected to stress, causing a net electric charge to appear across the electrodes. An inverse effect occurs when there is a potential difference across the electrodes that causes the material

to deform. Depending on the direction of the electric field, the direction in which the piezoelectric material is poled, and the mechanical clamping of the material, this deformation causes tensile or compressive stresses and strains in the material.

Wavelength is given mathematically as:

$$\lambda = \frac{c}{f} \tag{2.1}$$

where c is the speed of sound in the medium and f is the frequency of the wave.

The resonance frequencies of the piezoelectric element can be determined by treating the element as two separate vibrators, with one acting as an acoustic port in the front and the other in the back [6].

$$f_0 = n\,\frac{c_P}{2t} \tag{2.2}$$

Where n is an odd integer, c_P is the speed of sound in the piezoelectric and t is the thickness of the piezoelectric.

By merging Equations 2.1 and 2.2, and rearranging them, it becomes evident that resonance occurs when t equals odd multiples of one-half wavelength (λ_P) in the piezoelectric material.

$$t = n\,\frac{\lambda_P}{2} \tag{2.3}$$

A piezoelectric material is made up of molecules that have dipoles that oriented in the same direction. Because of an applied mechanical load, the piezoelectric material is mechanically deformed, the electric polarization changes macroscopically.

This conversion of energy is to and from mechanical domain (i.e., mechanical strain S and mechanical stress T) and electrical domain (i.e., electric field intensity E and electric displacement D). Because of covering of the piezoelectric with electrodes, the electrical voltages can be measured, applied to create mechanical deformation. For anisotropic solids, its mechanical properties can be described by its stiffness matrix from Hooke's law and its dielectric properties can be expressed with Voigt notation, also called matrix notation, as

$$\begin{bmatrix} T_1 \\ T_2 \\ T_3 \\ T_4 \\ T_5 \\ T_6 \end{bmatrix} = \begin{bmatrix} c_{11}^E & c_{12}^E & c_{13}^E & c_{14}^E & c_{15}^E & c_{16}^E \\ c_{21}^E & c_{22}^E & c_{23}^E & c_{24}^E & c_{25}^E & c_{26}^E \\ c_{31}^E & c_{32}^E & c_{33}^E & c_{34}^E & c_{35}^E & c_{36}^E \\ c_{41}^E & c_{42}^E & c_{43}^E & c_{44}^E & c_{45}^E & c_{46}^E \\ c_{51}^E & c_{52}^E & c_{53}^E & c_{54}^E & c_{55}^E & c_{56}^E \\ c_{61}^E & c_{62}^E & c_{63}^E & c_{64}^E & c_{65}^E & c_{66}^E \end{bmatrix} \begin{bmatrix} S_1 \\ S_2 \\ S_3 \\ S_4 \\ S_5 \\ S_6 \end{bmatrix} \tag{2.4}$$

$$\begin{bmatrix} D_1 \\ D_2 \\ D_3 \end{bmatrix} = \begin{bmatrix} \varepsilon_{11}^S & \varepsilon_{12}^S & \varepsilon_{13}^S \\ \varepsilon_{21}^S & \varepsilon_{22}^S & \varepsilon_{23}^S \\ \varepsilon_{31}^S & \varepsilon_{32}^S & \varepsilon_{33}^S \end{bmatrix} \begin{bmatrix} E_1 \\ E_2 \\ E_3 \end{bmatrix}$$

where T_i in the above matrix is the rank 2 mechanical stress tensor written as a 6 x 1 column vector, S_i is the rank 2 mechanical strain tensor written on the same format, $c_{i\,;j}^E$ is the elastic stiffness constants at constant electric field, $D_{1\,;2\,;3}$ is the electric displacement field, E_i is the electric field and "$S_{i\,;j}$ is the relative permittivity at constant strain, i.e. clamped conditions.

The piezoelectric material creates a coupling between electrical and mechanical domains. Thus, piezoelectricity affects both mechanical stress and strain, and vice versa, by induced electric fields and displacements. Following are the constitutive equations in stress charge form derived from the electrical and mechanical domains in above:

$$T = [c^E]S - e^t E \tag{2.5}$$

$$D = eS + [\varepsilon^S E]\, E \tag{2.6}$$

c^E, e and ε^S are the stiffness matrix at constant electric field, piezoelectric stress coefficient (Superscript t indicates matrix transpose) and clamped permittivity.

In class (3m) there are six independent elastic, four independent piezoelectric, and two independent dielectric constants, as shown in below matrix [4]:

$$C^E = \begin{bmatrix} c_{11} & c_{12} & c_{13} & c_{14} & 0 & 0 \\ c_{12} & c_{11} & c_{13} & -c_{14} & 0 & 0 \\ c_{13} & c_{13} & c_{33} & 0 & 0 & 0 \\ c_{14} & -c_{14} & 0 & c_{44} & 0 & 0 \\ 0 & 0 & 0 & 0 & c_{44} & c_{14} \\ 0 & 0 & 0 & 0 & c_{14} & c_{66} \end{bmatrix} \tag{2.7}$$

Where: $(c_{11} - c_{12}) = 2c_{66}$

$$\varepsilon = \begin{bmatrix} \varepsilon_{11} & 0 & 0 \\ 0 & \varepsilon_{11} & 0 \\ 0 & 0 & \varepsilon_{33} \end{bmatrix}$$

$$e = \begin{bmatrix} 0 & 0 & 0 & 0 & e_{15} & -e_{22} \\ -e_{22} & e_{22} & 0 & e_{15} & 0 & 0 \\ e_{31} & e_{31} & e_{33} & 0 & 0 & 0 \end{bmatrix}$$

Elasto-Piezo-dielectric matrix for the crystal class (3m)

One of the key material parameters crucial for the fabrication of a transducer is the electromechanical coupling coefficient, denoted as k_t. The electromechanical coupling

coefficient signifies the material's ability to convert electric energy into mechanical energy and vice versa. This coefficient is dependent upon the material geometry of the piezoelectric element. Specifically, when the lateral dimensions (width) of the transducer significantly exceed its thickness, the electromechanical coupling coefficient k_t associated with the thickness mode applies.

For a thin disk or plate operating in thickness mode, the electromechanical coupling factor is:

$$k_t = \frac{e_{33}}{\sqrt{c_{33}^D \varepsilon_{33}^S}} \tag{2.8}$$

When operating in thickness mode, a free long rod's coupling factor is typically expressed in d form as k_{33} which is also the maximum coupling factor of the piezoelectric material, hence, $k_{33} > k_t$.

$$k_{33} = \frac{d_{33}}{\sqrt{s_{33}^D \varepsilon_{33}^S}} \tag{2.9}$$

Where:

d_{33}= the piezoelectric strain constant.

c_{33}^D= the elastic stiffness along the thickness direction at constant electric displacement (constant charge or open circuit conditions).

s_{33}^D= the compliance constant.

The longitudinal wave velocity value will be defined to related elastic stiffness:

$$c_l = \sqrt{\frac{c_{33}^D}{\rho_P}} \tag{2.10}$$

ρ_P: the density of piezoelectric material.

So, the acoustic impedance is defined as:

$$Z_P = \sqrt{\rho_P \, c_{33}^D} \tag{2.11}$$

A thickness mode piezoelectric coupling coefficient h_{33} can be expressed as follows:

$$h_{33} = k_t \sqrt{\frac{c_{33}^D}{\varepsilon_{33}^S}} \tag{2.12}$$

Additional relations:

$$e_{33} = h_{33} \, \varepsilon_{33}^S \tag{2.13}$$

$$c_{33}^E = c_{33}^D \left(1 - {k_t}^2\right) = c_{33}^D - \frac{e_{33}^2}{\varepsilon_{33}^S} \tag{2.14}$$

2.3 Acoustic Impedance Matching

Another critical material parameter to consider is the acoustic impedance. Matching the acoustic impedance of the piezoelectric material with that of the load medium is essential for achieving optimal energy transmission. Typically, the piezoelectric material exhibits a characteristic acoustic impedance of approximately 30 MRayls, whereas the characteristic impedance of the load material, such as water or biological tissue, typically ranges around 1.5 MRayls [10]. This phenomenon results in pronounced reflections at the interface, constraining the outward transmission of acoustic energy from the piezoelectric plate and thereby reducing the bandwidth of the transducer. To address this, acoustic matching layers are introduced between the piezoelectric material and the load, effectively compensating for these impedance disparities.

The characteristic acoustic impedance for a material is equal to the acoustic impedance of a plane wave:

$$Z = \rho \, c \tag{2.15}$$

where Z is the characteristic acoustic impedance, ρ is density and c is longitudinal wave velocity in the medium of consideration.

Enhancing the performance of a transducer involves aligning the acoustic impedance at the transducer's front by employing matching layers. According to transmission line theory, achieving 100% transmission for a monochromatic plane wave necessitates the matching layer thickness to be $\lambda_m/_4$, where λ_m represents the wavelength in the matching layer material. This layer is characterized by the acoustic impedance Z_m [11].

$$Z_m = (Z_P\, Z_l)^{1/2} \tag{2.16}$$

For a wideband transducer, Desilets, et al. [3] found that effectively lower target values for the matching layer impedances could be derived based on the KLM equivalent circuit model. For a single matching layer, the matching layer impedance is:

$$Z_m = (Z_P\, {Z_l}^2)^{1/3} \tag{2.17}$$

For two matching layers, the acoustic impedances of the two layers should be:

$$Z_{m1} = ({Z_P}^4\, {Z_l}^3)^{1/7} \tag{2.18}$$

$$Z_{m2} = (Z_P\ {Z_l}^6)^{1/7} \tag{2.19}$$

The backing layer for the transducer also has an important role in the performance of the transduction. Backing layer can be used to adjust the mechanical quality factor, bandwidth, and sensitivity.

When an ultrasound pulse is emitted, it travels into the body and reflects echoes. The backing layer helps to absorb the acoustic energy that travels backward, preventing it from interfering with the reception of the returning echoes. This absorption reduces the ringing or reverberation of the transducer and improves image clarity.

Also, the backing layer dampens the vibration of the piezoelectric element after it has emitted an ultrasound pulse. This damping action helps to shorten the pulse length, which in turn improves axial resolution, meaning it enhances the ability to distinguish between closely spaced structures along the path of the ultrasound beam.

2.4 Different cuts of piezoelectric crystal (Z-cut and 36°/Y -cut)

To obtain the best piezoelectric properties from lithium niobate piezoelectric material, different crystal cuts must be chosen. This likes the situation for quartz. For bulk acoustic waves, longitudinal mode, a choice can be made between z-cut and $36°/\mathrm{Y}$ wafers. Piezoelectric efficiency is highest in plates with $36°/\mathrm{Y}$ orientation electrodes on the top and bottom faces.

However, they produce an asymmetric ultrasonic beam profile [12]. The parameters of interest for both cuts are given in table.1. It is important to consider the material's isotropy when considering its potential use in phased array probes. In both single array elements and steered beam configurations, monolithic lithium niobate plates have more sensitive 36°/Y -cut material that introduced asymmetric minima in the beam profile. Therefore, the z-cut material is preferred for array applications.

Table 1-1. Parameters of interest of lithium niobate z-cut and 36°/Y*-cut [13].*

Crystalline cut	k_t	Isotropy about the thickness axis	Wave type
36°/Y	0.49	Anisotropic	Quasi longitudinal
Z	0.17	Isotropic	Longitudinal

Lithium niobate is usually obtained in the form of single crystal wafers. Crystals with anisotropic structures have properties that vary with the cut used. While the properties of the 36°/Y-cut are highly asymmetric, it is the most efficient crystal cut. A symmetric cut that is commonly used is the z-cut (k_t = 0.17), which has a much lower efficiency.

2.5 Piezoelectric crystal (36°/Y-cut)

The material constants in the cross-section are obtainable by transforming the original matrices using the Euler angles (λ, μ, Θ). The Euler angle is defined as the rotation from the material axis to the device axis, following the Z-X-Z convention. For a rotated Y/cut $LiNbO_3$ with rotation Ψ, the Euler angles are λ= Θ= 0 and μ= Ψ -90°.

More specifically, the Euler angles for the cross-section along the X-axis in 36°/Y-cut $LiNbO_3$ is (0°,36°-90°,0°).

We can start with a transformation of stress:

$$\delta'_{ij} = a_{ik}\, a_{jl}\, a_{kl} \qquad (2.20)$$

$$= a_{i1}\, a_{j1}\, \delta_1 + a_{i2}\, a_{j2}\, \delta_2 + a_{i3}\, a_{j3}\, \delta_3$$

$$+(a_{i2}\, a_{j3} + a_{i3}\, a_{j2})\, \delta_4 \quad +(a_{i1}\, a_{j3} + a_{i3}\, a_{j1})\, \delta_5 + (a_{i1}\, a_{j2} + a_{i2}\, a_{j1})\, \delta_6 .$$

Using this in turn for each stress component, we get:

$$\delta' = \alpha(a)\delta \qquad (2.21)$$

Where: (2.22)

$$\alpha = \begin{bmatrix} a11a11 & a12a12 & a13a13 & 2a12a13 & 2a11a13 & 2a11a12 \\ a21a21 & a22a22 & a23a23 & 2a22a23 & 2a21a23 & 2a21a22 \\ a31a31 & a32a32 & a33a33 & 2a32a33 & 2a31a33 & 2a31a32 \\ a21a31 & a22a32 & a23a33 & a22a33 + a23a32 & a21a33 + a23a31 & a21a32 + a22a31 \\ a11a31 & a12a32 & a13a33 & a12a33 + a13a32 & a11a33 + a13a31 & a11a32 + a12a31 \\ a11a21 & a12a22 & a13a23 & a12a23 + a13a22 & a11a23 + a13a21 & a11a22 + a12a21 \end{bmatrix}$$

According to Hooke's law, elastic materials follow the following formula:

$$\delta_{ij} = c_{ijkl}\, \varepsilon_{kl} \qquad (2.23)$$

for some stiffness tensor c_{ijkl} that characterizes the material. Alternatively, compliance representations can be used:

$$\varepsilon_{ij} = s_{ijkl}\, \delta_{kl} \qquad (2.24)$$

where s_{ijkl} are compliance constants.

Hooke's law can be expressed in Voigt notation as follow: (2.25)

$$\delta_{ij} = c_{ij11}\, \varepsilon_{11} + c_{ij22}\, \varepsilon_{22} + c_{ij33}\, \varepsilon_{33} + c_{ij23}\, 2\varepsilon_{23} + c_{ij13}\, 2\varepsilon_{13} + c_{ij12}\, 2\varepsilon_{12}$$

$$= c_{ij11}\, \varepsilon_1 + c_{ij22}\, \varepsilon_2 + c_{ij33}\, \varepsilon_3 + c_{ij23}\, \varepsilon_4 + c_{ij13}\varepsilon_5 + c_{ij12}\, \varepsilon_6$$

Evaluating this for all stress components, we get:

$$\delta = C\, \varepsilon \qquad (2.26)$$

Where:

$$C = \begin{bmatrix} C_{11} & C_{12} & C_{13} & C_{14} & C_{15} & C_{16} \\ C_{21} & C_{22} & C_{23} & C_{24} & C_{25} & C_{26} \\ C_{31} & C_{32} & C_{33} & C_{34} & C_{35} & C_{36} \\ C_{41} & C_{42} & C_{43} & C_{44} & C_{45} & C_{46} \\ C_{51} & C_{52} & C_{53} & C_{54} & C_{55} & C_{56} \\ C_{61} & C_{62} & C_{63} & C_{64} & C_{65} & C_{66} \end{bmatrix} \qquad (2.27)$$

$$= \begin{bmatrix} C_{1111} & C_{1122} & C_{1133} & C_{1123} & C_{1113} & C_{1112} \\ C_{2211} & C_{2222} & C_{2233} & C_{2223} & C_{2213} & C_{2212} \\ C_{3311} & C_{3322} & C_{3333} & C_{3323} & C_{3313} & C_{3312} \\ C_{2311} & C_{2322} & C_{2333} & C_{2323} & C_{2313} & C_{2312} \\ C_{1311} & C_{1322} & C_{1333} & C_{1323} & C_{1313} & C_{1312} \\ C_{1211} & C_{1222} & C_{1233} & C_{1223} & C_{1213} & C_{1212} \end{bmatrix}$$

Hence, for stress, the compliance constants in Voigt notation are directly obtained by mapping indices. The matrix form of Hooke's law can be inverted to yield:

$$\mathrm{C} = \mathrm{S}\,\delta \tag{2.28}$$

where the compliance matrix is $\mathrm{S} = \mathrm{C}^{-1}$.

Transformations are readily obtained in matrix notation.

For stress $\delta' = \alpha\delta = \alpha\mathrm{C}\,\varepsilon = \alpha\mathrm{C}\alpha^{\mathrm{T}}\,\varepsilon'$ (2.29)

So that: $\mathrm{C}' = \alpha\,\mathrm{C}\,\alpha^{\mathrm{T}}$ (2.30)

To find the transformation properties of the compliance matrix, we start with strain [14].

That is: $\varepsilon' = [\alpha^{-1}]^{\mathrm{T}}\,\varepsilon = [\alpha^{-1}]^{\mathrm{T}}\,\mathrm{S}\,\delta = [\alpha^{-1}]^{\mathrm{T}}\,\mathrm{S}\,\alpha^{-1}\,\delta'$ (2.31)

And:

$$\mathrm{S}' = [\alpha^{-1}]^{\mathrm{T}}\,\mathrm{S}\,\alpha^{-1}. \tag{2.32}$$

2.6 Polymer Filler

The selection of passive polymer materials is indeed crucial in piezoelectric composite fabrication, especially in applications that involve high power and/or high-temperature conditions. The passive polymer components, which act as matrix or filler materials in piezocomposites, play a significant role in the overall performance and durability of these materials, particularly in harsh environmental conditions.

In certain scenarios, the presence of polymers within piezocomposites can be a limiting factor for their use in extreme environments due to factors such as: thermal stability, mechanical strength, and chemical resistance [15].

In the piezoelectric structures, the ideal condition for achieving the maximum coupling factor often involves the use of air because of its low density and the absence of mechanical restrictions. In air, however piezoceramic materials could vibrate with minimal mechanical constraints (which theoretically could maximize their performance in terms of generating electrical energy from mechanical vibrations or vice versa and

higher coupling factor), it is practically unsuitable for creating mechanically robust structures.

Therefore, in real-world applications where mechanical strength and structural stability are essential, employing a soft polymer with low elastic stiffness can serve as a compromise. The use of such a soft polymer around the vibrating piezoceramics can reduce lateral restrictions on their movement while still providing some mechanical support to the overall microstructure [21].

The reported properties of some of the polymer materials are compiled and listed in ref [15].

Elastic materials follow Hooke's law:

$$\delta = C\,\varepsilon \tag{2.33}$$

That δ is stress, C is stiffness matrix and ε is strain components.

The stiffness matrix can be written as below: (2.34)

$$C = \frac{E}{(1+\nu)(1-2\nu)}\begin{bmatrix} 1-\nu & \nu & \nu & 0 & 0 & 0 \\ \nu & 1-\nu & \nu & 0 & 0 & 0 \\ \nu & \nu & 1-\nu & 0 & 0 & 0 \\ 0 & 0 & 0 & 1-2\nu & 0 & 0 \\ 0 & 0 & 0 & 0 & 1-2\nu & 0 \\ 0 & 0 & 0 & 0 & 0 & 1-2\nu \end{bmatrix}$$

For an isotropic homogeneous material, the relevant elastic stiffness constants are:[21]

$$c_{11} = \frac{1-\nu}{\nu}\ \frac{E\,\nu}{(1+\nu)(1-2\nu)} \tag{2.35}$$

$$c_{12} = \frac{E\,\nu}{(1+\nu)(1-2\nu)} \tag{2.36}$$

where the Young's modulus E and Poisson's ratio v can indeed determine from literature or from speed of sound measurement of longitudinal wave velocity c_l and shear wave velocity c_s and they are related as [21]:

$$E = \rho_{filler}\, c_s^2\, \left(\frac{3c_l^2 - 4c_s^2}{c_l^2 - c_s^2}\right) \tag{2.37}$$

$$\nu = \frac{1-2(c_s/c_l)^2}{2-2(c_s/c_l)^2} \tag{2.38}$$

and the shear wave velocity inside the polymer can be approximated by [19]:

$$c_S = 0.45\ c_l \tag{2.39}$$

2.7 Modelling of single element transducers

2.7.1 Simulation in X.Trans

The most common equivalent circuits models for piezoelectric transducers are the Mason model and the KLM model. According to the KLM and Mason equivalent circuit models, the transducer can be treated as a three-port network consisting of two mechanical ports, representing the front and back surfaces, and one electrical port, representing the electrical connections.

In this section, the X. Trans package, a MATLAB program developed by the department of Circulation and Medical Imaging at NTNU is used to perform one dimensional modelling. For one piezoelectric element operating in thickness mode, it uses the equivalent circuit for the Mason model.

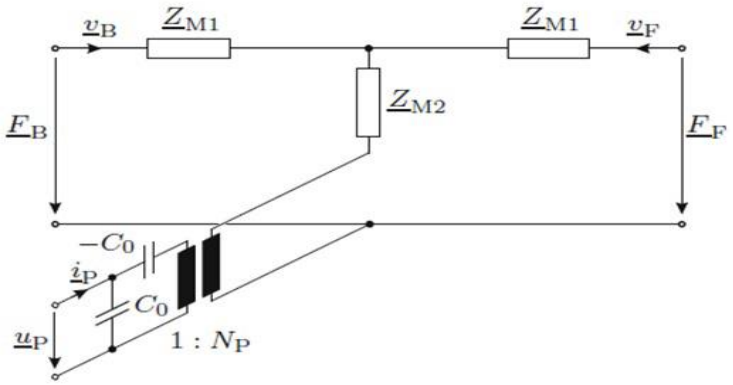

Figure 2.1 The equivalent circuit in Mason Model for thickness extensional operation of a piezoelectric element [20].

t_S: the piezoelectric element thickness.
k: the wave number.

$$Z_{M1} = j\, Z_P \tan\frac{kt_S}{2} \qquad N_P = h_{33}\, C_0 \qquad (2.40)$$

$$Z_{M2} = -j\, Z_P \csc kt_S \qquad h_{33} = k_t \sqrt{\frac{C_{33}^D}{\varepsilon^S{}_{33}}}$$

$$C_0 = \frac{\varepsilon_{33}^S\, A}{t_S}$$

N_P is the constant transmission ratio.

$\varepsilon^S{}_{33}$ is the clamped complex dielectric constant. C_{33}^D is the open circuit complex elastic stiffness. $k_t$is the complex electromechanical coupling coefficient.

The negative capacitance -C_0 serves as an ideal transformer that mechanical port is connected to an electrical port.

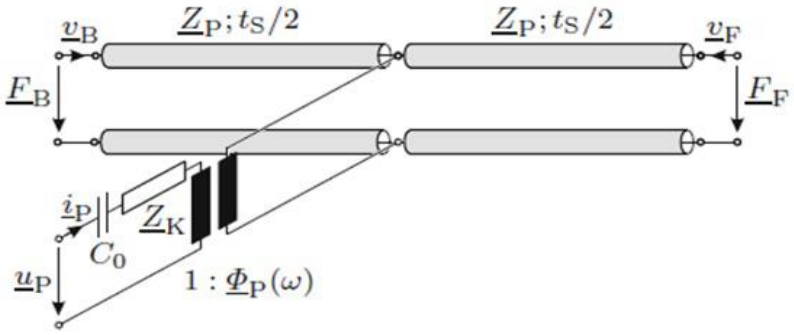

Figure 2.2 The KLM equivalent circuit model for a thickness extensional piezoelectric element [20].

$$\Phi_P(\omega) = \frac{\omega\, Z_P}{2\, h_{33}} \csc \frac{k\, t_S}{2} \tag{2.41}$$

$$Z_K = \frac{j\, h_{33}^2}{\omega^2\, Z_P} \sin k t_S \tag{2.42}$$

$\Phi_P(\omega)$: is the transmission ratio as a function of frequency.

Mason's model is suitable for studying the electrical behavior of the designed transducer since it has clamped capacitance C_0 at the electrical port. It provides insights into the electrical behavior of the transducer but does not directly model its mechanical properties.

Unlike the Mason model, the KLM model considers both the electrical and mechanical domains simultaneously, allowing for a more comprehensive analysis of the transducer's behavior. Due to its mechanical transmission lines, the KLM model can be used to investigate the effects of additional layers in the front and back of the piezoelectric material (i.e., matching layers) [20]. As a result, the two models are equivalent.

The choice between these models depends on the specific requirements of the analysis and the aspects of the transducer being studied.

2.7.2 Simulation in COMSOL

A finite element model (FEM) solves partial differential equations (PDEs) in two or three special coordinates when it is impossible to solve the phenomena analytically. The first step in the FEM process is solving the PDEs that govern the physical processes with boundary and initial conditions. After a model body's complicated geometry is

deconstructed using special discretization, FEM produces smaller models as finite elements. Using these finite points, we can approximate the real solution with an algebraic system of equations. In this work, a 2D model of the design transducer was developed and simulated using FEM. The two-dimensional Mason model allowed the investigation of lateral modes within composite structures, which were not included in the one-dimensional Mason model.

For this simulation, it is needed to define the physics in this problem that involves piezoelectricity, solid mechanics, and electrostatics. In the second step, define the geometric properties of the model based on the transducer design. After that we should define the material properties of elements and boundary conditions. In the next step, Define the mesh of the model. It is essential that the solution be converged to achieve a high level of accuracy. A mesh's shape and density have an impact on this. In the last part, Compute relevant variables and quantities.

3 Methods

3.1 Active piezoceramic- ($LiNbO_3$)

The material properties for the Z/cut lithium niobate used for the finite element simulations are listed in table below.

Table 3-1 Material properties of $LiNbO_3$ for Z/Cut in the finite element simulations [16].

$LiNbO_3$		
Elastic Constants [x 10^{11} N/m^2]	C^E_{11} C^E_{12} C^E_{13} C^E_{14} C^E_{33} C^E_{44} C^E_{66}	2.030 0.573 0.752 0.085 2.424 0.595 0.728
Compliance Constants [x 10^{-12} m^2 /N]	S^D_{11} S^D_{12} S^D_{13} S^D_{14} S^D_{33} S^D_{44} S^D_{66}	5.20 -0.44 -1.45 0.87 4.89 10.8 11.3
Piezo Strain constants [C/m^2] Piezo Strain constants [x 10^{-12}C/N]	e_{15} e_{22} e_{31} e_{33} d_{15} d_{22} d_{31} d_{33}	3.83 2.37 -0.23 1.3 69.2 20.8 -0.85 6.0
Relative Permittivity, Dielectric constant	$\varepsilon^S_{11} / \varepsilon_0$ $\varepsilon^S_{33} / \varepsilon_0$	44.3 27.9
Density [kg/m^3]	ρ	4650

3.2 Different Polymer materials (EpoTek 3012 and RTV 3140)

In this thesis, the EpoTek 3012 and RTV 3140 are used as passive polymer for making composite.

In composite materials, EpoTek 3012 is commonly used as a polymer filler. In general, it has good mechanical strength and stiffness, contributing to the composite's overall strength. Due to its excellent adhesive properties, it bonds well with various substrates, reinforcing the composite's structural integrity. Despite a wide range of temperatures, it retains its properties at both high and low temperatures.

EpoTek 3012, being an epoxy resin, doesn't have inherent piezoelectric properties. In fact, its use as a kerf filling material for ultrasonic transducers might suppress the motion or deformation of piezoelectric materials. Moreover, it's noted that EpoTek 3012 is easily available at the USN laboratories.

The Silicone rubbers like RTV 3140 are known for their flexibility and ability to maintain elasticity over a wide range of temperatures. They can accommodate some degree of movement in applications due to their flexibility.

For EpoTek 3012, the longitudinal velocity was measured using USN's ultrasonic lab's Speed of Sound setup, and shear velocity could be roughly 45% as described in [19].To obtain the effective material parameters for the one-dimensional Mason model, Young's modulus and Poisson's ratio were calculated using longitudinal and shear velocity.

For RTV 3140, because of limitations in lab equipment for degassing, longitudinal and shear velocity cannot be measured effectively. Hence, a typical value of Young's modulus (E), Poisson's ratio (v), longitudinal velocity (c_l) and shear velocity (c_s) has been taken from published literature [17] and [18].

The material parameters of different filler polymers as EpoTek 3012 and RTV 3140 are listed in Table 3-2 as shown below:

Table 3.2 Material Parameter of polymer fillers as EpoTek 3012 & RTV 3140 silicon rubber.

Properties	Symbols	EpoTek 3012	RTV 3140
Density	ρ_{filler} [kg/m^3]	1147 **	1050 [8]
Young 's Modulus	E [GPa]	4.10 *	0.0018 *
Poisson' s Ratio	v	0.37 [19]	0.49[20]
Long Velocity	c_l [m/s]	2587 **	1000 *
Shear Velocity	c_s [m/s]	1164 ***	90 *
Relative Permittivity	$\varepsilon / \varepsilon_0$	3.8 [7]	2.57 [8]

*Typical values measured for RTV silicone rubber has been taken from published literature [17] and [18].

** The values are measured in the USN lab.

***The shear velocity for EpoTek 3012 can calculate as 45% of the longitudinal velocity [19].

3.3 Piezocomposite material

The theory of piezocomposite materials is widely studied, and in this section, the electromechanical coupling coefficient k_{33} is calculated for a piezocomposite material with connectivity (2-2) and (1-3).

The composite piezoelectric has a high coupling and low acoustic impedance, making it an important tool for medical ultrasound imaging. PZT-rod/polymer composites are used in these medical transducers.

Sensitive transducers require adherence to specific criteria, including the electromechanical coupling constant (k_t), which denotes the degree of coupling between electrical and mechanical energies. Moreover, the specific acoustic impedance (Z) is crucial, as the piezoelectric material should be acoustically aligned with tissue to facilitate efficient coupling of acoustic waves during both transmission and reception. Additionally, the dielectric constant (ε^s) assumes significance, as it influences the compatibility of the electric properties with the driving and receiving electronics. Furthermore, in the context of sensitive transducers, considerations must be given to electrical and mechanical

losses. In another case, for piezopolymer material, there is lower Z but low k_t that degrades sensitivity.

Piezocomposite materials offer distinct advantages over piezoceramics and piezopolymers. With a larger electromechanical coupling constant (k_t ~ 0.6-0.75), significantly lower acoustic impedance (Z<10 MRayl), a wide range of dielectric constants (ε^s ~10-1000), and minimal electrical and mechanical losses, they present a compelling choice for various applications [1].

3.3.1 (1-3) Composite Piezoelectric (Z-cut)

When the rod dimension and spacing are fine enough in comparison with all relevant acoustic wavelengths, such composites can be treated as homogeneous media with new effective material parameters.; We can only apply this model if we remain within this regime safely. By focusing only on thickness-mode oscillations of large thin plates with negligible electrical and mechanical losses, we simplify the analysis substantially. The configuration of 1-3 composite is shown in below:

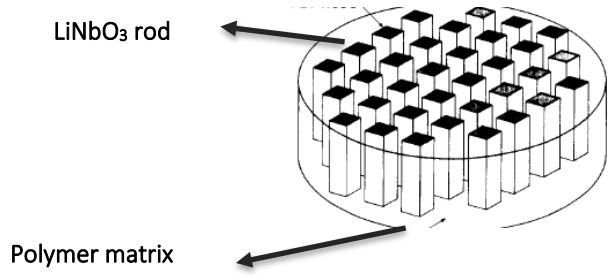

Figure 3.1 Schematic representation of 1-3 composite made from LiNbO3 rods in a polymer matrix. (Directly from [1])

Moreover, we focus sharply to treat an important physical effect-the lateral stresses generated within these plates-by means of a simple physical approximation.

Compared to thickness-mode resonances, lateral stopband resonances are pushed much higher. For frequencies near the thickness resonance, the composite is validly modeled as a homogeneous medium due to the fine spatial scale. For ultrasonic transducers in designing a composite material, it is needed to note that the lowest of these stopbands, at k = π/d, does not couple electrically in a uniformly electrode plate. At this lowest resonance, the rows of rods are separated by one half wavelength of the Lamb wave; as a result, rods oscillate out of phase with each other.

Connectivity is described by Newnham et al. into two numbers i,j. The two numbers can have values of 0, 1, 2, 3 and together they create 10 sets of connectivity patterns Active piezoceramics have a first digit, and passive polymers have a second digit. For example, when a material is only continuous in one direction, it is called '1', in two direction it is called '2', etc. An example is a 1-3 composite has piezoceramic rods being continuous in one direction a polymer phase being continuous in three directions.

Modelling a piezocomposite material accurately requires effective material parameters when embedded in piezoceramics. The main variable here is the volume fraction of piezoceramics or the polymer and their sum is [2]:

$$\mathrm{V_c} + \mathrm{V_p} = 1 \tag{3.1}$$

where $\mathrm{V_c}$ and $\mathrm{V_p}$ are the volume percentage of the ceramic material and the polymer _ material.

This section shows a simple physical model for the material parameters that govern the thickness-mode resonance in 1-3 piezoelectric composites. Orienting the composite plate in the x-y plane with the fundamental repeats of the rod lattice lying along the axes, we use strain and electric field as independent coordinates. The constitutive relations for the component phases give the stress and electric displacement at every point (x, y, z) within the plate. The polymer phase is an isotropic homogeneous medium that is piezoelectrically inactive, so for (x, y, z) within the polymer phase:

$$T_1 = c_{11} S_1 + c_{12} S_2 + c_{12} S_3 \tag{3.2}$$
$$T_2 = c_{12} S_1 + c_{11} S_2 + c_{12} S_3$$
$$T_3 = c_{12} S_1 + c_{12} S_2 + c_{11} S_3$$
$$T_4 = c_{44} S_4$$
$$T_5 = c_{44} S_5$$
$$T_6 = c_{44} S_6$$
$$D_1 = \varepsilon_{11} E_1$$
$$D_2 = \varepsilon_{11} E_2$$
$$D_3 = \varepsilon_{11} E_3$$

Here, T_i and S_i (i=1, 2, . . . 6) are the stress and strain components, respectively, in Voigt notation, E_i and D_i (i = 1, 2, 3) are the electric field and electric displacement, respectively, c_{ij} are the elastic stiffness constants and ε_{ij} are the dielectric constants.

For (x, y, z) within the ceramic phase, we assume that the ceramic rods as Lithium niobate material are perpendicular to the plate.

By using the equations for stress (T) and electrical displacement (D) in linear piezoelectric material as below:

$$T_{ij} = c_{ijkl} S_{kl} - e_{kij} E_k \tag{3.3}$$

And using the Voigt notation, we can show the stress and electrical displacement as below:

$$T_1 = c^E{}_{11} S_1 + c^E{}_{12} S_2 + c^E{}_{13} S_3 + 2 c^E{}_{14} S_4 - e_{21} E_2 - e_{31} E_3 \tag{3.4}$$

$$T_2 = c^E{}_{12} S_1 + c^E{}_{11} S_2 + c^E{}_{13} S_3 - 2 c^E{}_{14} S_4 - e_{22} E_2 - e_{32} E_3$$

$$T_3 = c^E{}_{13} S_1 + c^E{}_{13} S_2 + c^E{}_{33} S_3 - e_{33} E_3$$

$$T_4 = c^E{}_{14} S_1 - c^E{}_{14} S_2 + 2c^E{}_{44} S_4 - e_{24} E_2$$

$$T_5 = 2 c^E{}_{44} S_5 + 2 c^E{}_{14} S_6 - e_{15} E_1$$

$$T_6 = 2 c^E{}_{14} S_5 + c^E{}_{11} S_6 - c^E{}_{12} S_6 - e_{16} E_1$$

$$D_1 = 2 e_{15} S_5 + 2 e_{16} S_6 + \varepsilon^S_{11} E_1$$

$$D_2 = -e_{22} S_1 + e_{22} S_2 + 2e_{15} S_4 + \varepsilon^S_{22} E_2$$

$$D_3 = e_{31} S_1 + e_{31} S_2 + e_{33} S_3 + \varepsilon^S_{33} E_3$$

A ceramic phase can be distinguished from a polymer phase by using the superscripts E and S. Six simplifying approximations are presented to extract essential physics.

First, Throughout the individual phases, strain and electric field are assumed to be independent of x and y.

$$S_1 = S_2 \tag{3.5}$$

$$E_1 = E_2 \tag{3.6}$$

Second, as usual, we simplify the analysis of thickness mode oscillations in an electroded plate of large, thin dimensions. (symmetry in the x-y plane, E_1 = E_2 = 0, etc.)

The constitutive relations for the individual phases have a compact form,

namely, within the polymer (^{P}), phase,

$$T_1^P = (c_{11} + c_{12}) S_1^P + c_{12} S_3^P \tag{3.7}$$

$$T_3^P = 2c_{12} S_1^P + c_{11} S_3^P$$

$$D_3^P = \varepsilon_{11} E_3^P$$

Within the ceramic phase: (c phase)

$$T_1^C = (c^E{}_{11} + c^E{}_{12}) S_1^C + c^E{}_{13} S_3^C + 2c^E{}_{14} S_4^C - e_{31} E_3 \tag{3.8}$$

$$T_2^C = (c^E{}_{12} + c^E{}_{11}) S_1^C + c^E{}_{13} S_3^C - 2c^E{}_{14} S_4^C - e_{32} E_3$$

$$T_3^C = 2c^E{}_{13} S_1^C + c^E{}_{33} S_3^C - e_{33} E_3$$

$$T_4^C = 2c^E{}_{44}S_4^C$$
$$T_5^C = 2c^E{}_{44}S_5^C + 2c^E{}_{14}S_6^C$$
$$T_6^C = 2c^E{}_{14}S_5^C + c^E{}_{11}S_6^C - c^E{}_{12}S_6^C$$
$$D_1^C = 2e_{15}S_5^C + 2e_{16}S_6^C$$
$$D_2^C = 2e_{15}S_4^C$$
$$D_3^C = 2e_{31}S_1^C + e_{33}S_3^C + \varepsilon_{33}^S E_3$$

Based on our third approximation, ceramics and polymers oscillate together uniformly. Thus, in both phases, the vertical strains are the same,

$$S_3^P(Z) = S_3^C(Z) = \bar{S}_3(Z) \tag{3.9}$$

Fourth, we take the electric fields to be the same in both phases, namely,

$$E_3^P(Z) = E_3^C(Z) = \bar{E}_3(Z) \tag{3.10}$$

Now that the constitutive relations can be read more easily, for polymer phase:

$$T_1^P = (c_{11} + c_{12})S_1^P + c_{12}\bar{S}_3 \tag{3.11}$$
$$T_3^P = 2c_{12}S_1^P + c_{11}\bar{S}_3$$
$$D_3^P = \varepsilon_{11}\bar{E}_3$$

For ceramic phase:

$$T_1^C = (c^E{}_{11} + c^E{}_{12})S_1^C + c^E{}_{13}\bar{S}_3 + 2c^E{}_{14}S_4^C - e_{31}\bar{E}_3 \tag{3.12}$$
$$T_2^C = (c^E{}_{12} + c^E{}_{11})S_1^C + c^E{}_{13}\bar{S}_3 - 2c^E{}_{14}S_4^C - e_{32}\bar{E}_3$$
$$T_3^C = 2c^E{}_{13}S_1^C + c^E{}_{33}\bar{S}_3 - e_{33}\bar{E}_3$$
$$T_4^C = 2c^E{}_{44}S_4^C$$
$$T_5^C = 2c^E{}_{44}S_5^C + 2c^E{}_{14}S_6^C$$
$$T_6^C = 2c^E{}_{14}S_5^C + c^E{}_{11}S_6^C - c^E{}_{12}S_6^C$$
$$D_1^C = 2e_{15}S_5^C + 2e_{16}S_6^C$$
$$D_2^C = 2e_{15}S_4^C$$
$$D_3^C = 2e_{31}S_1^C + e_{33}\bar{S}_3 + \varepsilon_{33}^S\bar{E}_3$$

Our fifth approximation addresses the lateral interaction between the phases. We assume that the lateral stresses are equal in both phases and that the ceramic's lateral strain is compensated by a complimentary strain in the polymer so that the composite is lateral clamped:

$$T_1^P(Z) = T_1^C(Z) = \bar{T}_1(Z) \tag{3.13}$$
$$\bar{S}_1(Z) = \bar{v}\,S_1^P(Z) + v\,S_1^C(Z) = 0 \tag{3.14}$$

where v is the volume fraction of piezoceramic in the composite

and $\bar{\nu} = (1 - \nu)$ is the volume fraction of polymer.

Based on this, we expect the ceramic rods are clamped lateral to the polymer on an average basis. By using the vertical strain and electric field, we can describe the lateral strains as follows:

$$S^{C}_{1} = \bar{\nu}\,\frac{-(C^{E}_{13} - C_{12})\bar{S}_3 - 2C^{E}_{14}\,\bar{S}_4 + e_{31}\,\bar{E}_3}{\nu(C_{11} + C_{12}) + \bar{\nu}(C^{E}_{11} + C^{E}_{12})} \tag{3.15}$$

$$S^{P}_{1} = \nu\,\frac{(C^{E}_{13} - C_{12})\bar{S}_3 + 2C^{E}_{14}\,\bar{S}_4 - e_{31}\,\bar{E}_3}{\nu(C_{11} + C_{12}) + \bar{\nu}(C^{E}_{11} + C^{E}_{12})} \tag{3.16}$$

Then, the constitutive relations are simplified by removing the lateral strains and we obtain for the eliminated coordinate:

$$\bar{T_1}(Z) = \bar{C}^{E}_{13}\,\bar{S}_3 + 2\,\bar{C}^{E}_{14}\,\bar{S}_4 - \bar{e}_{31}\bar{E}_3 \tag{3.17}$$

Where:

$$\bar{C}^{E}_{13} = \frac{\nu\,C^{E}_{13}\,(C_{11} + C_{12}) + \bar{\nu}\,C_{12}(C^{E}_{11} + C^{E}_{12})}{\nu(C_{11} + C_{12}) + \bar{\nu}(C^{E}_{11} + C^{E}_{12})} \tag{3.18}$$

$$\bar{C}^{E}_{14} = \frac{\bar{\nu}\,(C^{E}_{11} + C^{E}_{12})C_{14}}{\nu(C_{11} + C_{12}) + \bar{\nu}(C^{E}_{11} + C^{E}_{12})} \tag{3.19}$$

$$\bar{e}_{31} = \frac{\nu\,e_{31}\,(C_{11} + C_{12})}{\nu(C_{11} + C_{12}) + \bar{\nu}(C^{E}_{11} + C^{E}_{12})} \tag{3.20}$$

And for the coordinates that remain:

$$T^{P}_{3} = \left[C_{11} + \frac{2\,\nu\;C_{12}(C^{E}_{13} - C_{12})}{\nu(C_{11} + C_{12}) + \bar{\nu}(C^{E}_{11} + C^{E}_{12})}\right]\bar{S}_3 + \left[\frac{4\,\nu\;C_{12}(C^{E}_{14})}{\nu(C_{11} + C_{12}) + \bar{\nu}(C^{E}_{11} + C^{E}_{12})}\right]\bar{S}_4 - \left[\frac{2\,\nu\;e_{31}\,C_{12}}{\nu(C_{11} + C_{12}) + \bar{\nu}(C^{E}_{11} + C^{E}_{12})}\right]\bar{E}_3 \tag{3.21}$$

$$D^{P}_{3} = \varepsilon_{11}\,\bar{E}_3 \tag{3.22}$$

$$T^{C}_{3} = \left[C^{E}_{33} - \frac{2\,\bar{\nu}\;C^{E}_{13}(C^{E}_{13} - C_{12})}{\nu(C_{11} + C_{12}) + \bar{\nu}(C^{E}_{11} + C^{E}_{12})}\right]\bar{S}_3 - \left[\frac{2\,\bar{\nu}\;C^{E}_{13}(C^{E}_{14})}{\nu(C_{11} + C_{12}) + \bar{\nu}(C^{E}_{11} + C^{E}_{12})}\right]\bar{S}_4 - \left[e_{33} - \frac{2\,\bar{\nu}\,e_{31}\;C_{13}}{\nu(C_{11} + C_{12}) + \bar{\nu}(C^{E}_{11} + C^{E}_{12})}\right]\bar{E}_3 \tag{3.23}$$

$$D^{C}_{3} = \left[e_{33} - \frac{2\,\bar{\nu}\,e_{31}\;(C^{E}_{13} - C_{12})}{\nu(C_{11} + C_{12}) + \bar{\nu}(C^{E}_{11} + C^{E}_{12})}\right]\bar{S}_3 - \tag{3.24}$$

$$[\frac{4\,\bar{\nu}\ e_{31}(C_{14}^{E})}{\nu(C_{11}+C_{12})+\bar{\nu}(C_{11}^{E}+C_{12}^{E})}]\ \bar{S}_4 +$$

$$[\varepsilon_{33}^{S}+\frac{2\,\bar{\nu}\ (e_{31})^2}{\nu(C_{11}+C_{12})+\bar{\nu}(C_{11}^{E}+C_{12}^{E})}]\ \bar{E}_3$$

The composites studied in this thesis are of 1-3 connectivity and with the volume percentage of the ceramics and the polymer.

Since the lateral periodicity is sufficiently fine, we can calculate the effective total stress and electric displacement by averaging over the contributions of the constituent phases, namely:

$$\bar{T_3}(Z) = \nu T_3^C(Z) + \bar{\nu} T_3^P(Z) \quad (3.25)$$

$$\bar{D_3}(Z) = \nu D_3^C(Z) + \bar{\nu} D_3^P(Z) \quad (3.26)$$

So, the final constitutive relations are:

$$\bar{T_3} = \bar{C_{33}^{E}}\,\bar{S_3} + \bar{C_{14}^{E}}\,S_4 - \bar{e_{33}}\,\bar{E_3} \quad (3.27)$$

$$\bar{D_3} = \bar{e_{33}}\,\bar{S_3} - \bar{e_{14}}\,S_4 - \bar{\varepsilon_{33}^{S}}\,\bar{E_3} \quad (3.28)$$

It is possible to eliminate the S_4 because we will be creating a frequency spurious mode, which S_4 will dominate the shear mode and it is out of frequency band.

So, we have:

$$\bar{T_3} = \bar{C_{33}^{E}}\,\bar{S_3} - \bar{e_{33}}\,\bar{E_3} \quad (3.29)$$

$$\bar{D_3} = \bar{e_{33}}\,\bar{S_3} - \bar{\varepsilon_{33}^{S}}\,\bar{E_3} \quad (3.30)$$

Then, we can derive the relation between $\bar{E}_3$, $\bar{D}_3$:

$$\bar{E_3} = {}^{1}\!/_{\bar{\varepsilon}_{33}} * \bar{D_3} - \left({}^{\bar{e}_{33}}\!/_{\bar{\varepsilon}_{33}}\right) * \bar{S_3} \quad (3.31)$$

The three principal effective material parameters:

$$\bar{C_{33}^{E}} = \nu\,[C_{33}^{E} - \frac{2\,\bar{\nu}\ (C_{13}^{E}-C_{12})^2}{\nu(C_{11}+C_{12})+\bar{\nu}(C_{11}^{E}+C_{12}^{E})}\ ] + \bar{\nu}\ C_{11} \quad (3.32)$$

$$\bar{e_{33}} = \nu\,[e_{33} - \frac{2\,\bar{\nu}\ e_{31}(C_{13}^{E}-C_{12})}{\nu(C_{11}+C_{12})+\bar{\nu}(C_{11}^{E}+C_{12}^{E})}\ ] \quad (3.33)$$

$$\bar{\varepsilon_{33}^{S}} = \nu\,[\varepsilon_{33}^{S} + \frac{2\,\bar{\nu}\ (e_{31})^2}{\nu(C_{11}+C_{12})+\bar{\nu}(C_{11}^{E}+C_{12}^{E})}\ ] + \bar{\nu}\ \varepsilon_{11} \quad (3.34)$$

where C_{12} and C_{11} are the stiffness constants and ε_{11} is the permittivity of the passive filler polymer.

For the transducer parameters, in terms of the properties of the component phases, $\bar{S}_3$ and $\bar{E}_3$ can be used as independent coordinates to evaluate the composite properties. As a result, it is easiest to analyse thin plate oscillations using $\bar{S}_3$, and $\bar{D}_3$ as independent variables. So, the equations are in h-form:

$$\bar{T_3} = \bar{c}_{33}^{D}\,\bar{S_3} - \bar{h}_{33}\,\bar{D_3} \tag{3.35}$$

$$\bar{E_3} = \bar{h}_{33}\bar{S_3} + \bar{\beta}_{33}^{S}\,\bar{D_3} \tag{3.36}$$

Where:

$$\bar{c}_{33}^{D} = \bar{c}_{33}^{E} + {(\bar{e}_{33})^2}\Big/{\bar{\varepsilon}_{33}^{S}} \tag{3.37}$$

$$\bar{h}_{33} = {\bar{e}_{33}}\Big/{\bar{\varepsilon}_{33}^{S}} \tag{3.38}$$

$$\bar{\beta}_{33}^{S} = {1}\Big/{\bar{\varepsilon}_{33}^{S}} \tag{3.39}$$

The composite density must be added to these relations, namely,

$$\bar{\rho} = \nu\,\rho^{c} + \bar{\nu}\,\rho^{P} \tag{3.40}$$

To calculate ultrasonic transducer quantities, these material parameters only need to be inserted into a thickness-mode oscillation analysis of a thin piezoelectric plate, namely, the electromechanical coupling constant:

$$\bar{k}_t = {\bar{h}_{33}}\Big/{(\bar{c}_{33}^{D}\,\bar{\beta}_{33}^{S})^{1/2}} = {\bar{e}_{33}}\Big/{(\bar{c}_{33}^{D}\,\bar{\varepsilon}_{33}^{S})^{1/2}} \tag{3.41}$$

the specific acoustic impedance,

$$\bar{Z} = (\,\bar{c}_{33}^{D}\,\bar{\rho})^{1/2} \tag{3.42}$$

and the longitudinal velocity,

$$\bar{v}_l = ({\bar{c}_{33}^{D}}\Big/{\bar{\rho}})^{1/2}\,. \tag{3.43}$$

When we compress the rod that is surrounded by air, it is free to move in lateral. While we use polymer as made composite, the movement in back and forth will be smaller than free (air) one.

As the volume fraction will be large, the lateral clamping of the rods by the polymer has a sensible effect on the piezoelectric and elastic behavior which the elastic stiffness increases and the piezoelectric strain constant reduces.

In analyzing the behavior of a free long rod operating in thickness mode, we assume that there is no stiffness in the filler material (free pillars), with $\boldsymbol{\nu}$=1. Consequently, we derive [1]:

$$\varepsilon_S = \varepsilon_{33} + \left(2\, e_{31}^2 \Big/ C_{11}^E + C_{12}^E\right) \quad (3.44)$$

$$e = e_{33} - \left(2\, e_{31} \cdot C_{13}^E \Big/ C_{11}^E + C_{12}^E\right) \quad (3.45)$$

$$C^E = C_{33}^E - \left(2\, {C_{13}^E}^2 \Big/ C_{11}^E + C_{12}^E\right) \quad (3.46)$$

$$C^D = C^E + \left(e^2 / \varepsilon_S\right) \quad (3.47)$$

$$k_{33} = \frac{e}{\sqrt{C^D \cdot \varepsilon_S}} \quad (3.48)$$

3.3.2 (1-3) Composite Piezoelectric (36°/Y-cut)

The composites studied in this thesis are of 1-3 connectivity and with the volume percentage of the ceramics and the polymer. composite has piezoceramic rods being continuous in one direction a polymer phase being continuous in three directions.

Modelling a piezocomposite material accurately requires effective material parameters when embedded in piezoceramics. The main variable here is the volume fraction of piezoceramics or the polymer and their sum is:

$$\mathrm{V_c} + \mathrm{V_p} = 1 \quad (3.49)$$

where $\mathrm{V_c}$ and $\mathrm{V_p}$ are the volume percentage of the ceramic material and the polymer material.

The constitutive relations for the component phases give the stress and electric displacement at every point (x, y, z) within the plate. The polymer phase is the same as previous section as an isotropic homogeneous medium that is piezoelectrically inactive, so for (x, y, z) within the polymer phase:

$$T_1 = c_{11} S_1 + c_{12} S_2 + c_{12} S_3 \quad (3.50)$$

$$T_2 = c_{12} S_1 + c_{11} S_2 + c_{12} S_3$$

$$T_3 = c_{12} S_1 + c_{12} S_2 + c_{11} S_3$$

$$T_4 = c_{44} S_4$$

$$T_5 = c_{44} S_5$$

$$T_6 = c_{44} S_6$$

$$D_1 = \varepsilon_{11} E_1$$

$$D_2 = \varepsilon_{11} E_2$$

$$D_3 = \varepsilon_{11} E_3$$

we assume that the ceramic rods as Lithium niobate material are perpendicular to the plate.

By using the equations for stress (T) and electrical displacement (D) in linear piezoelectric material as below:

$$T_{ij} = c_{ijkl} S_{kl} - e_{kij} E_k \quad (3.51)$$

And using the Voigt notation, we can show the stress and electrical displacement as below:

$$T_1 = c^E{}_{11} S_1 + c^E{}_{12} S_2 + c^E{}_{13} S_3 + 2 c^E{}_{14} S_4 - e_{21} E_2 - e_{31} E_3 \quad (3.52)$$

$$T_2 = c^E{}_{12} S_1 + c^E{}_{22} S_2 + c^E{}_{23} S_3 + 2 c^E{}_{24} S_4 - e_{22} E_2 - e_{32} E_3$$

$$T_3 = c^E{}_{13} S_1 + c^E{}_{23} S_2 + c^E{}_{33} S_3 + 2 c^E{}_{34} S_4 - e_{23} E_2 - e_{33} E_3$$

$$T_4 = c^E{}_{14} S_1 + c^E{}_{24} S_2 + c^E{}_{34} S_3 + 2c^E{}_{44} S_4 - e_{24} E_2 - e_{34} E_3$$

$$T_5 = 2 c^E{}_{55} S_5 + 2 c^E{}_{56} S_6 - e_{15} E_1$$

$$T_6 = 2 c^E{}_{56} S_5 + 2 c^E{}_{66} S_6 - e_{16} E_1$$

$$D_1 = 2 e_{15} S_5 + 2 e_{16} S_6 + \varepsilon^S_{11} E_1$$

$$D_2 = e_{21} S_1 + e_{22} S_2 + e_{23} S_3 + 2e_{24} S_4 + \varepsilon^S_{22} E_2 + \varepsilon^S_{23} E_3$$

$$D_3 = e_{31} S_1 + e_{32} S_2 + e_{33} S_3 + 2e_{34} S_4 + \varepsilon^S_{32} E_2 + \varepsilon^S_{33} E_3$$

We can assume that Six simplifying approximations are presented to extract essential physics for ceramic phase as 36˚/Y oriented Lithium niobate.

The Lithium niobate is the anisotropic crystal that varies with respect to different cuts. so, for the 36˚/ Y-cut because of highly asymmetric properties, we cannot assume the strains in x and y directions are the same.

$$S_1 \neq S_2 \quad (3.53)$$

First, Throughout the individual phases, electric field are assumed to be independent of X and Y.

$$E_1 = E_2 \quad (3.54)$$

Second, as usual, we simplify the analysis of thickness mode oscillations in an electroded plate of large, thin dimensions. (symmetry in the x-y plane, $E_1 = E_2 = 0$, etc.)

The constitutive relations for the individual phases have a compact form,
namely, within the polymer (^{P}), phase,

$$T_1^P = c_{11} S_1^P + c_{12} S_2^P + c_{12} S_3^P \quad (3.55)$$

$$T_3^P = c_{12}S_1^P + c_{12}S_2^P + c_{11}S_3^P$$

$$D_3^P = \varepsilon_{11} E_3^P$$

Within the ceramic phase: (c phase)

$$T_1^C = c^E{}_{11}S_1^C + c^E{}_{12}S_2^C + c^E{}_{13}S_3^C + 2c^E{}_{14}S_4^C - e_{31} E_3 \quad (3.56)$$

$$T_2^C = c^E{}_{12}S_1^C + c^E{}_{22}S_2^C + c^E{}_{23}S_3^C + 2c^E{}_{24}S_4^C - e_{32} E_3$$

$$T_3^C = c^E{}_{13}S_1^C + c^E{}_{23}S_2^C + c^E{}_{33}S_3^C + 2c^E{}_{34}S_4^C - e_{33} E_3$$

$$T_4^C = c^E{}_{14}S_1^C + c^E{}_{24}S_2^C + c^E{}_{34}S_3^C + 2c^E{}_{44} S_4^C - e_{34} E_3$$

$$T_5^C = 2c^E{}_{55}S_5^C + 2c^E{}_{56}S_6^C$$

$$T_6^C = 2c^E{}_{56}S_5^C + 2c^E{}_{66}S_6^C$$

$$D_1^C = 2e_{15}S_5^C + 2e_{16}S_6^C$$

$$D_2^C = e_{21}S_1^C + e_{22}S_2^C + e_{23}S_3^C + 2e_{24}S_4^C + \varepsilon_{23}^S E_3$$

$$D_3^C = e_{31}S_1^C + e_{32}S_2^C + e_{33}S_3^C + 2e_{34}S_4^C + \varepsilon_{33}^S E_3$$

Based on our third approximation, ceramics and polymers oscillate together uniformly. Thus, in both phases, the vertical strains are the same,

$$S_3^P(Z) = S_3^C(Z) = \bar{S}_3(Z) \quad (3.57)$$

Fourth, we take the electrice fields to be the same in both phases, namely,

$$E_3^P(Z) = E_3^C(Z) = \bar{E}_3(Z) \quad (3.58)$$

Fifth approximation is, the S_4^C can be eliminated because we will create a frequency spurious mode, in which S_4^C will dominate the shear mode, which is out of frequency range.
Now that the constitutive relations can be read more easily, for polymer phase:

$$T_1^P = c_{11}S_1^P + c_{12}S_2^P + c_{12}\bar{S}_3 \quad (3.59)$$

$$T_3^P = c_{12}(S_1^P + S_2^P) + c_{11}\bar{S}_3$$

$$D_3^P = \varepsilon_{11} \bar{E}_3$$

Within the ceramic phase: (c phase)

$$T_1^C = c^E{}_{11}S_1^C + c^E{}_{12}S_2^C + c^E{}_{13}\bar{S}_3 - e_{31} \bar{E}_3 \quad (3.60)$$

$$T_2^C = c^E{}_{12} S_1^C + c^E{}_{22} S_2^C + c^E{}_{23} \bar{S}_3 - e_{32} \bar{E}_3$$

$$T_3^C = c^E{}_{13} S_1^C + c^E{}_{23} S_2^C + c^E{}_{33} \bar{S}_3 - e_{33} \bar{E}_3$$

$$T_4^C = c^E{}_{14} S_1^C + c^E{}_{24} S_2^C + c^E{}_{34} \bar{S}_3 - e_{34} \bar{E}_3$$

$$T_5^C = 2c^E{}_{55} S_5^C + 2c^E{}_{56} S_6^C$$

$$T_6^C = 2c^E{}_{56} S_5^C + 2c^E{}_{66} S_6^C$$

$$D_1^C = 2e_{15} S_5^C + 2e_{16} S_6^C$$

$$D_2^C = e_{21} S_1^C + e_{22} S_2^C + e_{23} \bar{S}_3 + \varepsilon_{23}^S \bar{E}_3$$

$$D_3^C = e_{31} S_1^C + e_{32} S_2^C + e_{33} \bar{S}_3 + \varepsilon_{33}^S \bar{E}_3$$

Our sixth approximation addresses the lateral interaction between the phases for both S_1 and S_2. It is assumed that both phases have equal lateral stresses, and that lateral strains of the ceramic and polymer compensate for each other so that lateral clamping occurs [1]:

$$T_1^P(Z) = T_1^C(Z) = \bar{T_1}(Z)$$

$$\bar{S_1}(Z) = \bar{\nu} S_1^P(Z) + \nu S_1^C(Z) = 0 \quad (3.61)$$

$$T_2^P(Z) = T_2^C(Z) = \bar{T_2}(Z)$$

$$\bar{S_2}(Z) = \bar{\nu} S_2^P(Z) + \nu S_2^C(Z) = 0 \quad (3.62)$$

where ν is the volume fraction of piezoceramic in the composite and $\bar{\nu} = (1 - \nu)$ is the volume fraction of polymer.

Based on this, we expect the ceramic rods are clamped lateral to the polymer on an average basis. The lateral strains can be described as follows using vertical strains and electric fields that derive from Eq (3.61) that we assumed some alphabetic terms to simplify these complicated equations:

$$S^C{}_1 = -\bar{\nu}[AS_2^C + B\bar{S}_3 - C\bar{E}_3] \quad (3.63)$$

$$S^P{}_1 = \nu [AS_2^C + B\bar{S}_3 - C\bar{E}_3]$$

Where:

$$A = \frac{C_{12}^E + \frac{\nu}{\bar{\nu}} C_{12}}{\bar{\nu} C_{11}^E + \nu C_{11}} \quad (3.64)$$

$$B = \frac{C_{13}^{E} - C_{12}}{\bar{\nu}C_{11}^{E}+\nu C_{11}}$$

$$C = \frac{e_{31}}{\bar{\nu}C_{11}^{E}+\nu C_{11}}$$

In similarly, by solving the Eq (3.62), we can derive the lateral strain for the second direction by assuming that it is presented by some terms for simplifying.

$$S^{C}_{2} = -\bar{\nu}[DS_1^C + E\bar{S}_3 - F\bar{E}_3\,] \tag{3.65}$$

$$S^{P}_{2} = \nu\,[DS_1^C + E\bar{S}_3 - F\bar{E}_3\,]$$

Where:

$$D = \frac{C_{12}^{E} + \frac{\nu}{\bar{\nu}}\,C_{12}}{\bar{\nu}C_{22}^{E}+\nu C_{11}} \tag{3.66}$$

$$E = \frac{C_{23}^{E} - C_{12}}{\bar{\nu}C_{22}^{E}+\nu C_{11}}$$

$$F = \frac{e_{32}}{\bar{\nu}C_{22}^{E}+\nu C_{11}}$$

By substituting the S_2^C in the equation of S_1^C, we can write the lateral strain in relation to vertical strain and electric field.

$$S_1^C = -\bar{\nu}\,\frac{(B-A\bar{\nu}E)\bar{S}_3+(A\bar{\nu}F-C)\bar{E}_3}{1-A\bar{\nu}^2D} \tag{3.67}$$

$$S_1^P = \nu\,\frac{(B-A\bar{\nu}E)\bar{S}_3+(A\bar{\nu}F-C)\bar{E}_3}{1-A\bar{\nu}^2D}$$

By inserting the equation of S_1^C Eq (3.67) in S_2^C Eq (3.65), we can write this lateral strain dependent on vertical strain and electric field.

$$S_2^C = -\bar{\nu}\,\frac{(E-\bar{\nu}BD)\bar{S}_3+(\bar{\nu}CD-F)\bar{E}_3}{1-A\bar{\nu}^2D} \tag{3.68}$$

$$S_2^P = \nu\,\frac{(E-\bar{\nu}BD)\bar{S}_3+(\bar{\nu}CD-F)\bar{E}_3}{1-A\bar{\nu}^2D}$$

And for the coordinates that remain:

$$T^{P}_{3} = [C_{11}+\frac{\nu\;C_{12}(B-A\bar{\nu}E+E-\bar{\nu}BD)}{1-A\bar{\nu}^2D}\,]\,\bar{S}_3- \tag{3.69}$$

$$\left[\frac{\nu\ C_{12}(C-A\bar{\nu}F+F-\bar{\nu}CD)}{1-A\bar{\nu}^{2}D}\right]\bar{E}_3$$

$$D_3^P = \varepsilon_{11}\bar{E}_3 \tag{3.70}$$

$$T^C{}_3 = \left[C_{33}^E\text{-}\bar{\nu}\ \frac{C_{13}^E(B-A\bar{\nu}E)+C_{23}^E(E-\bar{\nu}BD)}{1-A\bar{\nu}^{2}D}\right]\bar{S}_3 - \tag{3.71}$$

$$\left[e_{33}-\bar{\nu}\frac{C_{13}^E\,(C-A\bar{\nu}F)+C_{23}^E(F-\bar{\nu}CD)}{1-A\bar{\nu}^{2}D}\right]\bar{E}_3$$

$$D^C{}_3 = \left[e_{33}-\bar{\nu}\frac{e_{31}\ (B-A\bar{\nu}E)+e_{32}\ (E-\bar{\nu}BD)}{1-A\bar{\nu}^{2}D}\right]\bar{S}_3 + \tag{3.72}$$

$$\left[\varepsilon_{33}^S-\ \bar{\nu}\frac{e_{31}\ (A\bar{\nu}F-C)+e_{32}\ (\bar{\nu}CD-F)}{1-A\bar{\nu}^{2}D}\right]\bar{E}_3$$

By averaging over the contributions of the constituent phases, we can determine the total effective stress and electric displacement, namely:

$$\bar{T_3}(Z) = \nu T_3^C(Z) + \bar{\nu}T_3^P(Z) \tag{3.73}$$

$$\bar{D_3}(Z) = \nu D_3^C(Z) + \bar{\nu}D_3^P(Z)$$

So, the final constitutive relations are:

$$\bar{T_3} = \bar{C}_{33}^E\bar{S_3} - \bar{e}_{33}\bar{E_3} \tag{3.74}$$

$$\bar{D_3} = \bar{e}_{33}\bar{S_3} + \bar{\varepsilon}_{33}^S\bar{E_3}$$

Then, we can derive the relation between $\bar{E}_3$, $\bar{D}_3$:

$$\bar{E_3} = {}^{1}\!/_{\bar{\varepsilon}_{33}} * \bar{D_3} - \left({}^{\bar{e}_{33}}\!/_{\bar{\varepsilon}_{33}}\right) * \bar{S_3} \tag{3.75}$$

The three principal effective material parameters:

$$\bar{C}_{33}^E = \nu\left[C_{33}^E\text{-}\bar{\nu}\ \frac{C_{13}^E(B-A\bar{\nu}E)+C_{23}^E(E-\bar{\nu}BD)-C_{12}(B-A\bar{\nu}E+E-\bar{\nu}BD)}{1-A\bar{\nu}^{2}D}\right]+\bar{\nu}\ C_{11} \tag{3.76}$$

$$\bar{e}_{33} = \nu\left[e_{33}\text{-}\bar{\nu}\ \frac{C_{13}^E\,(C-A\bar{\nu}F)+C_{23}^E(F-\bar{\nu}CD)-C_{12}(C-A\bar{\nu}F+F-\bar{\nu}CD)}{1-A\bar{\nu}^{2}D}\right]$$

$$\bar{\varepsilon}_{33}^S = \nu\left[\varepsilon_{33}^S\text{-}\bar{\nu}\ \frac{e_{31}\ (A\bar{\nu}F-C)+e_{32}\ (\bar{\nu}CD-F)}{1-A\bar{\nu}^{2}D}\right]+\bar{\nu}\ \varepsilon_{11}$$

where C_{12} and C_{11} are the stiffness constants and ε_{11} is the permittivity of the passive filler polymer.

For the transducer parameters, in terms of the properties of the component phases, $\bar{S}_3$ and $\bar{E}_3$ can be used as independent coordinates to evaluate the composite properties. As a result, it is easiest to analyse thin plate oscillations using $\bar{S}_3$, and $\bar{D}_3$ as independent variables. So, the equations are in h-form:

$$\bar{T_3} = \bar{c}_{33}^{D}\,\bar{S_3} - \bar{h}_{33}\,\bar{D_3} \tag{3.77}$$

$$\bar{E_3} = \bar{h}_{33}\bar{S_3} + \bar{\beta}_{33}^{S}\,\bar{D_3}$$

Where:

$$\bar{c}_{33}^{D} = \bar{c}_{33}^{E} + {(\bar{e}_{33})^2}\Big/{\bar{\varepsilon}_{33}^{S}} \tag{3.78}$$

$$\bar{h}_{33} = {\bar{e}_{33}}\Big/{\bar{\varepsilon}_{33}^{S}} \tag{3.79}$$

$$\bar{\beta}_{33}^{S} = {1}\Big/{\bar{\varepsilon}_{33}^{S}} \tag{3.80}$$

The composite density must be added to these relations, namely,

$$\bar{\rho} = \nu\,\rho^{c} + \bar{\nu}\,\rho^{P} \tag{3.81}$$

To calculate ultrasonic transducer quantities, these material parameters only need to be inserted into a thickness-mode oscillation analysis of a thin piezoelectric plate, namely, the electromechanical coupling constant:

$$k_t = {\bar{h}_{33}}\Big/{(\bar{c}_{33}^{D}\,\bar{\beta}_{33}^{S})^{1/2}} = {\bar{e}_{33}}\Big/{(\bar{c}_{33}^{D}\,\bar{\varepsilon}_{33}^{S})^{1/2}} \tag{3.82}$$

the specific acoustic impedance,

$$\bar{Z} = (\,\bar{c}_{33}^{D}\,\bar{\rho})^{1/2} \tag{3.83}$$

and the longitudinal velocity,

$$\bar{v}_l = ({\bar{c}_{33}^{D}}\Big/{\bar{\rho}})^{1/2}\,. \tag{3.84}$$

Compressing an air-surrounded rod allows it to move in lateral directions. In composites made from polymer, the back-and-forth movement will be smaller than in free air.

Due to the large volume fraction, the lateral clamping of the rods by the polymer has a significant impact on the piezoelectric and elastic behavior, resulting in an increase in elastic stiffness and a decrease in piezoelectric strain constant.

To determine the behavior of a free long rod operating in thickness mode, it is assumed that there is no stiffness in the filler material (free pillars) and that *v =1*.

$$T_1^{C} = 0 \qquad , T_2^{C} = 0 \tag{3.85}$$

Thus, we obtain the lateral strains by taking some alphabetic terms to simplify the equations:

$$S_1^C = \frac{A\,\tilde{S_3} + B\,\tilde{E_3}}{C} \tag{3.86}$$

$$S_2^C = -\frac{D\,\tilde{S_3} + F\,\tilde{E_3}}{C}$$

Where:

$$A = \frac{-c_{12}^E\,c_{23}^E + c_{13}^E\,c_{22}^E}{c_{22}^E} \tag{3.87}$$

$$B = \frac{c_{12}^E\,e_{32} - c_{22}^E\,e_{31}}{c_{22}^E}$$

$$C = \left(1 - \frac{(c_{12}^E)^2}{c_{22}^E\,c_{11}^E}\right).c_{11}^E$$

$$D = \frac{-c_{12}^E\,A + c_{23}^E\,C}{c_{22}^E}$$

$$F = \frac{-c_{12}^E\,B - e_{32}\,C}{c_{22}^E}$$

By removing the lateral strains, the vertical strain and electrical displacement can be derived as:

$$T_3^C = (c_{33}^E - \frac{c_{13}^E\,A + c_{23}^E\,D}{C})\,\tilde{S_3} - \tag{3.88}$$

$$(e_{33} + \frac{c_{13}^E\,B + c_{23}^E\,F}{C})\,\tilde{S_3}$$

$$D_3^C = (e_{33} - \frac{e_{31}\,A + e_{32}\,D}{C})\,\tilde{S_3} + \tag{3.89}$$

$$(\varepsilon_{33}^S - \frac{e_{31}\,B + e_{32}\,F}{C})\,\tilde{S_3}$$

So, the constitutive equations will be shown as:

$$\varepsilon_S = \varepsilon_{33}^S - \frac{e_{31}\,B + e_{32}\,F}{C} \tag{3. 90}$$

$$e = e_{33} + \frac{c_{13}^E\,B + c_{23}^E\,F}{C} \tag{3. 91}$$

$$C^E = C_{33}^E - \frac{c_{13}^E\,A + c_{23}^E\,D}{C} \tag{3. 92}$$

$$C^D = C^E + (e^2/\varepsilon_S) \tag{3. 93}$$

$$k_{33} = \frac{e}{\sqrt{C^D\,.\varepsilon_S}} \tag{3. 94}$$

3.3.3 (2-2) Composite Piezoelectric(Z-cut)

A composite of ceramics and polymer is studied in this thesis with a 2-2 connectivity.

The active and passive phases of 2-2 composite are continuous in two directions and stacked on top of each other.

A typical 2-2 composite is shown in figure 2. It is a layered structure of alternating polymer and piezoceramic constituents.

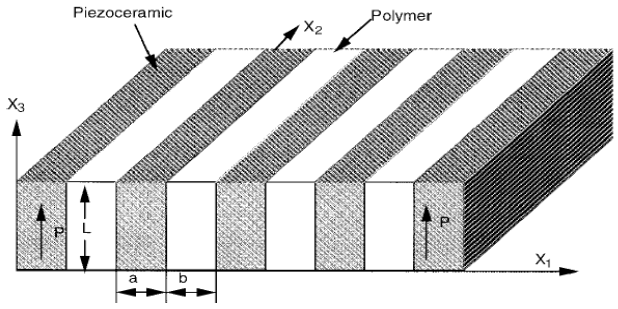

Figure 3.2 Configuration of 2-2 composite. (directly from [2])

The effective material parameters can be derived from a 1-3 composite procedure by assuming the strain is clamped in one direction.

$$S_2 = 0 \tag{3. 95}$$

So, the effective material parameters for this composite can be shown as below:

1. effective stiffness at constant electric field c_{33}^{E*}:

$$c_{33}^{E*} = V_c \left(c_{33}^{E} - \frac{V_P (c_{12} - c_{13}^{E})^2}{V_P\, c_{11}^{E} + V_c\, c_{11}} \right) + V_P\, c_{11} \tag{3. 96}$$

2. effective dielectric permittivity ε_{33}^{S*}:

$$\varepsilon_{33}^{S*} = V_c \left(\varepsilon_{33}^{S} + \frac{e_{31}^2\, V_P}{V_P\, c_{11}^{E} + V_c\, c_{11}} \right) + V_P\, \varepsilon_{11} \tag{3. 97}$$

3. effective piezoelectric stress coefficient e_{33}^{*} :

$$e_{33}^{*} = V_c \left(e_{33} - \frac{V_P\, e_{31}\, (c_{13}^{E} - c_{12})}{V_P\, c_{11}^{E} + V_c\, c_{11}} \right) \tag{3. 98}$$

where C_{11} and C_{12} are the stiffness constant and ε_{11} is the permittivity of the passive filler polymer.

The parameters of c_{11}^{E}, c_{13}^{E} and c_{33}^{E} are the stiffness constants of piezoelectric material, e_{31} and e_{33} are the piezoelectric stress coefficient and ε_{33} is the dielectric permittivity of the piezoelectric material [2].

The following are other effective parameters that can be calculated:

1. stiffness at constant electric displacement field:

$$c_{33}^{D*} = c_{33}^{E*} + \frac{e_{33}^{*\,2}}{\varepsilon_{33}^{S*}} \tag{3. 99}$$

2. effective density:

$$\rho^* = \rho_c V_c + \rho_P V_P \quad (3.100)$$

3. effective longitudinal speed of sound along the thickness direction:

$$c_L^* = \sqrt{\frac{c_{33}^{D*}}{\rho^*}} \quad (3.101)$$

4. effective acoustic impedance:

$$Z^* = \sqrt{\rho^* c_{33}^{D*}} = \rho^* c_L^* \quad (3.102)$$

5. effective piezoelectric stiffness constant:

$$h_{33}^* = \frac{e_{33}^*}{\varepsilon_{33}^{S*}} \quad (3.103)$$

6. The thickness mode electromechanical coupling coefficient for the plate:

$$k_t^* = \frac{e_{33}^*}{\sqrt{c_{33}^{D*}\,\varepsilon_{33}^{S*}}} = h_{33}^* \sqrt{\frac{\varepsilon_{33}^{S*}}{c_{33}^{D*}}} \quad (3.104)$$

3.3.4 (2-2) Composite Piezoelectric (36°/Y-cut):

A 2-2 composite consists of polymers (softer materials) and ceramics together as a continuous phase, making it softer than a 1-3 composite. Despite the ease of fabrication, this composite arrangement has a lower coupling coefficient than composites 1-3.

For the 36°/ Y-cut, within the polymer (^{P}), phase,

$$T_1^P = c_{11}S_1^P + c_{12}S_2^P + c_{12}S_3^P \quad (3.105)$$
$$T_2^P = c_{12}S_1^P + c_{11}S_2^P + c_{12}S_3^P$$
$$T_3^P = c_{12}S_1^P + c_{12}S_2^P + c_{11}S_3^P$$
$$D_3^P = \varepsilon_{11} E_3^P$$

Within the ceramic phase: (c phase)

$$T_1^C = c^E{}_{11}S_1^C + c^E{}_{12}S_2^C + c^E{}_{13}S_3^C + 2c^E{}_{14}S_4^C - e_{31} E_3 \quad (3.106)$$
$$T_2^C = c^E{}_{12}S_1^C + c^E{}_{22}S_2^C + c^E{}_{23}S_3^C + 2c^E{}_{24}S_4^C - e_{32} E_3$$
$$T_3^C = c^E{}_{13}S_1^C + c^E{}_{23}S_2^C + c^E{}_{33}S_3^C + 2c^E{}_{34}S_4^C - e_{33} E_3$$
$$T_4^C = c^E{}_{14}S_1^C + c^E{}_{24}S_2^C + c^E{}_{34}S_3^C + 2c^E{}_{44}S_4^C - e_{34} E_3$$
$$T_5^C = 2c^E{}_{55}S_5^C + 2c^E{}_{56}S_6^C$$
$$T_6^C = 2c^E{}_{56}S_5^C + 2c^E{}_{66}S_6^C$$
$$D_1^C = 2e_{15}S_5^C + 2e_{16}S_6^C$$
$$D_2^C = e_{21}S_1^C + e_{22}S_2^C + e_{23}S_3^C + 2e_{24}S_4^C + \varepsilon_{23}^S E_3$$
$$D_3^C = e_{31}S_1^C + e_{32}S_2^C + e_{33}S_3^C + 2e_{34}S_4^C + \varepsilon_{33}^S E_3$$

First, we assume that the terms that consists of shear stress are equal zero.

$$S_4^C = 0 \tag{3. 107}$$

Secondly, for this type of piezocomposite, we can consider the strain are continuous in 2 direction and is clamped in one direction for both polymer and ceramic materials. The point for this type of composite is that which direction must be clamped, and which directions are continuous. As a result, we need to consider two ways for this assumption.

1) The first way is when we assume that strain in 2nd direction is clamped: $S_2 = 0$

So, we can simplify the equations for both stress and displacement.

$$S_2^C = S_2^P = 0 \tag{3. 108}$$

For polymer phase:

$$T_1^P = c_{11}S_1^P + c_{12}S_3^P \tag{3. 109}$$

$$T_2^P = c_{12}S_1^P + c_{12}S_3^P$$

$$T_3^P = c_{12}S_1^P + c_{11}S_3^P$$

$$D_3^P = \varepsilon_{11} E_3^P$$

For ceramic phase:

$$T_1^C = c^E{}_{11}S_1^C + c^E{}_{13}S_3^C - e_{31} E_3 \tag{3. 110}$$

$$T_2^C = c^E{}_{12}S_1^C + c^E{}_{23}S_3^C - e_{32} E_3$$

$$T_3^C = c^E{}_{13}S_1^C + c^E{}_{33}S_3^C - e_{33} E_3$$

$$T_4^C = c^E{}_{14}S_1^C + c^E{}_{34}S_3^C - e_{34} E_3$$

$$T_5^C = 2c^E{}_{55}S_5^C + 2c^E{}_{56}S_6^C$$

$$T_6^C = 2c^E{}_{56}S_5^C + 2c^E{}_{66}S_6^C$$

$$D_1^C = 2e_{15}S_5^C + 2e_{16}S_6^C$$

$$D_2^C = e_{21}S_1^C + e_{23}S_3^C + \varepsilon_{23}^S E_3$$

$$D_3^C = e_{31}S_1^C + e_{33}S_3^C + \varepsilon_{33}^S E_3$$

Third assumption is that ceramics and polymers oscillate together uniformly. Thus, in both phases, the vertical strains are the same,

$$S_3^P(Z) = S_3^C(Z) = \bar{S}_3(Z) \tag{3. 111}$$

Fourth, we take the electrice fields to be the same in both phases, namely,

$$E_3^P(Z) = E_3^C(Z) = \bar{E_3}(Z) \quad (3.112)$$

So, for polymer phase we have:

$$T_1^P = c_{11}S_1^P + c_{12}\bar{S_3} \quad (3.113)$$

$$T_2^P = c_{12}S_1^P + c_{12}\bar{S_3}$$

$$T_3^P = c_{12}S_1^P + c_{11}\bar{S_3}$$

$$D_3^P = \varepsilon_{11}\bar{E_3}$$

For ceramic phase:

$$T_1^C = c^E{}_{11}S_1^C + c^E{}_{13}\bar{S_3} - e_{31}\bar{E_3} \quad (3.114)$$

$$T_2^C = c^E{}_{12}S_1^C + c^E{}_{23}\bar{S_3} - e_{32}\bar{E_3}$$

$$T_3^C = c^E{}_{13}S_1^C + c^E{}_{33}\bar{S_3} - e_{33}\bar{E_3}$$

$$T_4^C = c^E{}_{14}S_1^C + c^E{}_{34}\bar{S_3} - e_{34}\bar{E_3}$$

$$T_5^C = 2c^E{}_{55}S_5^C + 2c^E{}_{56}S_6^C$$

$$T_6^C = 2c^E{}_{56}S_5^C + 2c^E{}_{66}S_6^C$$

$$D_1^C = 2e_{15}S_5^C + 2e_{16}S_6^C$$

$$D_2^C = e_{21}S_1^C + e_{23}\bar{S_3} + \varepsilon_{23}^S\bar{E_3}$$

$$D_3^C = e_{31}S_1^C + e_{33}\bar{S_3} + \varepsilon_{33}^S\bar{E_3}$$

Our fifth approximation addresses the lateral interaction between the phases. It is assumed that both phases have equal lateral stresses, and that lateral strains of the ceramic and polymer compensate for each other so that lateral clamping occurs:

$$T_1^P(Z) = T_1^C(Z) = \bar{T_1}(Z) \quad (3.115)$$

$$\bar{S_1}(Z) = \bar{\nu}\,S_1^P(Z) + \nu\,S_1^C(Z) = 0$$

where ν is the volume fraction of piezoceramic in the composite

and $\bar{\nu} = (1-\nu)$ is the volume fraction of polymer.

By using these assumptions refer to Eq (3. 115), we can write the lateral strain depends on vertical strain and electric field as shown below:

$$S_1^C = -\bar{\nu}\frac{(C_{13}^E - C_{12})\bar{S_3} - e_{31}\bar{E_3}}{\bar{\nu}C_{11}^E + \nu C_{11}} \quad (3.116)$$

$S_2^P = \nu \frac{(C_{13}^E - C_{12})\bar{S}_3 - e_{31}\bar{E}_3}{\bar{\nu}C_{11}^E + \nu C_{11}}$

Then, the constitutive relations are simplified by removing the lateral strains and we obtain for the eliminated coordinate:

$$\bar{T_1}(Z) = \bar{C_{13}^E}\,\bar{S_3} - \bar{e_{31}}\bar{E_3} \quad (3.117)$$

Where:

$\bar{C}^E_{13} = C_{13}^E - \bar{\nu}\frac{C_{12}(C_{13}^E - C_{12})}{\bar{\nu}C_{11}^E + \nu C_{11}}$ (3.118)

$\bar{e}_{31} = e_{31} - \bar{\nu}\frac{e_{31}(C_{12})}{\bar{\nu}C_{11}^E + \nu C_{11}}$ (3.119)

And for the coordinates that remain:

$T^P_3 = [C_{11} + \frac{\nu\ C_{12}(C_{13}^E - C_{12})}{\bar{\nu}C_{11}^E + \nu C_{11}}]\,\bar{S}_3 -$ (3.120)

$[\frac{\nu\ e_{31}\,C_{12}}{\bar{\nu}C_{11}^E + \nu C_{11}}]\,\bar{E}_3$

$D_3^P = \varepsilon_{11}\bar{E_3}$

$T^C_3 = [C^E_{33} - \frac{\bar{\nu}\,C_{13}^E(C_{13}^E - C_{12})}{\bar{\nu}C_{11}^E + \nu C_{11}}]\,\bar{S}_3 -$

$[e_{33} - \frac{\bar{\nu}\,e_{31}\,C_{13}^E}{\bar{\nu}C_{11}^E + \nu C_{11}}]\,\bar{E}_3$

$D^C_3 = [e_{33} - \frac{\bar{\nu}\,e_{31}(C_{13}^E - C_{12})}{\bar{\nu}C_{11}^E + \nu C_{11}}]\,\bar{S}_3 +$

$[\varepsilon_{33}^S + \frac{\bar{\nu}(e_{31})^2}{\bar{\nu}C_{11}^E + \nu C_{11}}]\,\bar{E}_3$

Since the lateral periodicity is sufficiently fine, we can calculate the effective total stress and electric displacement by averaging over the contributions of the constituent phases, namely:

$$\bar{T_3}(Z) = \nu T_3^C(Z) + \bar{\nu}T_3^P(Z) \quad (3.121)$$

$$\bar{D_3}(Z) = \nu D_3^C(Z) + \bar{\nu}D_3^P(Z)$$

So, the final constitutive relations are:

$$\bar{T_3} = \bar{C_{33}^E}\,\bar{S_3} - \bar{e_{33}}\,\bar{E_3} \quad (3.122)$$

$$\bar{D_3} = \bar{e_{33}}\,\bar{S_3} + \bar{\varepsilon_{33}^S}\,\bar{E_3}$$

The three principal effective material parameters:

effective stiffness at constant electric field c_{33}^{E*}:

$$c_{33}^{E*} = \nu \left(c_{33}^{E} - \frac{\bar{\nu} \left(c_{13}^{E} - c_{12} \right)^2}{\bar{\nu} C_{11}^{E} + \nu C_{11}} \right) + \bar{\nu}\, c_{11} \quad (3.123)$$

effective dielectric permittivity ε_{33}^{S*} :

$$\varepsilon_{33}^{S*} = \nu \left(\varepsilon_{33}^{S} + \frac{\bar{\nu} \left(e_{31} \right)^2}{\bar{\nu} C_{11}^{E} + \nu C_{11}} \right) + \bar{\nu}\, \varepsilon_{11} \quad (3.124)$$

effective piezoelectric stress coefficient e_{33}^{*} :

$$e_{33}^{*} = \nu \left(e_{33} - \frac{\bar{\nu}\, e_{31} \left(c_{13}^{E} - c_{12} \right)}{\bar{\nu} C_{11}^{E} + \nu C_{11}} \right) \quad (3.125)$$

where C_{11} and C_{12} are the stiffness constant and ε_{11} is the permittivity of the passive filler polymer.

The calculation for other effective parameters like coupling coefficient and acoustic impedance are like previous section for Z-cut (3.6.3), so to prevent the duplication, we have ignored to mention again in this part.

2) The second way is when we assume that the first direction is clamped. So, we should consider: $S_1 = 0$

So, we can simplify the equations for both stress and displacement.

$$S_1^C = S_1^P = 0 \quad (3.126)$$

For polymer phase:

$$T_1^P = c_{12} S_2^P + c_{12} S_3^P \quad (3.127)$$

$$T_2^P = c_{11} S_2^P + c_{12} S_3^P$$

$$T_3^P = c_{12} S_2^P + c_{11} S_3^P$$

$$D_3^P = \varepsilon_{11} E_3^P$$

For ceramic phase:

$$T_1^C = c^E{}_{12} S_2^C + c^E{}_{13} S_3^C - e_{31} E_3 \quad (3.128)$$

$$T_2^C = c^E{}_{22} S_2^C + c^E{}_{23} S_3^C - e_{32} E_3$$

$$T_3^C = c^E{}_{23} S_2^C + c^E{}_{33} S_3^C - e_{33} E_3$$

$$T_4^C = c^E{}_{24} S_2^C + c^E{}_{34} S_3^C - e_{34} E_3$$

$$T_5^C = 2c^E{}_{55} S_5^C + 2c^E{}_{56} S_6^C$$

$$T_6^C = 2c^E{}_{56} S_5^C + 2c^E{}_{66} S_6^C$$

$$D_1^C = 2e_{15} S_5^C + 2e_{16} S_6^C$$

$$D_2^C = e_{22} S_2^C + e_{23} S_3^C + \varepsilon_{23}^S E_3$$

$$D_3^C = e_{32}S_2^C + e_{33}S_3^C + \varepsilon_{33}^S E_3$$

Third assumption is that ceramics and polymers oscillate together uniformly. As a result, the vertical strains are the same in both phases,

$$S_3^P(Z) = S_3^C(Z) = \bar{S_3}(Z) \quad (3.129)$$

Fourth, we take the electrice fields to be the same in both phases, namely,

$$E_3^P(Z) = E_3^C(Z) = \bar{E_3}(Z) \quad (3.130)$$

So, for polymer phase we have:

$$T_1^P = c_{12}S_2^P + c_{12}\bar{S_3} \quad (3.131)$$

$$T_2^P = c_{11}S_2^P + c_{12}\bar{S_3}$$

$$T_3^P = c_{12}S_2^P + c_{11}\bar{S_3}$$

$$D_3^P = \varepsilon_{11}\bar{E_3}$$

For ceramic phase:

$$T_1^C = c^E{}_{12}S_2^C + c^E{}_{13}\bar{S_3} - e_{31}\bar{E_3} \quad (3.132)$$

$$T_2^C = c^E{}_{22}S_2^C + c^E{}_{23}\bar{S_3} - e_{32}\bar{E_3}$$

$$T_3^C = c^E{}_{23}S_2^C + c^E{}_{33}\bar{S_3} - e_{33}\bar{E_3}$$

$$T_4^C = c^E{}_{24}S_2^C + c^E{}_{34}\bar{S_3} - e_{34}\bar{E_3}$$

$$T_5^C = 2c^E{}_{55}S_5^C + 2c^E{}_{56}S_6^C$$

$$T_6^C = 2c^E{}_{56}S_5^C + 2c^E{}_{66}S_6^C$$

$$D_1^C = 2e_{15}S_5^C + 2e_{16}S_6^C$$

$$D_2^C = e_{22}S_2^C + e_{23}\bar{S_3} + \varepsilon_{23}^S\bar{E_3}$$

$$D_3^C = e_{32}S_2^C + e_{33}\bar{S_3} + \varepsilon_{33}^S\bar{E_3}$$

Our fifth approximation addresses the lateral interaction between the phases. It is assumed that both phases have equal lateral stresses, and that lateral strains of the ceramic and polymer compensate for each other so that lateral clamping occurs:

$$T_2^P(Z) = T_2^C(Z) = \bar{T_2}(Z) \quad (3.133)$$

$$\bar{S_2}(Z) = \bar{\nu}\, S_2^P(Z) + \nu\, S_2^C(Z) = 0$$

where ν is the volume fraction of piezoceramic in the composite and $\bar{\nu} = (1 - \nu)$ is the volume fraction of polymer.

By using these assumptions refer to Eq (3. 133), we can write the lateral strain depends on vertical strain and electric field as shown below:

$$S_2^C = -\bar{\nu}\frac{(C_{23}^E - C_{12})\bar{S_3} - e_{32}\bar{E_3}}{\bar{\nu}C_{22}^E + \nu C_{11}} \quad (3.\ 134)$$

$$S_2^P = \nu\frac{(C_{23}^E - C_{12})\bar{S_3} - e_{32}\bar{E_3}}{\bar{\nu}C_{22}^E + \nu C_{11}}$$

Then, the constitutive relations will have simplified by removing the lateral strains, and we obtain for the coordinates that have been eliminated:

$$\bar{T_1}(Z) = \bar{C}_{23}^E\,\bar{S_3} - \bar{e}_{32}\bar{E_3} \quad (3.\ 135)$$

Where:

$$\bar{C}^E{}_{23} = C_{23}^E - \bar{\nu}\frac{C_{12}\,(C_{23}^E - C_{12})}{\bar{\nu}C_{22}^E + \nu C_{11}}, \quad \bar{e}_{32} = e_{32} - \bar{\nu}\frac{e_{32}\,(C_{12})}{\bar{\nu}C_{22}^E + \nu C_{11}} \quad (3.\ 136)$$

And for the coordinates that remain:

$$T^P{}_3 = \left[C_{11} + \frac{\nu\, C_{12}(C_{23}^E - C_{12})}{\bar{\nu}C_{22}^E + \nu C_{11}}\right]\bar{S_3} - \quad (3.\ 137)$$

$$\left[\frac{\nu\, e_{32}\, C_{12}}{\bar{\nu}C_{22}^E + \nu C_{11}}\right]\bar{E_3}$$

$$D_3^P = \varepsilon_{11}\,\bar{E_3}$$

$$T^C{}_3 = \left[C^E{}_{33} - \frac{\bar{\nu}\, C_{23}^E\,(C_{23}^E - C_{12})}{\bar{\nu}C_{22}^E + \nu C_{11}}\right]\bar{S_3} -$$

$$\left[e_{33} - \frac{\bar{\nu}\, e_{32}\, C_{23}^E}{\bar{\nu}C_{22}^E + \nu C_{11}}\right]\bar{E_3}$$

$$D^C{}_3 = \left[e_{33} - \frac{\bar{\nu}\, e_{32}\,(C_{23}^E - C_{12})}{\bar{\nu}C_{22}^E + \nu C_{11}}\right]\bar{S_3} +$$

$$\left[\varepsilon_{33}^S + \frac{\bar{\nu}\,(e_{32})^2}{\bar{\nu}C_{22}^E + \nu C_{11}}\right]\bar{E_3}$$

With a fine lateral periodicity, we can average the contributions of each component phase to calculate the effective total stress and electric displacement, namely:

$$\bar{T_3}(Z) = \nu T_3^C(Z) + \bar{\nu}T_3^P(Z) \quad (3.\ 138)$$

$$\bar{D_3}(Z) = \nu D_3^C(Z) + \bar{\nu}D_3^P(Z)$$

So, the final constitutive relations are:

$$\bar{T_3} = \bar{C}^{E}_{33}\,\bar{S_3} - \bar{e}_{33}\,\bar{E_3} \quad (3.\ 139)$$

$$\bar{D_3} = \bar{e}_{33}\,\bar{S_3} + \bar{\varepsilon}^{S}_{33}\,\bar{E_3}$$

The three principal effective material parameters:

effective stiffness at constant electric field c^{E*}_{33}:

$$c^{E*}_{33} = \nu\,(\,c^{E}_{33} - \frac{\bar{\nu}\,(c^{E}_{23}-c_{12})^2}{\bar{\nu}C^{E}_{22}+\nu C_{11}}) + \bar{\nu}\,c_{11} \quad (3.\ 140)$$

effective dielectric permittivity ε^{S*}_{33} :

$$\varepsilon^{S*}_{33} = \nu\,\left(\varepsilon^{S}_{33} + \frac{\bar{\nu}\,(e_{32})^2}{\bar{\nu}C^{E}_{22}+\nu C_{11}}\right) + \bar{\nu}\,\varepsilon_{11} \quad (3.\ 141)$$

effective piezoelectric stress coefficient e^{*}_{33} :

$$e^{*}_{33} = \nu\,(e_{33} - \frac{\bar{\nu}\,e_{32}\,(c^{E}_{23}-c_{12})}{\bar{\nu}C^{E}_{22}+\nu C_{11}}) \quad (3.\ 142)$$

where C_{11} and C_{12} are the stiffness constant and ε_{11} is the permittivity of the passive filler polymer.

3.4 Finite Element Modelling

This section presents the finite element modelling (COMSOL simulation) for two different Z-cut and 36˚/Y-cut in various steps like plate, free rod.

In the definition part, electrical impedance is defined as voltage over current. in this study, Solid Mechanics and Electrostatics were used to model the transducer behavior. In Solid Mechanics, the linear Elastic Material and Piezoelectric Material were selected as default for Isotropic symmetric structures.

3.4.1 Finite Element Modelling of $LiNbO_3$ Free Plate in Z-Cut

In this part, lithium niobate was chosen as the main material which it ‘s properties are listed in table 3.1. Parameters in Global definitions part was defined as table 3.3. Frequency domain is selected between 1 and 12 [MHz].

Table 3-3 Material parameters for Z/Cut in COMSOL Model

Parameter	Expression
$LiNbO_3$-Width	10[mm]
$LiNbO_3$-Thickness	1.1 [mm]
F-min	1[MHz]
F-max	12[MHz]
F-step	0.05[MHz]
V_{in}	5[V]
F_0	3[MHz]
T_0	1/ F_0
$LiNbO_3$-c	7316[m/s]
$LiNbO_3$-lambda	$LiNbO_3$-c/ F_0
Q	10000

The COMSOL physics domains selected for the structure were Solid Mechanics (Piezoelectric Effect) and Electrostatics. For Solid Mechanics, Free conditions were applied to all sides and loss factor damping (1/Q) for having the imagine part of impedance. When Roller was activated on both sides of the structure to simulate a plate which restricts lateral expansion, like a 1D simulation in the X direction without any lateral peaks.

In the Electrostatics domain, one element on the bottom was connected to a Terminal set at 5V, while the plate's top was connected to Ground. In the Multiphysics aspect, the Piezoelectric Effect was enabled for the entire structure. The mapped mesh was selected with an Extra Fine setting to ensure precise representation.

Figure 3.3 shows the structure of Lithium niobate as a Free plate.

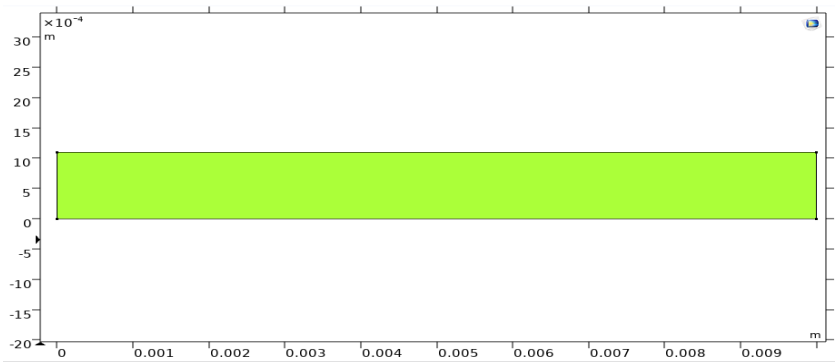

(a) Model structure.

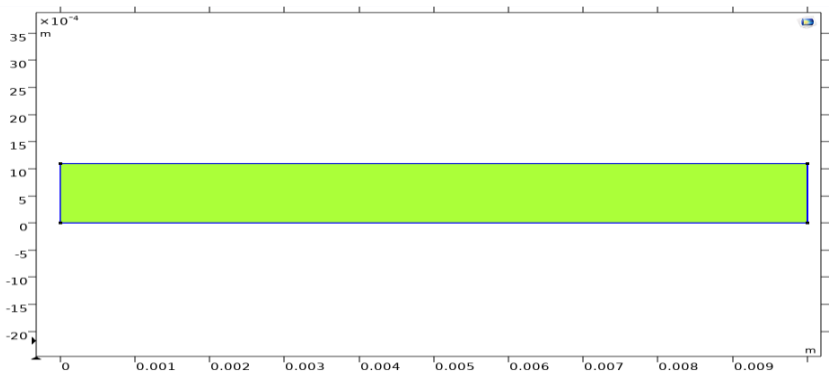

(b) Free. Solid Mechanics

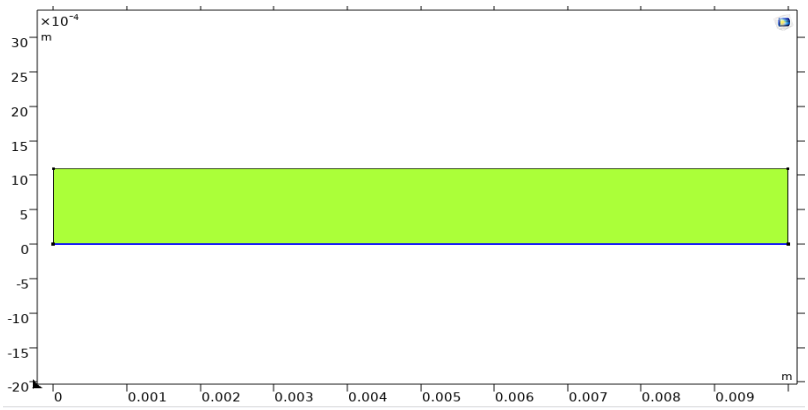

(c) Terminal

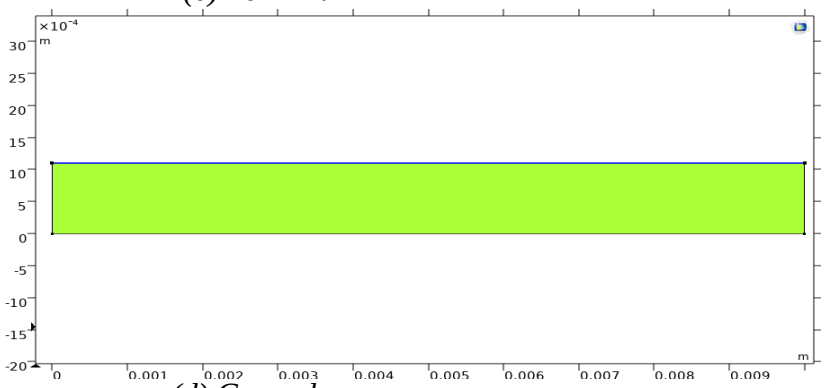

(d) Ground

Figure 3.3 COMSOL Model of a bulk $LiNbO_3$ plate for Z-cut.

3.4.2 Finite Element Modelling of $LiNbO_3$ Free Rod in Z-Cut

This part presents the $LiNbO_3$ as a Free Rod which can move freely in all directions without any lateral clamping. The material parameters are based on table 3.1 and 3.3 but only the width was changed to 0.1 [mm].

The Solid Mechanics domain consists of Linear Elastic material, with Free boundary conditions, and incorporates Piezoelectric material throughout the entire structure. In the Electrostatics domain, a Charge Conservation Piezoelectric approach is applied, with

Ground conditions specified for the top and Terminal conditions set with an applied voltage of 5[V] for the bottom sides. For accurate simulation, the mapped mesh was chosen with an Extra Fine setting.

Figure 3.4 demonstrates the structure of Lithium niobate represented as a Free Rod.

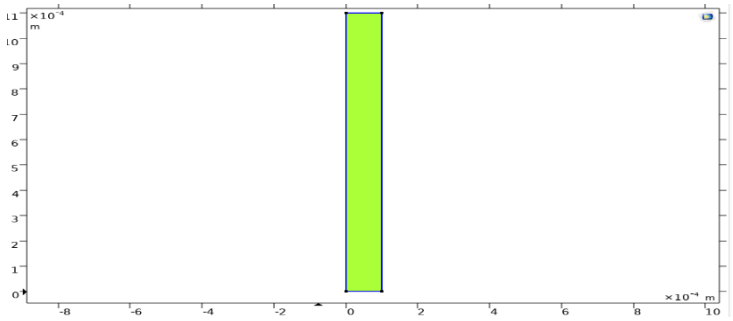

a) Free conditions.

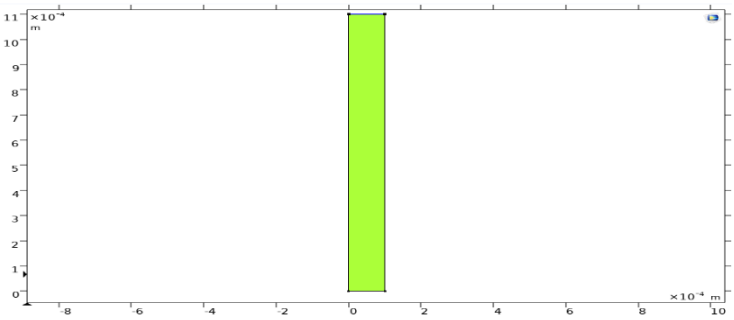

b) Ground.

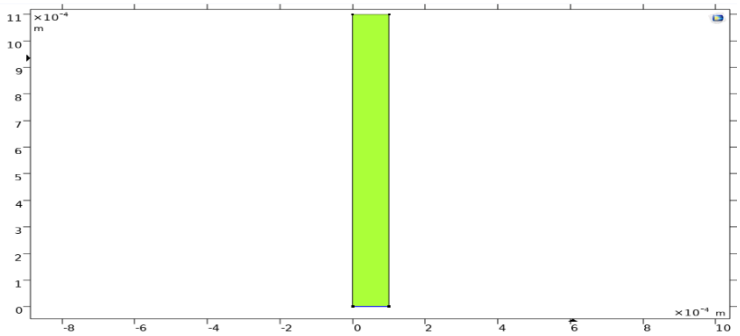

c) Terminal.

Figure 3.4 COMSOL Model of a $LiNbO_3$ Free Rod for Z-cut.

3.4.3 Finite Element Modelling of $LiNbO_3$ Free Plate in 36˚/Y-Cut

In this segment, the model was constructed in a 2D-Axisymmetric format, utilizing Lithium niobate as the material like Z-cut plate, with parameters derived from tables 3.1 and 3.3. Within the component definitions, the Rotated System was selected for this orientation, employing Euler angles (Z-X-Z) in reference to section 2.5.

$\alpha = 0$, $\beta = 54$[deg], $\gamma = 0$

In Solid Mechanics, the Piezoelectric material as a Rotated System, Axial symmetry for the left side of the structure and Free conditions for other sides. When Roller for right side were selected (that allows only movement in one direction while restraining motion in other directions), it will be similar 1D simulation without any lateral vibration. In Electrostatics Axial symmetry applied to the left side. The structure was modeled as a Charge conservation Piezoelectric setup, with Terminal condition specifying an applied voltage of 5[V] for the top and Ground condition was set for bottom. The mapped mesh was selected with an Extra Fine setting to ensure precise representation.

Figure 3.5 illustrates the model structure for $LiNbO_3$ plate in 36° / Y -cut.

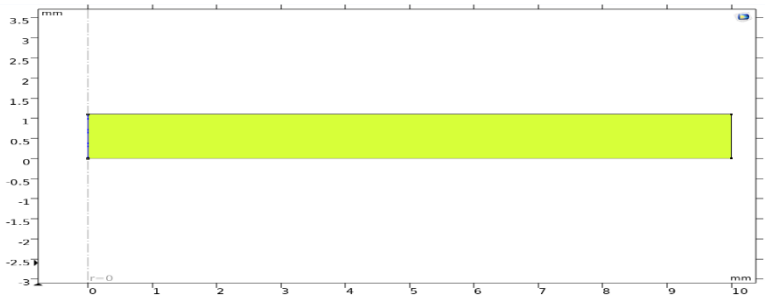

(a) Axial symmetry

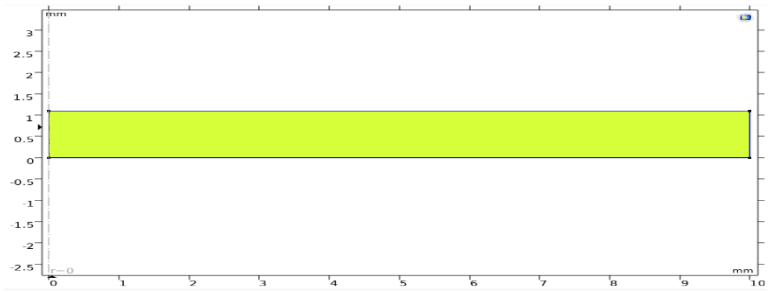

(b) Free. Solid Mechanics

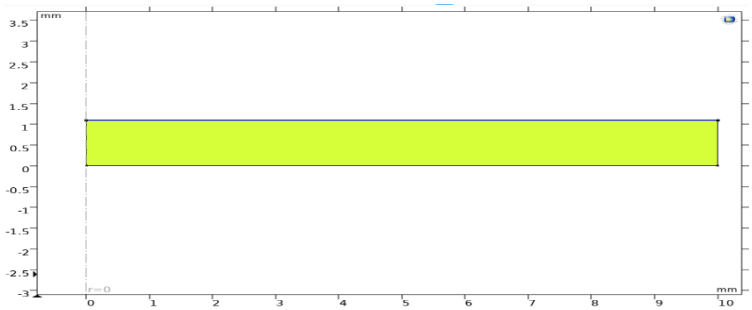

(c) *Terminal.*

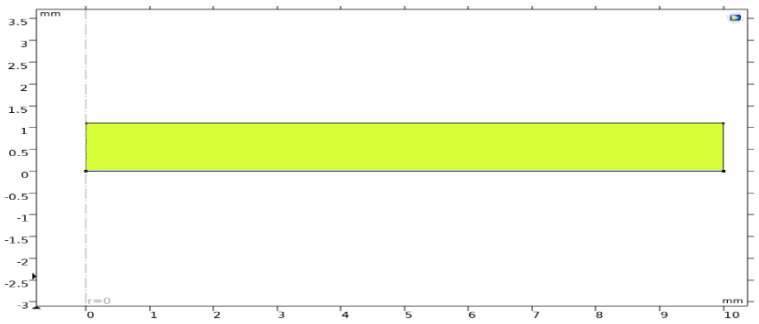

(d) Ground.

Figure 3.5 COMSOL Model and the meshed result of a bulk $LiNbO_3$ plate for 36° Y – cut.

3.4.4 Finite Element Modelling of $LiNbO_3$ Free Rod in 36° / Y -cut

In this part, the structure has been considered as free Rod with small width 0.1 [mm] which can move or vibrates freely. In Solid Mechanics, the Piezoelectric material was implemented as a Rotated System, Axial symmetry for the left side and Free conditions applied to the remaining sides of the structure.

In Electrostatics, Axial symmetry applied to the left side. The structure was configured as a Charge conservation Piezoelectric setup, with Terminal dictating an applied voltage of 5[V] for the top and Ground established for the bottom. For accurate representation, a mapped mesh was chosen with an Extra Fine setting.

Figure 3.6 shows the Model of a LiNbO3 Free Rod in 36° / Y -cut.

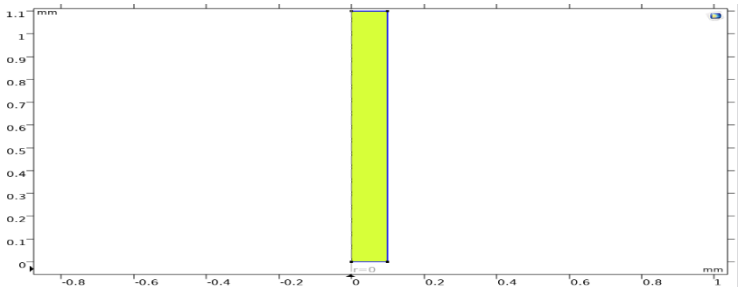

(a) Free conditions.

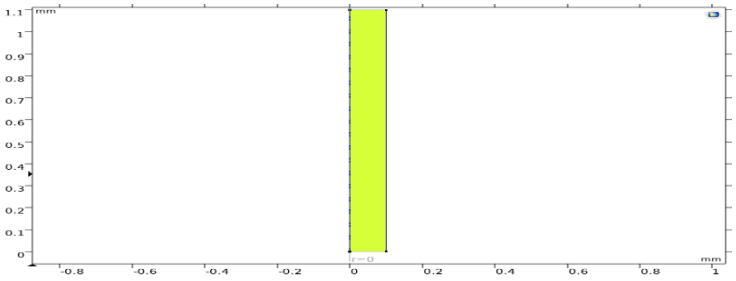

(b) Axial symmetry.

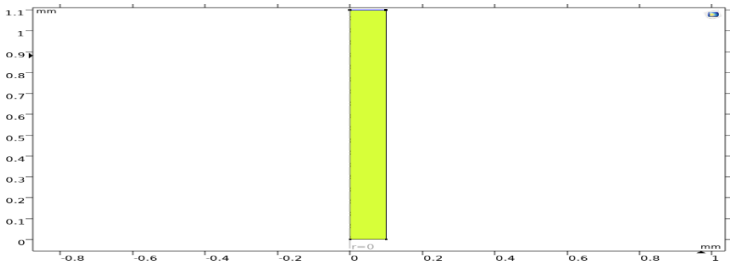

(c) Terminal.

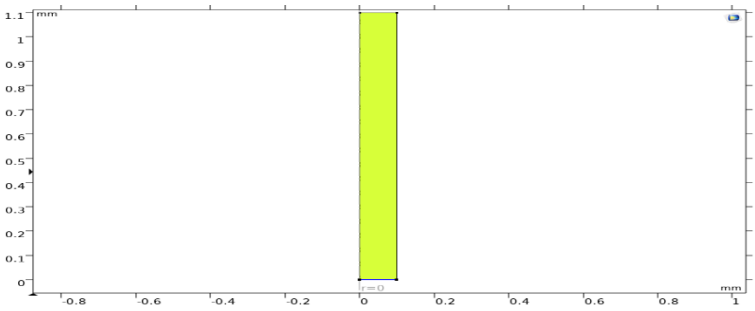

(d) Ground

Figure 3.6 COMSOL Model of a $LiNbO_3$ Free Rod in 36° Y -cut.

If the resonance f_r and anti-resonance frequency f_a is obtained, the thickness mode electromechanical coupling constant can be found from [9] as:

$$k_t^2 = \frac{\pi f_r}{2 f_a} \tan\left[\frac{\pi}{2}\left(1 - \frac{f_r}{f_a}\right)\right] \qquad (3.143)$$

4 Result

This chapter is organized based on the list of material properties and simulation for two different cuts of Lithium Niobate ($LiNbO_3$).

4.1 Simulation in X-Trans for Lithium Niobate (Z-Cut)

The simulation methodology utilized in X-Trans employs a configuration consisting of three layers: one active layer, exemplified by $LiNbO_3$ in our context, and accompanying matching and backing layers. Initially, these layers are assigned the properties of air, denoting a free boundary condition. Furthermore, the surrounding medium, serving as the load, is also represented by air. in the table below, it has shown the properties of active and passive layers.

Table 4-1 Material properties for Z/Cut in one dimensional Mason Model

Layer	Piezoelectric constant (h_{33}) $*10^8$[V/m]	Relative permittivity ($\varepsilon_{33}^S/\varepsilon_0$)	Acoustic impedance(Z) [MRayl]	Longitudinal Velocity (V_l) [m/s]	Mechanical Loss Factor (Q_m)
Backing layer (Air)	-	-	0.000413	343	10
Piezoelectric	51	27.9	33.6	7316	10000
Matching layer (Air)	-	-	0.000413	343	10000
Load (Air)	-	-	0.000413	343	10

Center frequency(F_0) = 3 [MHz], F_{min}= 0.1 [MHz], F_{max}= 12 [MHz]

Area= 78.5 mm^2, Thickness= 1.1 mm

The result graphs for electrical impedance of Z/Cut of $LiNbO_3$ are shown below.

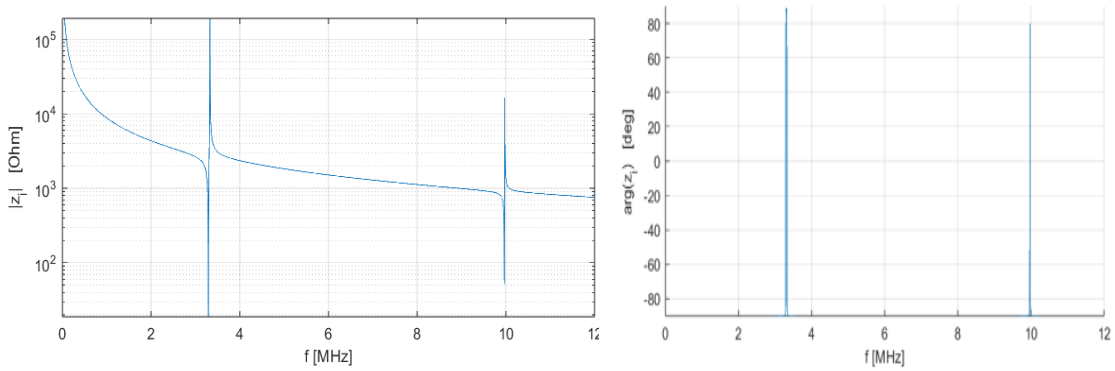

Figure 4.1 The electrical impedance for Z/Cut Lithium Niobate.

Transfer function is defined as the ratio across mechanical velocity and electrical voltage. When the load is designated as air, the displacement and vibration exhibit heightened levels, thereby resulting in comparatively reduced damping in contrast to a water load. The transfer function for Z/Cut is specified as follows.

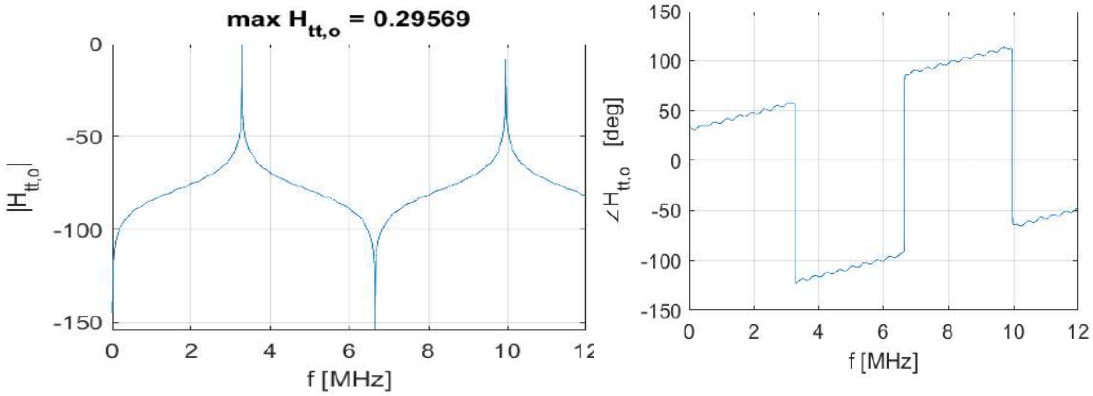

Figure 4.2 The Transfer function for Z/Cut Lithium Niobate.

4.2 Simulation in COMSOL for $LiNbO_3$ (Z-Cut)

This section shows the result which related to simulation of $LiNbO_3$ material in Z-cut when it has been considered as Free plate, Clamped plate, and Free Rod.

The first part illustrates the result for Free plate with the structure that is described in 3.4.1 Section.

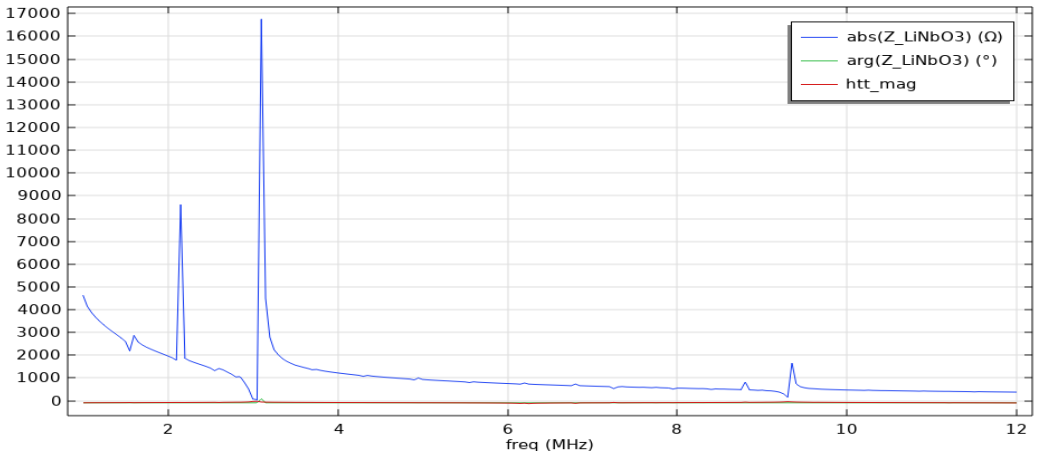

Figure 4.3 COMSOL simulation for Free plate Lithium Niobate in Z-cut.

f_r (Resonance)= 3.05[MHz], f_a(anti-resonance) =3.1 [MHz]

The 2D simulation conducted in COMSOL reveals lateral vibrations alongside primary peaks associated with resonance and anti-resonance. These lateral vibrations can be mitigated by treating the plate with clamped conditions (Roller), thereby confining the material's behavior to a single direction. Alternatively, a composite material approach can be employed, which will be elaborated upon in subsequent analysis. The plate is clamped when the Roller is applied in both sides of the structure, so it will be like 1D simulation in X. Trans without any lateral vibrations.

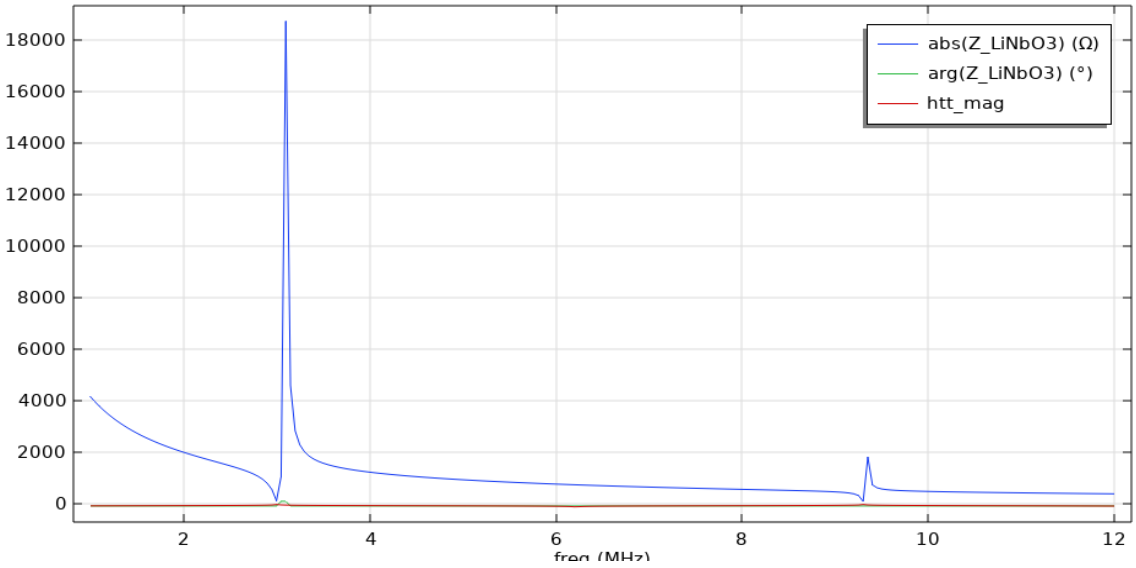

Figure 4.4 COMSOL simulation for Clamped plate Lithium Niobate in Z-cut.

f_r (Resonance)= 3[MHz], f_a(anti-resonance) =3.1 [MHz]

As we can see in this graph that related to electrical impedance in COMSOL simulation, the Z contains two parts refer to real component (resistance) and imaginary component (reactance). Resistance represents the opposition to the flow of current in a circuit due to factors like wire resistance, while reactance accounts for the opposition because of capacitance or inductance in the circuit.

In a circuit, electrical impedance is determined by resistance, inductance, and capacitance. Mathematically, impedance (Z) is represented as the complex sum of resistance (R) and reactance (X):

$$Z = R + jX \quad (4.1)$$

R (Resistance) is the real part and X (Reactance) is imaginary part that is difference between inductive and capacitive reactance.

Inductive reactance: $X_L = 2\pi fL$, Capacitive reactance: $X_C = {}^{1}/_{2\pi fC}$ (4.2)

This part shows the result about the condition when the width of the structure is very small compared to plate and the Rod is free in all conditions refer to section 3.4.2.

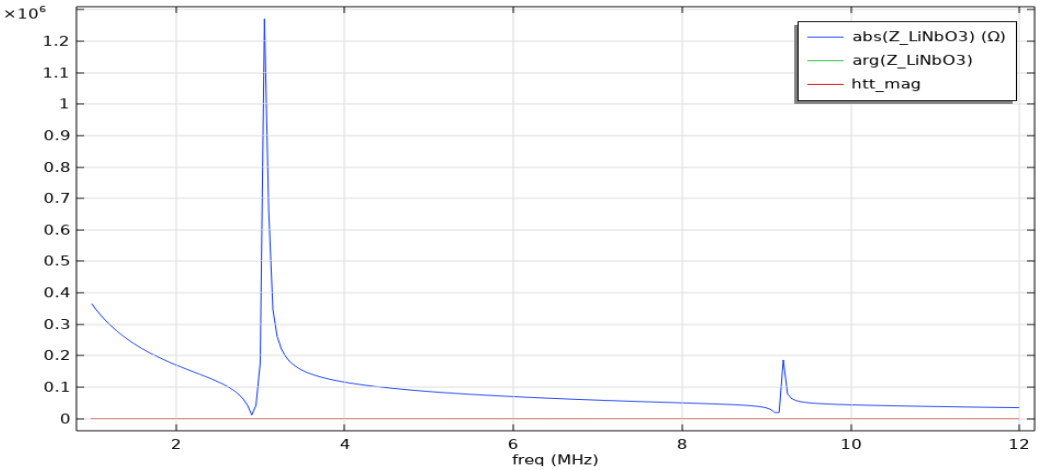

Figure 4.5 COMSOL simulation for Free Rod Lithium Niobate in Z-cut.

f_r (Resonance)= 2.9[MHz], f_a(anti-resonance) =3.05 [MHz]

4.3 Simulation in X-Trans for Lithium Niobate (36 ̊/ Y-Cut)

Based on the X-Trans simulation methodology, there are three layers: one active layer, $LiNbO_3$ in our context, and matching and backing layers. The simulation methodology mirrors the configuration detailed in the Z-cut, as previously presented in the preceding section, maintaining identical parameters regarding area and frequency domain. To determine the piezoelectric constant (h_{33}) and relative permittivity (ε_{33}^{S}), it necessitated

the utilization of transformed matrices generated via MATLAB coding. This section illustrates the transformed matrices concerning stiffness, piezo strain, and dielectric constants.

The determination of material constants within the cross-section involves transforming the original matrices utilizing Euler angles (λ, μ, Θ). These Euler angles denote the rotation from the material axis to the device axis, adhering to the Z-X-Z convention. Specifically, for a rotated 36°/Y-cut $LiNbO_3$ with a rotation of ψ, the Euler angles are defined as follows: $\lambda = \theta = 0^{\circ}$ and $\mu = 36^{\circ} - 90^{\circ}$.

Utilizing the equations presented in the preceding chapter, we conducted simulations and computations to derive the constant matrices corresponding to this specific cut, as illustrated below.

Elastic stiffness:

$C^T = 6 \times 6$ (4.3)

$10^{11} \times$

$$\begin{bmatrix} 2.03 & 0.609 & 0.715 & -0.111 & 0 & 0 \\ 0.609 & 2.214 & 0.905 & -0.088 & 0 & 0 \\ 0.715 & 0.905 & 1.93 & -0.073 & 0 & 0 \\ -0.111 & -0.088 & -0.073 & 0.749 & 0 & 0 \\ 0 & 0 & 0 & 0 & 0.763 & 0.037 \\ 0 & 0 & 0 & 0 & 0.037 & 0.56 \end{bmatrix}$$

Piezoelectric constant:

$e^T = 3 \times 6$

$$\begin{bmatrix} 0 & 0 & 0 & 0 & 0.33 & -4.49 \\ -1.58 & -2.41 & 2.57 & 0.38 & 0 & 0 \\ -1.78 & -1.74 & 4.55 & -0.34 & 0 & 0 \end{bmatrix}$$

Clamped dielectric constant:

$\varepsilon^T =$

$$\begin{bmatrix} 44.3 & 0 & 0 \\ 0 & 33.57 & 7.8 \\ 0 & 7.8 & 38.6 \end{bmatrix}$$

Through the utilization of the matrices transformed as indicated above, we have conducted calculations to determine the piezoelectric constant in accordance with the following equation:

h_{33}^{T}= $\frac{e_{33}^{T}}{\varepsilon_{33}^{T}}$ (4.4)

Table.4-2 presents the properties of 36°/Y-cut $LiNbO_3$ as the active layer and the passive layers, selected as air for indicating a free boundary condition.

Table 4-2 Material properties for 36° Y -Cut in one dimensional Mason Model

Layer	Piezoelectric constant (h_{33}) $*10^8$[V/m]	Relative permittivity ($\varepsilon_{33}^{S}/\varepsilon_0$)	Acoustic impedance (Z) [MRayl]	Longitudinal Velocity (V_l) [m/s]	Mechanical Loss Factor (Q_m)
Backing layer, load (Air)	-	-	0.000413	343	10
Piezoelectric	133	38.6	33.7	7340	10000
Matching layer (Air)	-	-	0.000413	343	10000

The electrical impedance result for this cut is presented below:

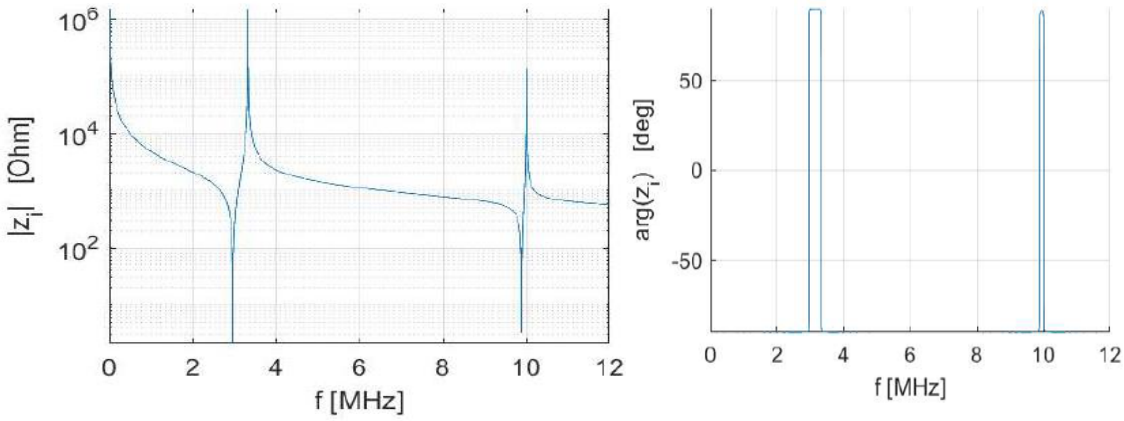

Figure 4.6 The electrical impedance for 36°/Y-cut Lithium Niobate.

As evident from the depicted figure and upon comparison with (Figure 4.1) pertaining to the Z-cut, the significantly higher value of h_{33} for the 36°/Y-cut results in obvious difference between the resonance and anti-resonance frequencies compared to the Z-cut configuration.

This cut has some benefits in compared to Z-cut. Y-cut with higher h_{33} value produce wider bandwidths due to the larger difference between resonance and anti-resonance frequencies. By having a wide frequency range, the transducer is adaptable and can be applied to a wide range of applications. The transducer becomes more sensitive to electrical signals with a higher h_{33} value. As a result of this increased sensitivity, more precise measurements and actuations are possible. Increasing sensitivity results in improved signal-to-noise ratios, leading to clearer, more accurate readings or outputs.

Transfer function is defined as the ratio between mechanical velocity(u) and electrical voltage(V). As can be seen in the following figure, the simulation result was obtained using X-Trans

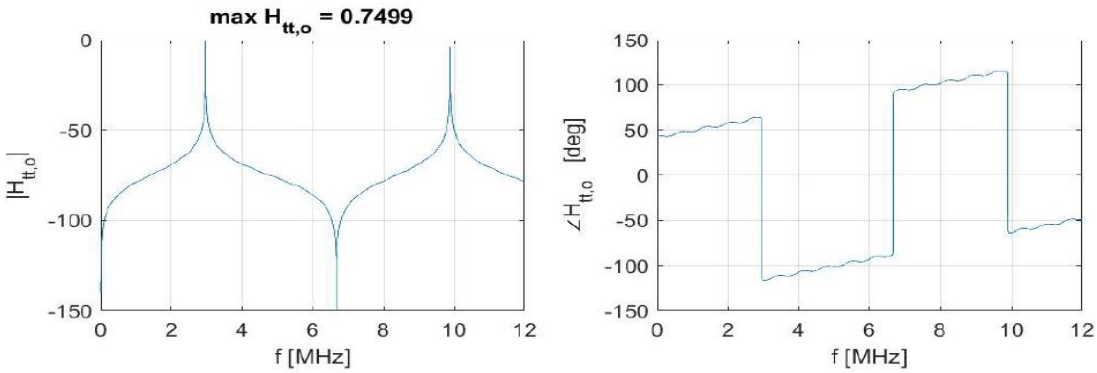

Figure 4.7 The transfer function for 36°/Y-cut Lithium Niobate.

The difference in transfer function figures is attributed to the variance in piezoelectric coefficients between the 36°/Y-cut and Z-cut crystals. Specifically, the h_{33} coefficient (signifying the piezoelectric response along the crystal's thickness direction) is typically greater for 36°/Y-cut crystals when compare with Z-cut crystals. This difference in coefficients impacts the transfer function, particularly in terms of the conversion between mechanical stress or strain and electrical voltage.

36°/Y-cut transducers commonly demonstrate heightened sensitivity perpendicular to the crystal surface in contrast to Z-cut transducers. This variation in directional sensitivity is evident in their respective transfer functions. The bandwidth of the transfer function can be defined as the range of frequencies over which the magnitude of the transfer function is -3dB.

4.4 Simulation in COMSOL for $LiNbO_3$ (36° / Y-Cut)

This section shows the result which related to simulation of $LiNbO_3$ material in 36° / Y -cut when it has been considered as Free plate, Clamped plate, and Free Rod.

This section shows the results of $LiNbO_3$ in 36° / Y-Cut in applied Rotated System that is described in 3.4.3 Section.

Figure 4.8 illustrates the COMSOL simulation for Electrical impedance of Free plate $LiNbO_3$ in 36° / Y-Cut.

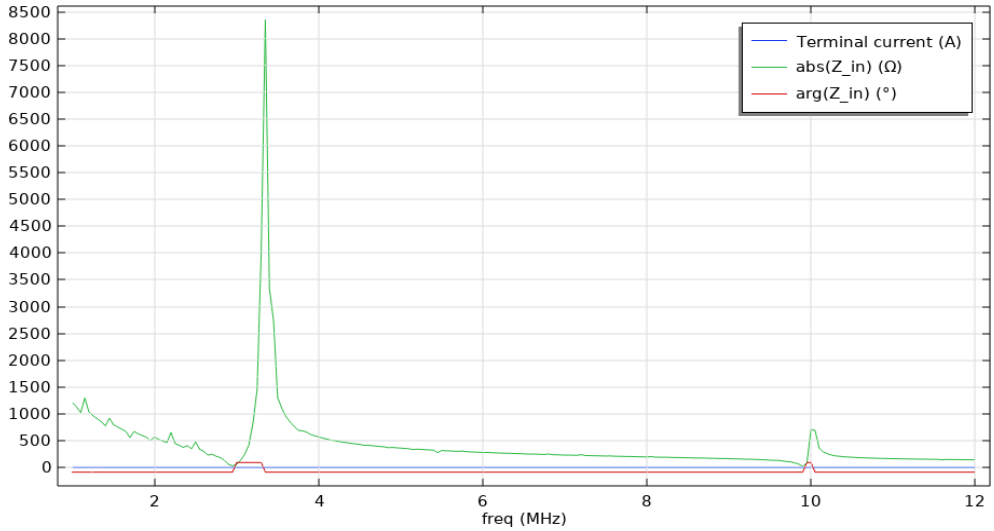

Figure 4.8 COMSOL simulation for Electrical impedance of Free plate $LiNbO_3$ in 36° / Y-Cut.

F_r (resonance peak) = 2.95[MHz]

F_a (anti-resonance peak) = 3.35[MHz]

The above figure shows the lateral vibrations because of simulation in 2-dimensional structure, and it can be eliminated by imposing clamped condition on the plate in a single direction (This condition is achieved by applying a Roller to one side of the plate, restricting its vibration to one direction only).

Figure 4.9 shows the Electrical impedance for clamped plate of $LiNbO_3$ in 36°/ Y-Cut.

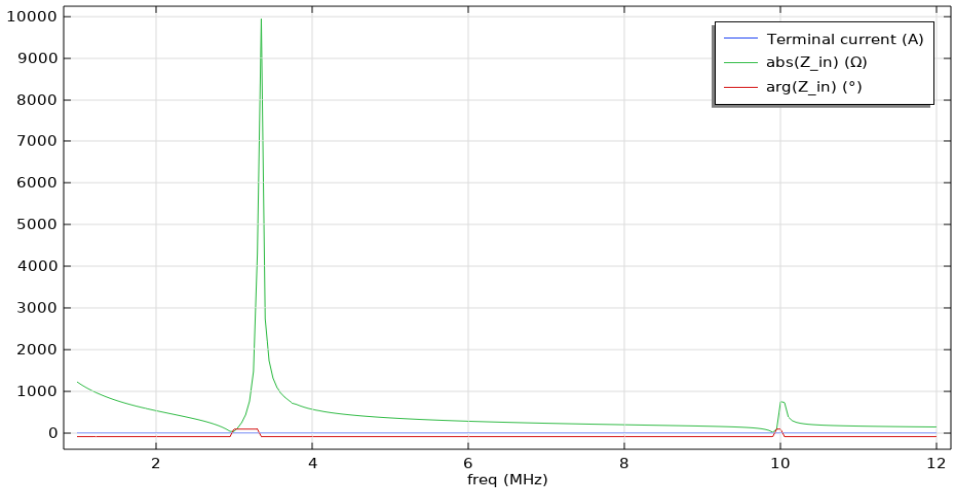

Figure 4.9 COMSOL simulation for Electrical impedance of Clamped plate $LiNbO_3$ in 36° Y-Cut.

F_r (resonance peak) = **3[**MHz], F_a (anti-resonance peak) = **3.35**[MHz]

This part is related to Free Rod with small width for structure refer to section 3.4.4. This structure shows the highest value for electromechanical coupling factor related to resonance and anti-resonance frequencies based on Eq (3.143).

Figure 4.10 shows the Electrical impedance for Free Rod of $LiNbO_3$ in 36°/ Y-Cut.

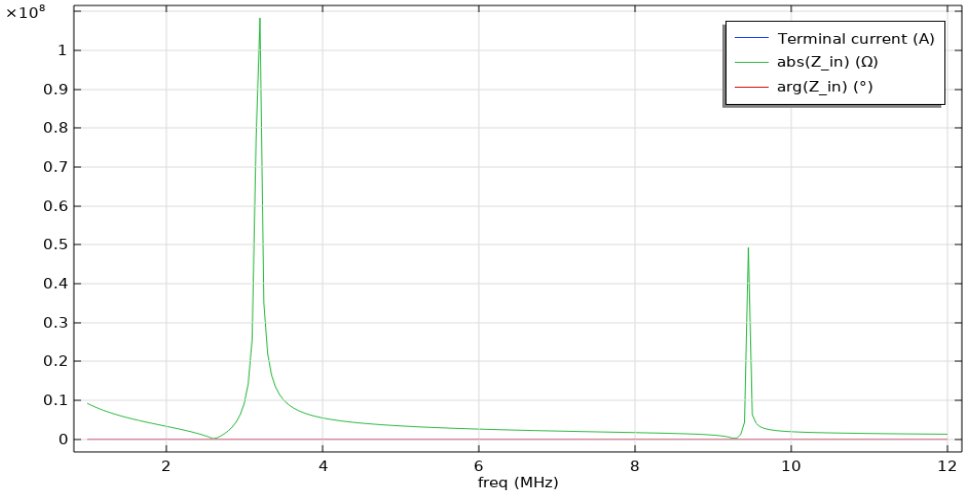

Figure 4.10 COMSOL simulation for Electrical impedance of Free Rod $LiNbO_3$ in 36° Y-Cut.

F_r (resonance peak) = **2.6[**MHz], F_a (anti-resonance peak) = **3.2**[MHz]

To calculate the electromechanical coupling coefficient related to these two frequencies, the equation is:

The difference between resonance and anti-resonance is higher than in compared to Z-cut structure in the previous section, so is shows that the $LiNbO_3$ in 36̊/ Y-Cut has higher electromechanical coupling factor.

4.5 Composite properties for Z-cut

In this section, simulations have been conducted using MATLAB to model the 1-3 and 2-2 composites of $LiNbO_3$ with various polymer materials, including EpoTek 3012 and RTV 3140 (silicone rubber), specifically oriented in the Z-cut configuration showing how piezoceramic volume fraction affects composite properties.

The coding utilized in this analysis relies on the constitutive equations and material constants provided in the preceding section.

Piezocomposite design is characterized by coupling coefficients and acoustic impedances that depend on volume fraction. By modifying the volume fraction, piezocomposite design aims to achieve the highest thickness mode coupling coefficient.

4.5.1 Composite of $LiNbO_3$ and EpoTek 3012 polymer for Z-cut

This section is considered as composite of $LiNbO_3$ with EpoTek 3012 filler material. Figure 4.11 demonstrates the material parameters with respect to volume fraction of ceramic phase.

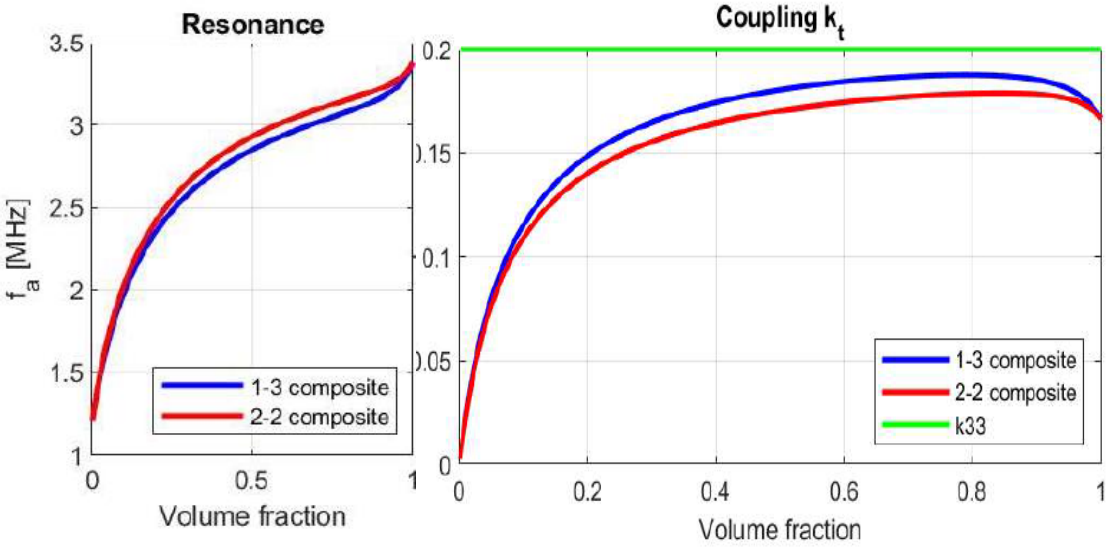

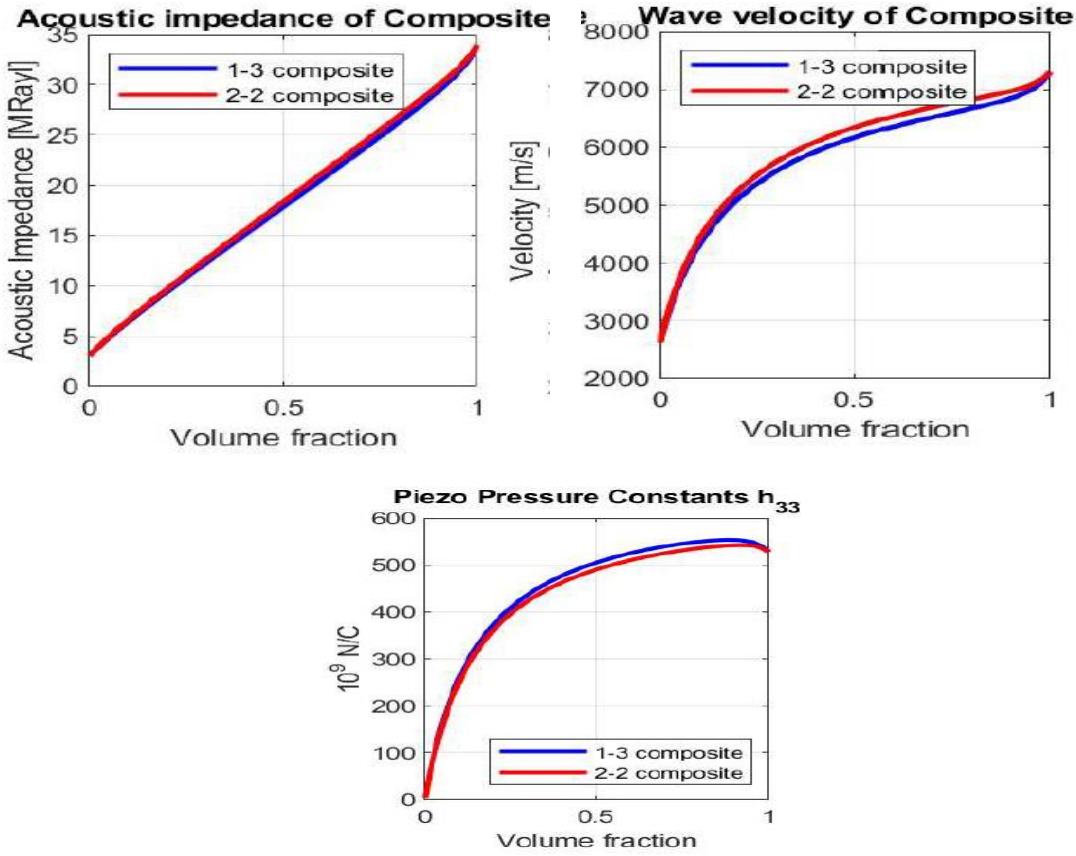

Figure 4.11 Variation with volume fraction of piezoelectric ceramic, v, of a composite's transducer parameters: specific acoustic impedance(Z); longitudinal-velocity (V_l); and thickness-mode electromechanical coupling constant (k_t), Material parameters are for $LiNbO_3$ ceramic and EpoTek 3012 polymer for Z-cut.

Figure of coupling coefficient (4.11b) demonstrates that when the volume fraction equals 1 (representing a bulk piezoelectric plate), the coupling coefficient reaches the thin plate coupling coefficient of k_t= 0.166. Conversely, when the volume fraction approaches zero, indicating a simple polymer without piezoelectric characteristics, k_t tends toward 0. For EpoTek 3012 epoxy material, the coupling coefficient peaks in 2-2 composite at around 0.178 and in 1-3 composite has higher value at around 0.187 for a volume fraction of roughly 0.8, as indicated in Figure above.

The K_{33} that shows there is no stiffness in filler material (free pillars) is equal to 0.2.

For X-Trans simulation, we utilized the material parameters based on acoustic impedance, wave velocity, and piezo pressure constant provided earlier. The corresponding values for both composites are listed in the table presented below, the material values for bulk $LiNbO_3$ were also included for comparison with the composite plate.

We assumed that the area for both 1-3 and 2-2 composites is the same as bulk $LiNbO_3$.

To simulate the one-dimensional Mason model in Xtrans, we have used the material parameters related to Figure 4.11 to list the material parameters of 1-3 and 2-2 composites of $LiNbO_3$ with EpoTek 3012 filler in table 4.3 as below.

Table 4-3 Fitting of material parameters of the $LiNbO_3$, EpoTek 3012-filled piezocomposite for one-dimensional Mason modelling in Xtrans for Z-cut.

Parameter	Bulk $LiNbO_3$	1-3 composite ($LiNbO_3$/ EpoTek3012)	2-2 composite ($LiNbO_3$/ EpoTek3012)
A [mm^2]	78.5	78.5	78.5
h_{33} [10^8	51	55.3	53.7
V/m]	27.9	23.2	23.13
$\varepsilon^S / \varepsilon_0$	33.6	27.06	27.12
Z[MRayls]	7316	6669.3	6832.2
c_l [m/s]			

The central frequency of the designed transducer is approximate 3MHz.

The wavelength is calculated as below equation:

$$\lambda = \frac{c}{f} \quad (4.5)$$

where c is speed of sound in load material which assumed to be as water (1540 m/s) and steel (5980 m/s), and f is the central frequency (3MHz). In this case, the wavelength is 513.3 e-6 m for water and 1993.3 e-6 m for steel material.

To select the appropriate matching layer based on the relationship with piezocomposite and load impedances according to Eq (2.17), EpoTek 3012 mixed with 10% Al_2O_3 emerges as the optimal material for achieving impedance matching when the load was chosen as water [22] and the matching layer is Niobium when the load was selected as steel [23] .

Material parameters for different layers are listed in table 4.4 for composite of $LiNbO_3$ and EpoTek 3012 filler.

Table 4-4 Material properties for different layers of the $LiNbO_3$, EpoTek 3012-filled 1-3 piezocomposite in one dimensional Mason Model for Z-cut.

Material	Z [MRayls]	C [m/s]	Q
Backing layer (Air)	0.000413	343	10
Matching layer Load (water)	3.93 1.5	2580.6 1540	10
Matching layer [23] Load (Steel)	38.54 46	4920 5980	10

Air backing was chosen for this work due to its ability to achieve high sensitivity. By using the X-Trans simulation, we have computed the Electrical impedance of the transducer that has 1 matching layer, backing layer and load. The load is chosen as water because of similarity to biological tissues and reduces the acoustic impedance mismatch due to matching of transducer and load, so allows for more efficient transmission of ultrasound waves. Figure 4.12 shows the electrical impedance of 1-3 composite of $LiNbO_3$ and EpoTek 3012 filler as amplitude and phase with considering the load as water in this cut as Z-cut.

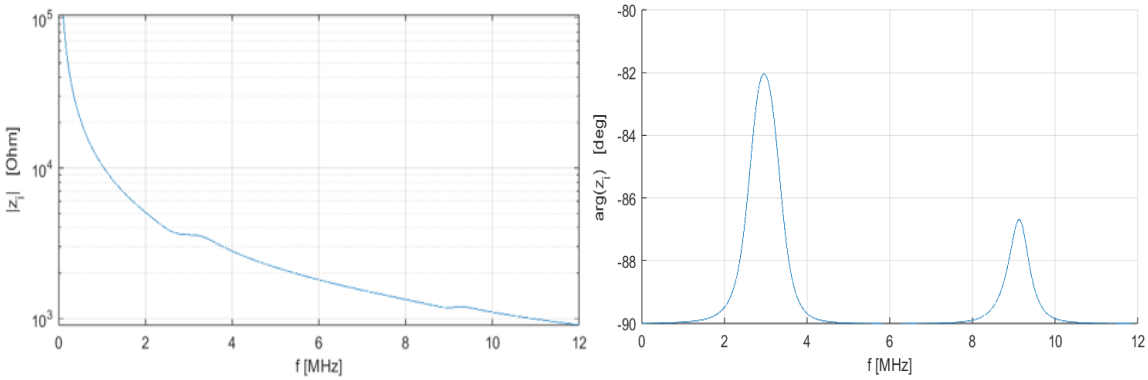

Figure 4.12 Electrical impedance of 1-3 composite of $LiNbO_3$ and EpoTek 3012 filler with water as load for Z-cut.

As is shown in the above figures, the peaks of graph are related to resonances and anti-resonances in special frequencies. The resonance peak is related to lower value which electrons can flow (short circuit) easier than the open circuit in anti-resonance peak.

Figure 4.13 shows the transfer function of 1-3 composite of $LiNbO_3$ and EpoTek 3012 filler for Z-cut.

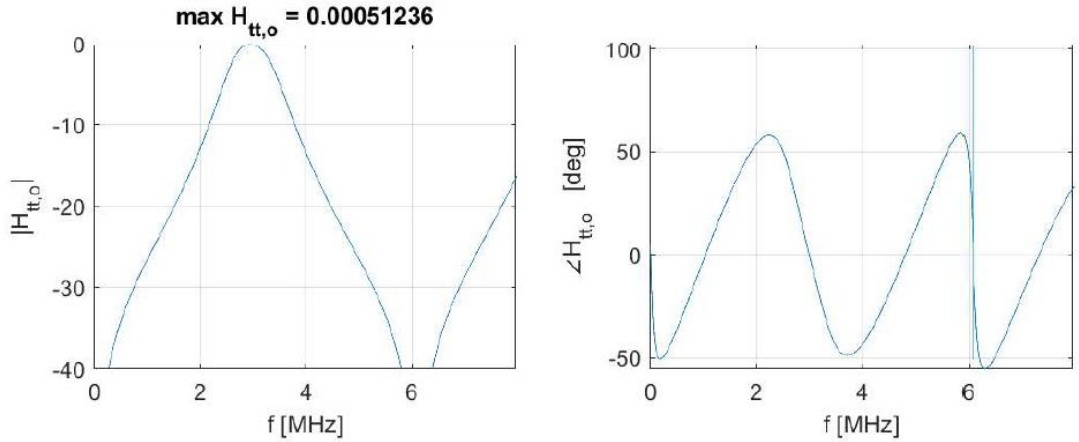

Figure 4.13 Transfer function of 1-3 composite of LiNbO3 and EpoTek 3012 filler with water as load for Z-cut.

In this section, we aim to present the simulation results for this composite by utilizing steel as the load material.

The load is chosen as steel because of high temperature stability that it can be suitable for high temperature applications. It can tolerate high temperature without degradation in mechanical or acoustic properties.

As shown in figure 4.14, the electrical impedance of 1-3 composites of $LiNbO_3$ and EpoTek 3012 filler with steel as load is displayed as amplitude and phase.

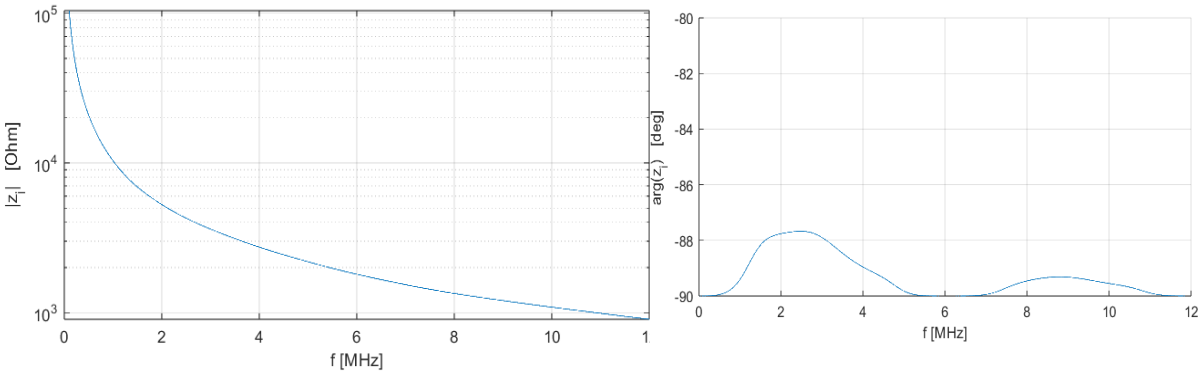

Figure 4.14 Electrical impedance of 1-3 composite of $LiNbO_3$ and EpoTek 3012 filler with steel as load for Z-cut.

Figure 4.15 shows the transfer function of 1-3 composite of $LiNbO_3$ and EpoTek 3012 filler for Z-cut with steel material as is chosen for load.

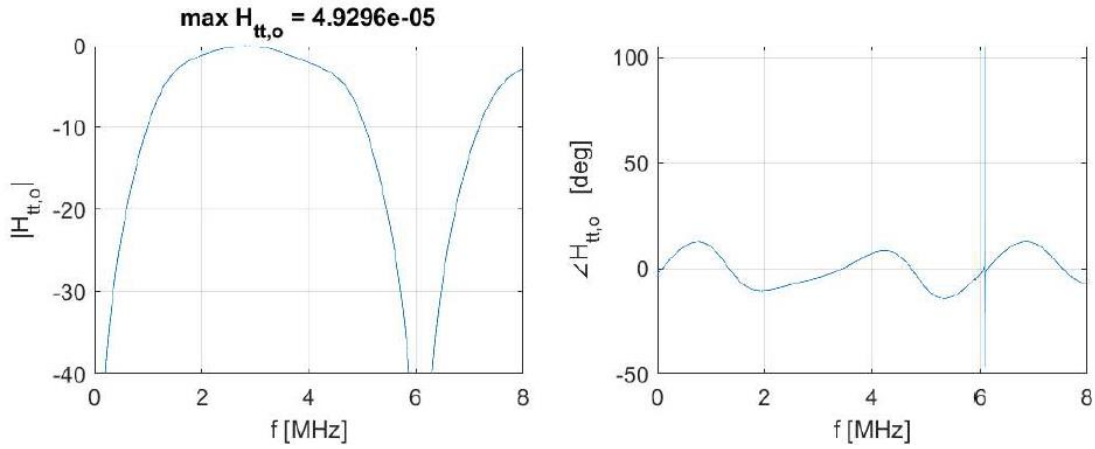

Figure 4.15 Transfer function of 1-3 composite of $LiNbO_3$ and EpoTek 3012 filler with steel as load for Z-cut.

In the next step, material parameters for different layers for 2-2 composite of $LiNbO_3$ and EpoTek 3012 filler in Z-cut are listed as table 4.5.

Table 4-5 Material properties for different layers of the $LiNbO_3$, EpoTek 3012-filled 2-2 piezocomposite in one dimensional Mason Model for Z-cut.

Material	Z [MRayls]	C [m/s]	Q
Backing layer (Air)	0.000413	343	10
Matching layer	3.94	2580.6	10
load(water)	1.5	1540	
Matching layer [23]	38.54	4920	10
load (Steel)	46	5980	

Figure 4.16shows the electrical impedance of 2-2 composite of $LiNbO_3$ and EpoTek 3012 filler as amplitude and phase with considering the load as water in this cut as Z-cut.

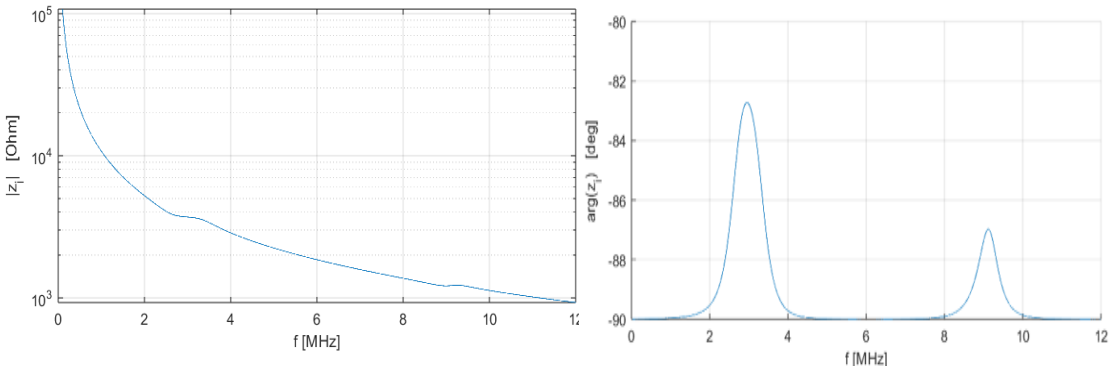

Figure 4.16 Electrical impedance of 2-2 composite of $LiNbO_3$ and EpoTek 3012 filler with water as load for Z-cut.

Figure 4.17 shows the transfer function of 2-2 composite of $LiNbO_3$ and EpoTek 3012 filler for Z-cut.

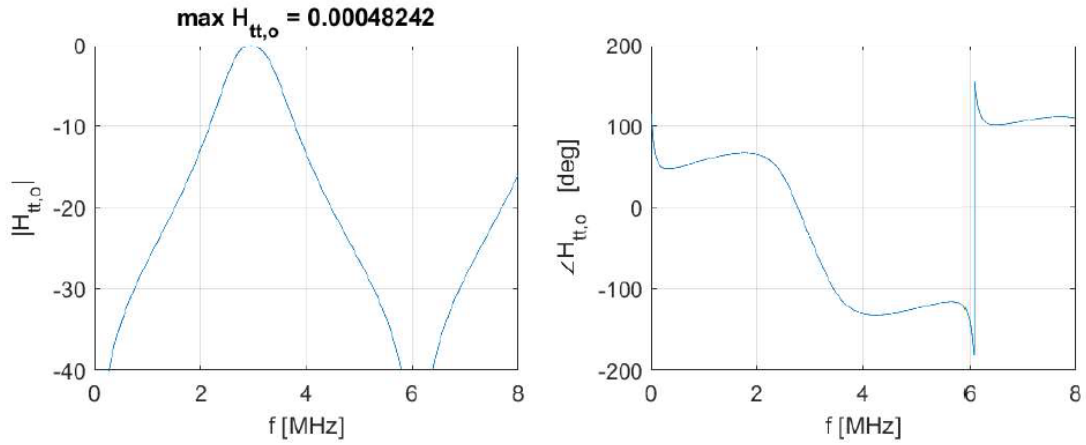

Figure 4.17 Transfer function of 2-2 composite of $LiNbO_3$ and EpoTek 3012 filler with water as load for Z-cut.

Next part is related to 2-2 composite and steel as load for Z-cut. With the load as steel in this cut, the electrical impedance as amplitude and phase is shown in figure 4.18.

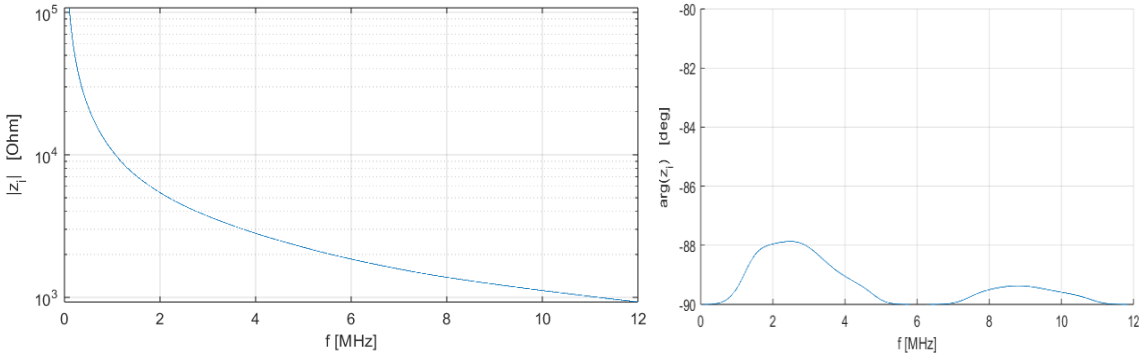

Figure 4.18 Electrical impedance of 2-2 composite of LiNbO3 and EpoTek 3012 filler with steel as load for Z-cut.

For Z-cut with steel material as load, Figure 4.19 shows the transfer function of 2-2 composites of $LiNbO_3$ and EpoTek 3012 filler.

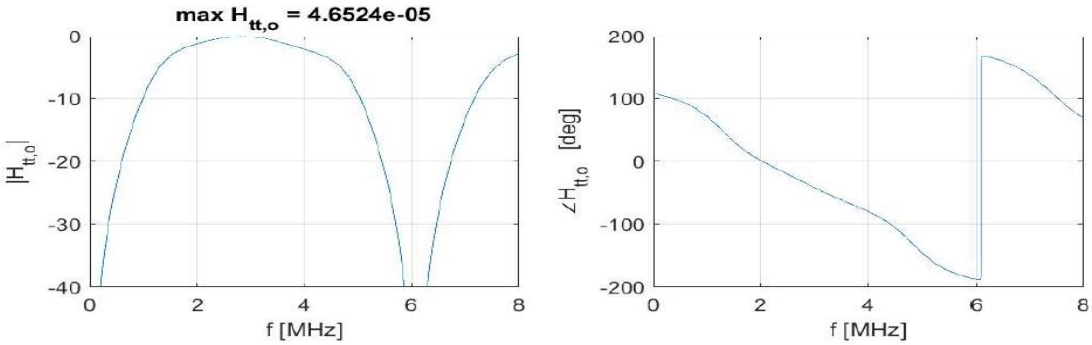

Figure 4.19 Transfer function of 2-2 composite of $LiNbO_3$ and EpoTek 3012 filler with steel as load for Z-cut.

4.5.2 Composite of $LiNbO_3$ and RTV 3140 polymer for Z-cut

Piezocomposite is filled with RTV 3140 as a polymer material in this section. This composite that contains softer polymer is expected to have a higher electromechanical coupling coefficient than EpoTek 3012.

This figure 4.20 illustrates the piezocomposite parameters for $LiNbO_3$ with RTV 3140 filler as a function of volume fraction.

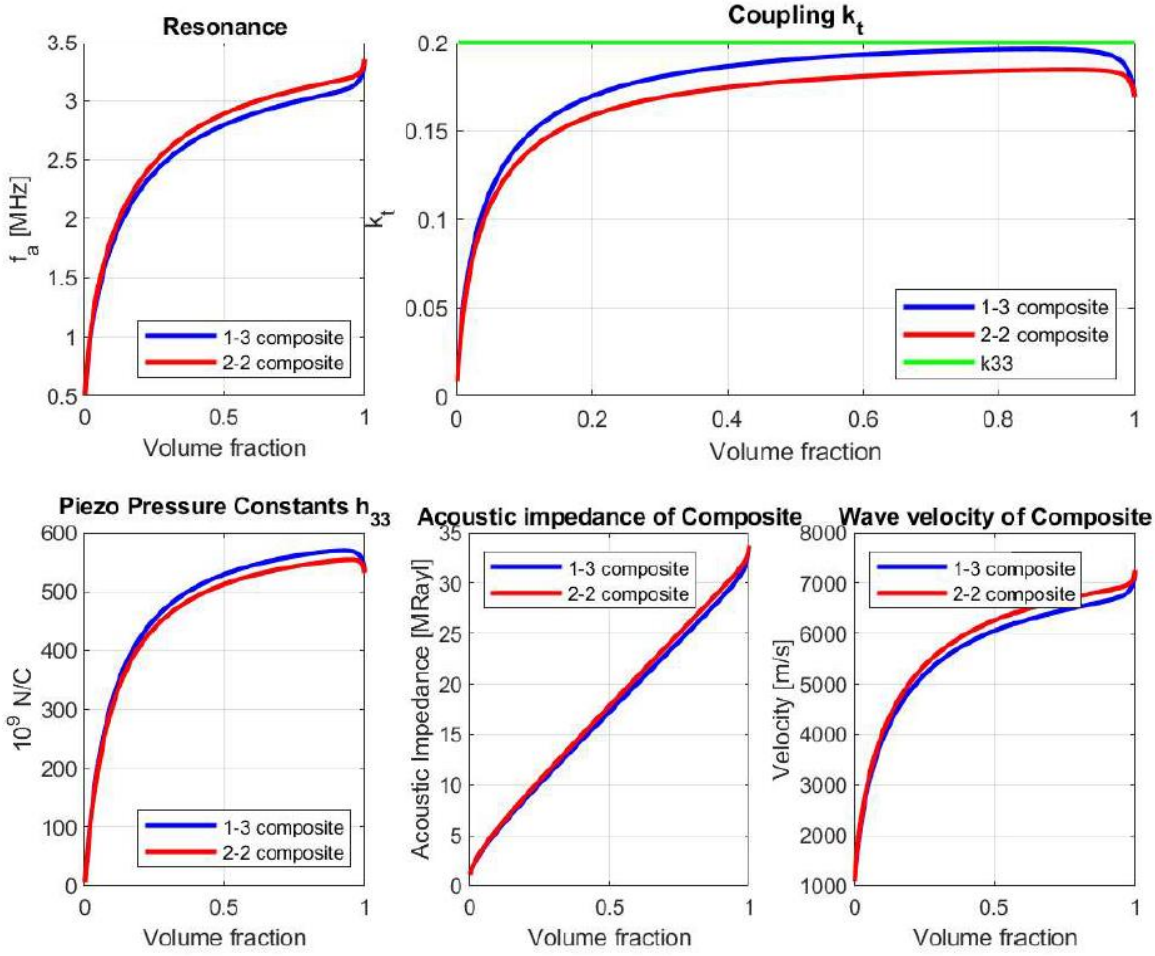

Figure 4.20 Variation with volume fraction of piezoelectric ceramic, v, of a composite's transducer parameters: specific acoustic impedance(Z); longitudinal-velocity (V_l); and thickness-mode electromechanical coupling constant (k_t), Material parameters are for $LiNbO_3$ ceramic and RTV 3140 polymer for Z-cut.

The coupling coefficient figure (4.20b) illustrates that when the volume fraction equals 1, representing a bulk piezoelectric plate, the coupling coefficient reaches the thin plate coupling coefficient of k_t =0.166. Conversely, as the volume fraction approaches zero, indicating a simple polymer devoid of piezoelectric characteristics, k_t tends toward 0. For

RTV 3140 epoxy material, the coupling coefficient peaks in 2-2 composite at around 0.184 and in 1-3 composite has higher value at around 0.196 for a volume fraction of roughly 0.8, as indicated in Figure above.

For 2-2 composite, the highest value for coupling coefficient is corresponding to volume fraction of 0.9 but for simplify dicing procedures, we assume that the volume fraction is the same for both polymer materials and both cuts as identical dicing dimensions.

By comparing the figures above concerning composite of $LiNbO_3$ as an active material with various surroundings polymers like EpoTek 3012 and RTV 3140 (rubber silicone), we can see the higher electromechanical coupling coefficient and lower acoustic impedance and wave velocity for rubber silicone as a softer material.

Table 4.6: Fitting of material parameters of the $LiNbO_3$, RTV 3140-filled piezocomposite for one-dimensional Mason modelling in Xtrans for Z-cut.

Parameter	Bulk $LiNbO_3$	1-3 composite ($LiNbO_3$/ RTV 3140)	2-2 composite ($LiNbO_3$/ RTV 3140)
A [mm^2]	78.5	78.5	78.5
h_{33} [10^8 V/m]	51	56	54.1
$\varepsilon^S / \varepsilon_0$	27.9	22.9	22.8
Z[MRayls]	33.6	25.74	26.6
c_l [m/s]	7316	6534.58	6748.84

Table 4-7: Material properties for different layers of the $LiNbO_3$, RTV 3140-filled, 1-3piezocomposite in one dimensional Mason Model for Z-cut.

Material	Z [MRayls]	C [m/s]	Q
Backing layer (Air)	0.000413	343	10
Matching layer	3.86	2580.6	10
Load (water)	1.5	1540	
Matching layer,Niobium [23]	38.54	4920	10
Load (Steel)	46	5980	

Figure 4.21 shows the electrical impedance for 1-3 piezocomposite of $LiNbO_3$ and RTV polymer for Z-cut that water is chosen as load.

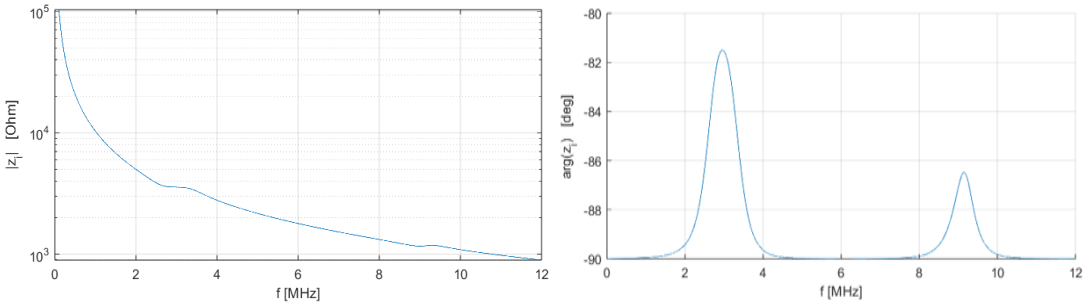

Figure 4. 21 *Electrical impedance of 1-3 composite of $LiNbO_3$ and RTV 3140 filler with water as load for Z-cut.*

The transfer function for this composite demonstrates as figure 4.22 as below.

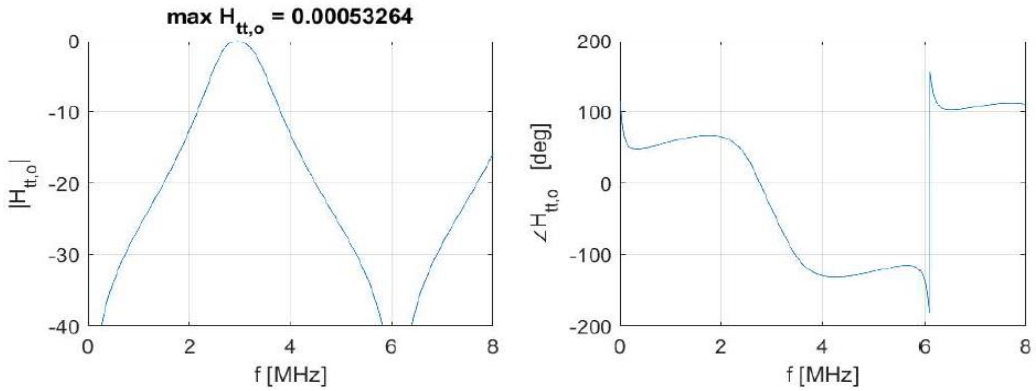

Figure 4.22 Transfer function of 1-3 composite of $LiNbO_3$ and RTV 3140 filler with water as load for Z-cut.

In this part, steel is chosen as a load instead of water. Because of close its acoustic impedance with Lithium niobate, there is no need for using the any specific matching layer. figures 4.23 and 4.24 show the electrical impedance and transfer function for 1-3 composite of $LiNbO_3$ and RTV 3140 filler with steel as load in Z-cut, respectively.

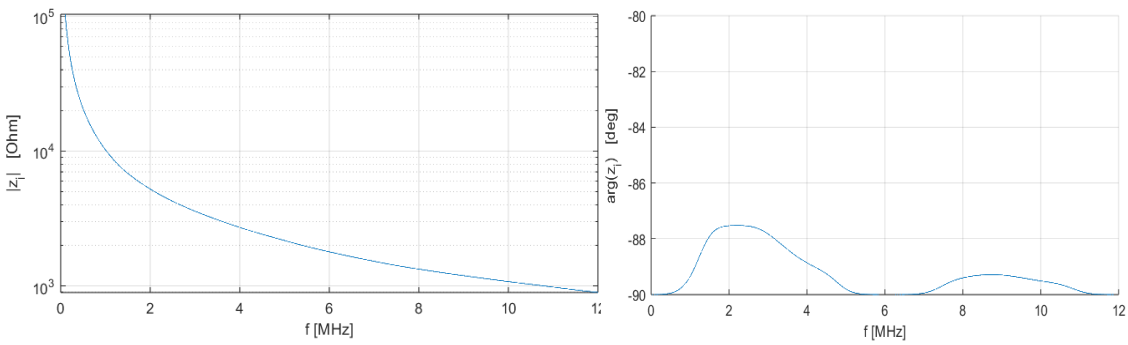

Figure 4.23 Electrical impedance of 1-3 composite of $LiNbO_3$ and RTV 3140 filler with steel as load for Z-cut.

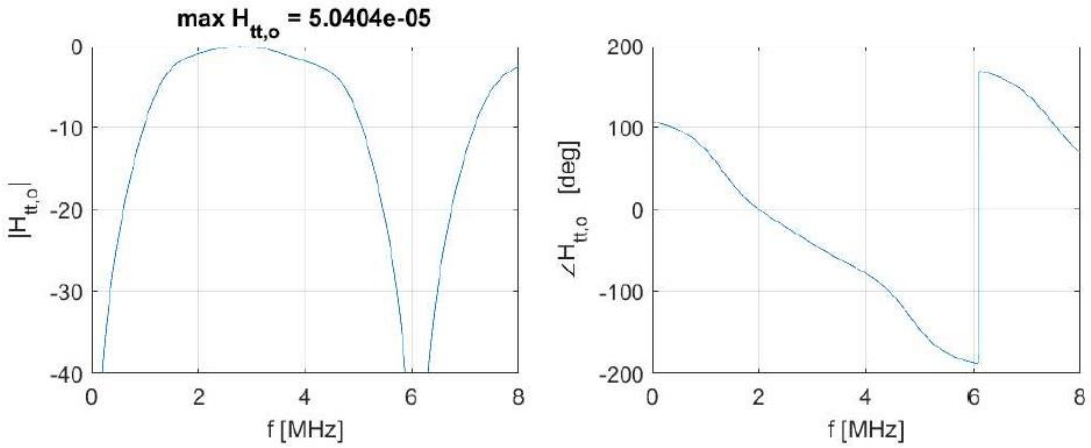

Figure 4.24 Transfer function of 1-3 composite of $LiNbO_3$ and RTV 3140 filler with steel as load for Z-cut.

The one-dimensional Mason Model is used to simulate the 2-2 piezocomposite of lithium niobate and RTV 3140 filler for Z-cut. The values of piezoelectric constant (h_{33}), acoustic impedance, speed of sound and dielectric constant have shown before as table 4.8. As shown in table 4.8, material parameters for backing, matching, and load are listed.

The matching layer is the same as before that is related to the EpoTek 3012 with 10% Al_2O_3 for the load as water and Niobium for the load as steel [22],[23].

Table 4-8: Material properties for different layers of the $LiNbO_3$, RTV 3140-filled 2-2piezocomposite in one dimensional Mason Model for Z-cut.

Material	Z [MRayls]	C [m/s]	Q
Backing layer (Air)	0.000413	343	10
Matching layer	3.91	2580.6	10
Load (water)	1.5	1540	
Matching layer, Niobium [23]	38.54	4920	10
Load (Steel)	46	5980	

The electrical impedance for 2-2 piezocomposite of $LiNbO_3$ and RTV 3140 filler for Z-cut by assuming water as load, is shown as figure 4.25.

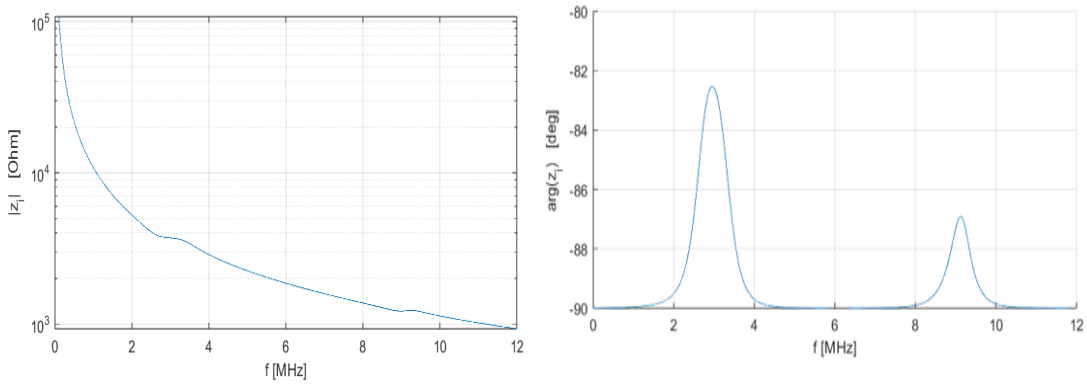

Figure 4.25 Electrical impedance of 2-2 composite of $LiNbO_3$ and RTV 3140 filler with water as load for Z-cut.

The transfer function for this model demonstrates as figure 4.26.

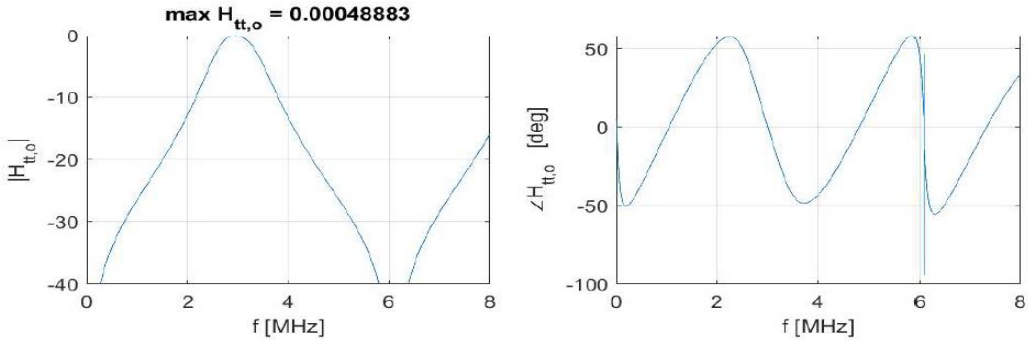

Figure 4.26 Transfer function of 2-2 composite of $LiNbO_3$ and RTV 3140 filler with water as load for Z-cut.

Due to the steel material being considered as the load instead of water, that is more suitable for high temperature applications, the ideal matching layer is considered as Niobium which is suitable because of its thermal stability at elevated temperatures.

The electrical impedance and transfer function for this 2-2 piezocomposite and steel as load are shown in figures 4.27 and 4.28, respectively.

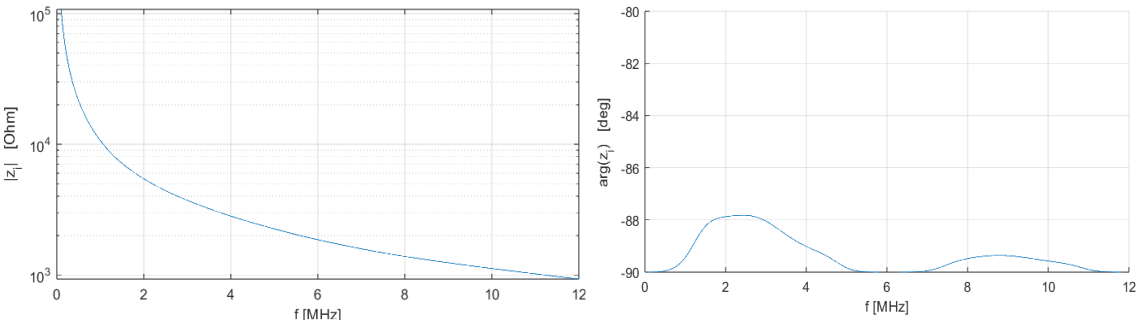

Figure 4.27 Electrical impedance of 2-2 composite of $LiNbO_3$ and RTV 3140 filler with steel as load for Z-cut.

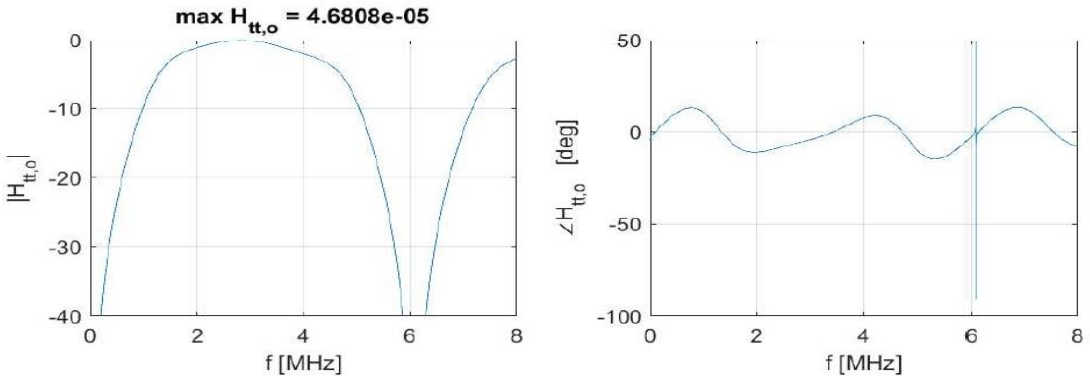

Figure 4.28 Transfer function of 2-2 composite of $LiNbO_3$ and RTV 3140 filler with steel as load for Z-cut.

4.5.3 Composite of $LiNbO_3$ and Air polymer for Z-cut

This section is considered as a composite of $LiNbO_3$ with air filler material. Figure 4.29 demonstrates the material parameters with respect to volume fraction of ceramic phase.

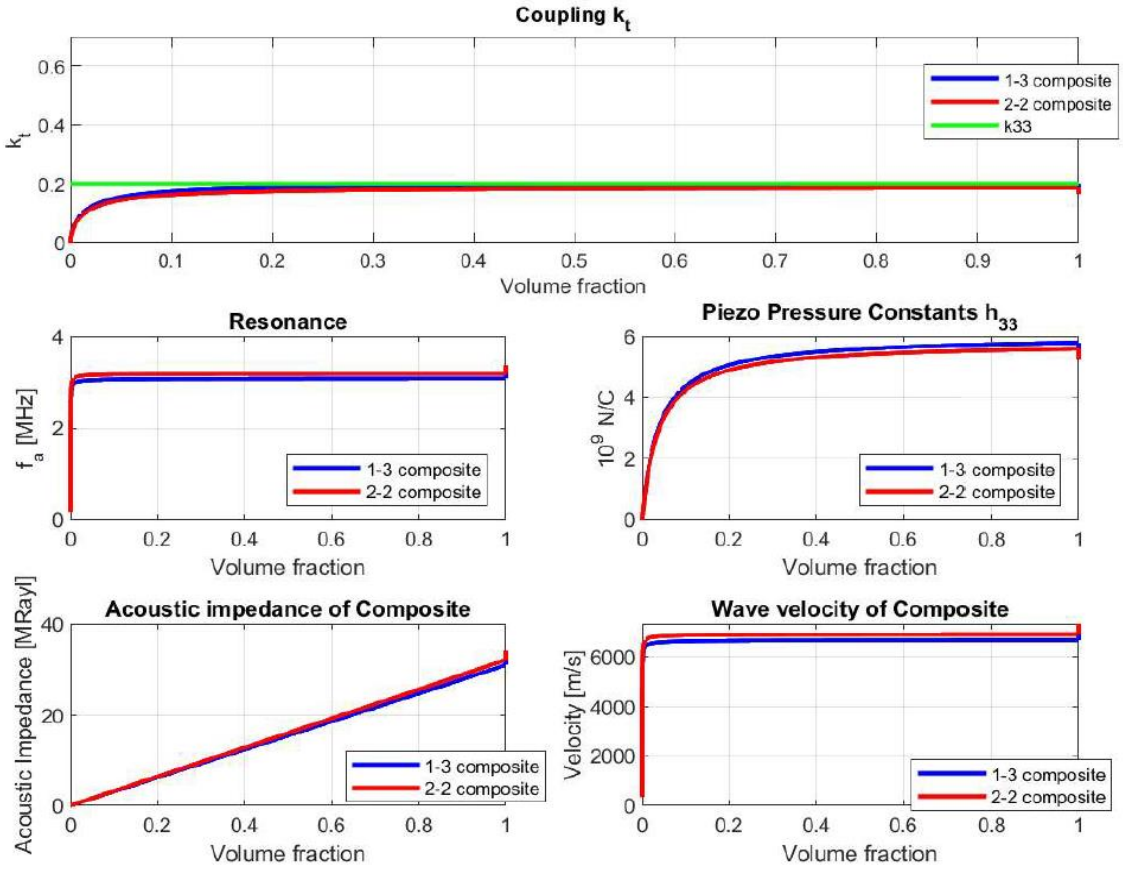

Figure 4.29 Variation with volume fraction of piezoelectric ceramic, v, of a composite's transducer parameters: specific acoustic impedance(Z); longitudinal-velocity (V_l); and thickness-mode electromechanical coupling constant (k_t), Material parameters are for $LiNbO_3$ ceramic and air polymer for Z-cut.

Figure of coupling coefficient (4.29a) demonstrates that when the volume fraction equals 1 (representing a bulk piezoelectric plate), the coupling coefficient reaches the thin plate coupling coefficient of k_t= 0.166. Conversely, when the volume fraction approaches zero, indicating a simple polymer without piezoelectric characteristics, k_t tends toward 0. For air epoxy material, the coupling coefficient peaks in 2-2 composite at around 0.186 and in 1-3 composite has higher value at around 0.190 for a volume fraction of roughly 0.8, as indicated in Figure above.

The K_{33} that shows there is no stiffness in filler material (free pillars) is equal to 0.2.

For X-Trans simulation, we utilized the material parameters based on acoustic impedance, wave velocity, and piezo pressure constant provided earlier. The corresponding values for both composites are listed in the table presented below, the material values for bulk $LiNbO_3$ were also included for comparison with the composite plate.

We assumed that the area for both 1-3 and 2-2 composites is the same as bulk $LiNbO_3$.

To simulate the one-dimensional Mason model in Xtrans, it has been used the material parameters related to Figure 4.29 to list the material parameters of 1-3 and 2-2 composites of $LiNbO_3$ with air filler in table 4.9 as below.

Table 4.9: Fitting of material parameters of the $LiNbO_3$, air-filled piezocomposite for one-dimensional Mason modelling in Xtrans for Z-cut.

Parameter	Bulk $LiNbO_3$	1-3 composite ($LiNbO_3$/ air)	2-2 composite ($LiNbO_3$/ air)
A [mm^2]	78.5	78.5	78.5
h_{33} [10^8 V/m]	51	57.4	55.5
$\varepsilon^S / \varepsilon_0$	27.9	22.6	22.5
Z[MRayls]	33.6	24.9	25.7
c_l [m/s]	7316	6674.7	6913

The electrical impedance and transfer function are shown in future figures for both water and steel as load. The matching layer is used as EpoTek3012+ 10% Al_2O_3 when the load is water [22] and is selected as Niobium when the load is steel [23].

Table 4-10: Material properties for different layers of the air-filled, 1-3piezocomposite in one dimensional Mason Model for Z-cut.

Material	Z [MRayls]	C [m/s]	Q
Backing layer (Air)	0.000413	343	10
Matching layer Load(water)	3.83 1.5	2580.6 1540	10
Matching layer Load (Steel)	38.54 46	4920 5980	10

The simulation is done by X-trans with using the values refer to table 4.9and table 4.10 and center frequency of 3MHz.

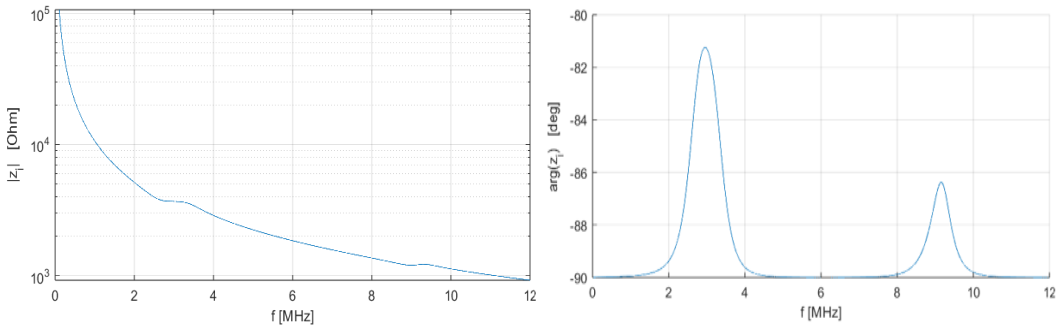

Figure 4.30 Electrical impedance of 1-3 composite of $LiNbO_3$ and air filler with water as load for Z-cut.

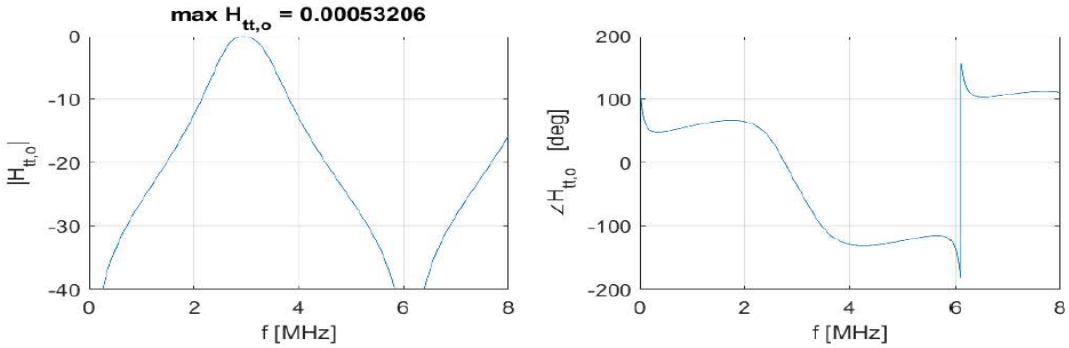

Figure 4.31 Transfer function of 1-3 composite of $LiNbO_3$ and air filler with water as load for Z-cut.

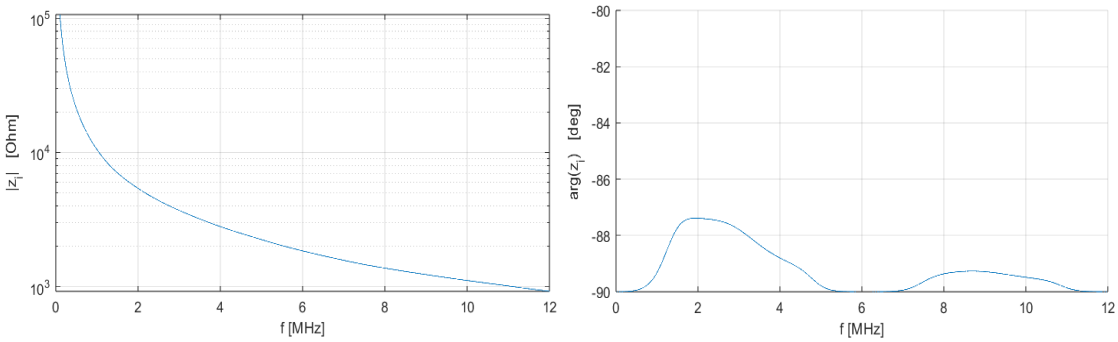

Figure 4.32 Electrical impedance of 1-3 composite of $LiNbO_3$ and air filler with steel as load for Z-cut.

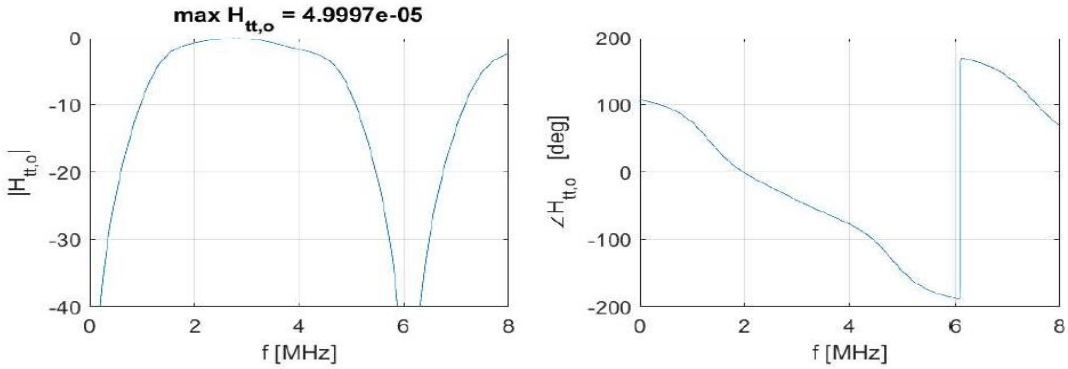

Figure 4.33 Transfer function of 1-3 composite of $LiNbO_3$ and air filler with steel as load for Z-cut.

This part is dedicated to simulation of 2-2 composite of $LiNbO_3$ and air as polymer material which it is used the values from table 4.9 and table 4.11 for different layers and both load as water and steel. The matching layer choosing is the same as 1-3 composite that has explained before.

Table 4-11: Material properties for different layers of the air -filled 2-2piezocomposite in one dimensional Mason Model for Z-cut.

Material	Z [MRayls]	C [m/s]	Q
Backing layer (Air)	0.000413	343	10
Matching layer Load (water)	3.87 1.5	2580.6 1540	10
Matching layer [23] Load (Steel)	38.54 46	4920 5980	10

The electrical impedance and transfer function are illustrated as figures below.

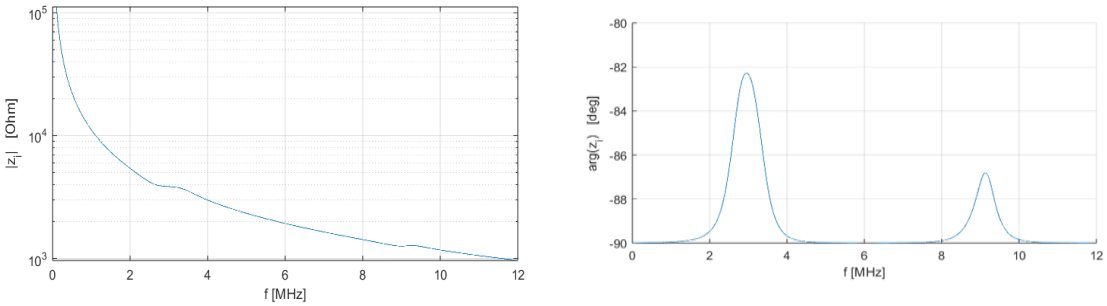

Figure 4.34 Electrical impedance of 2-2 composite of $LiNbO_3$ and air filler with water as load for Z-cut.

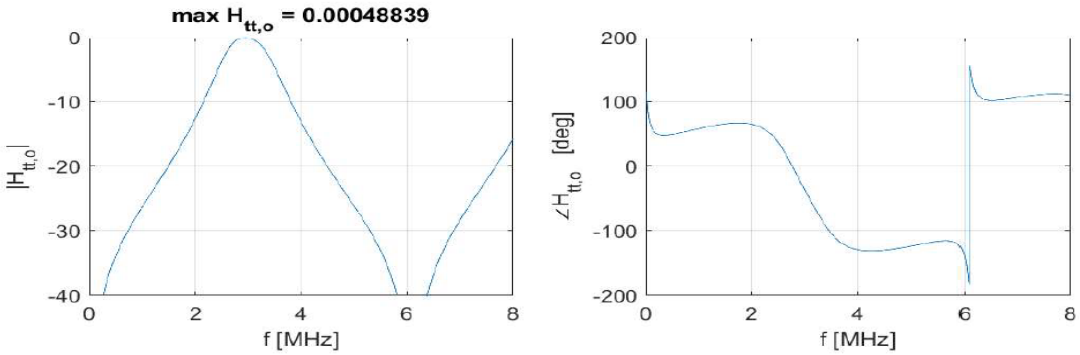

Figure 4.35 Transfer function of 2-2 composite of $LiNbO_3$ and air filler with water as load for Z-cut.

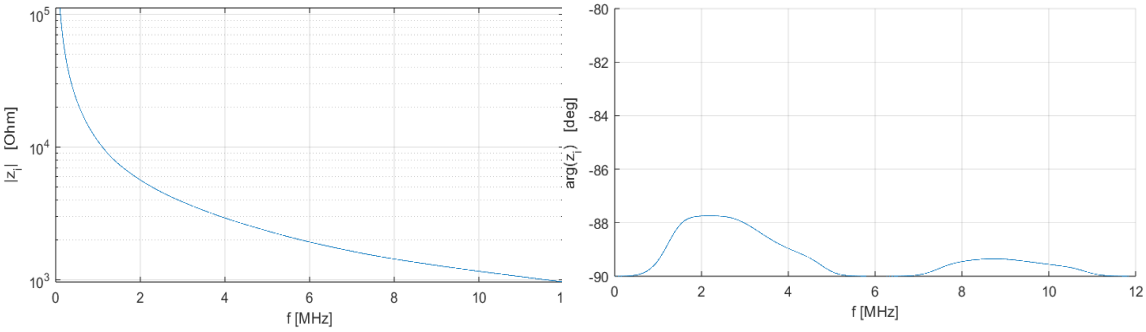

Figure 4.36 Electrical impedance of 2-2 composite of $LiNbO_3$ and air filler with steel as load for Z-cut

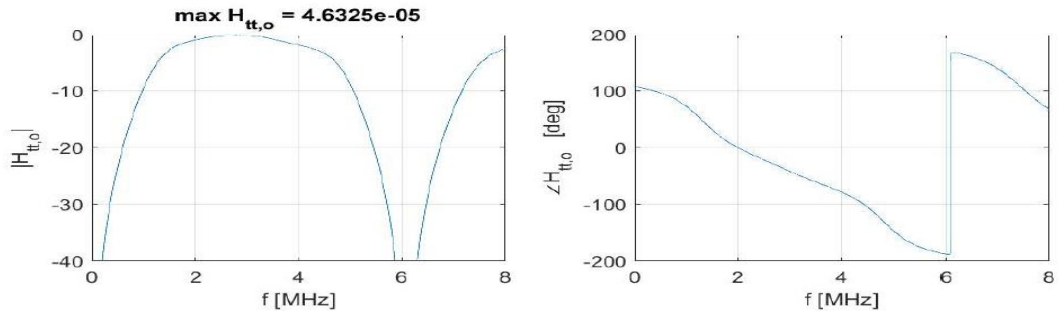

Figure 4.37 Transfer function of 2-2 composite of $LiNbO_3$ and air filler with steel as load for Z-cut.

4.6 Composite properties for 36˚/Y -cut

4.6.1 Composite of $LiNbO_3$ and EpoTek 3012 polymer for 36˚/Y-cut

This section is considered as composite of $LiNbO_3$ with EpoTek 3012 filler material. Figure 4.38 demonstrates the material parameters with respect to volume fraction of ceramic phase.

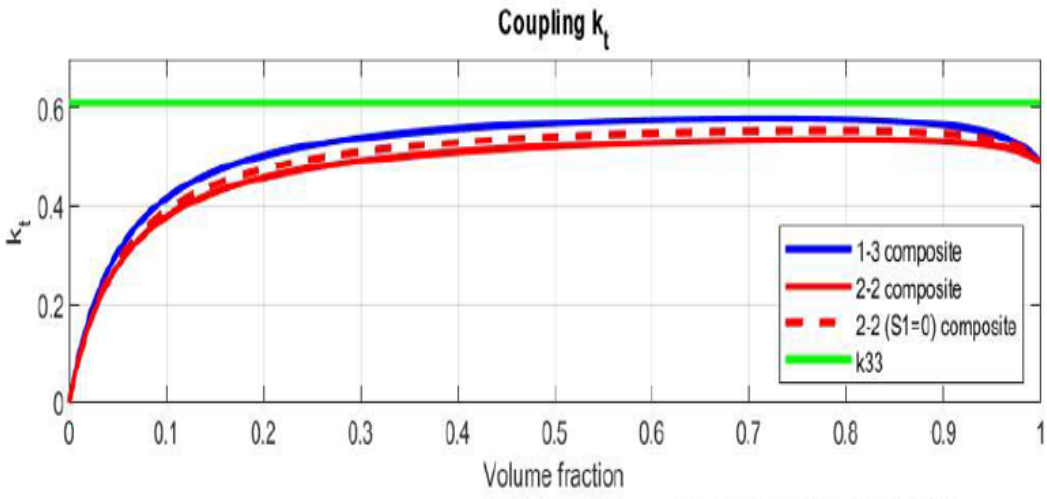

(a)

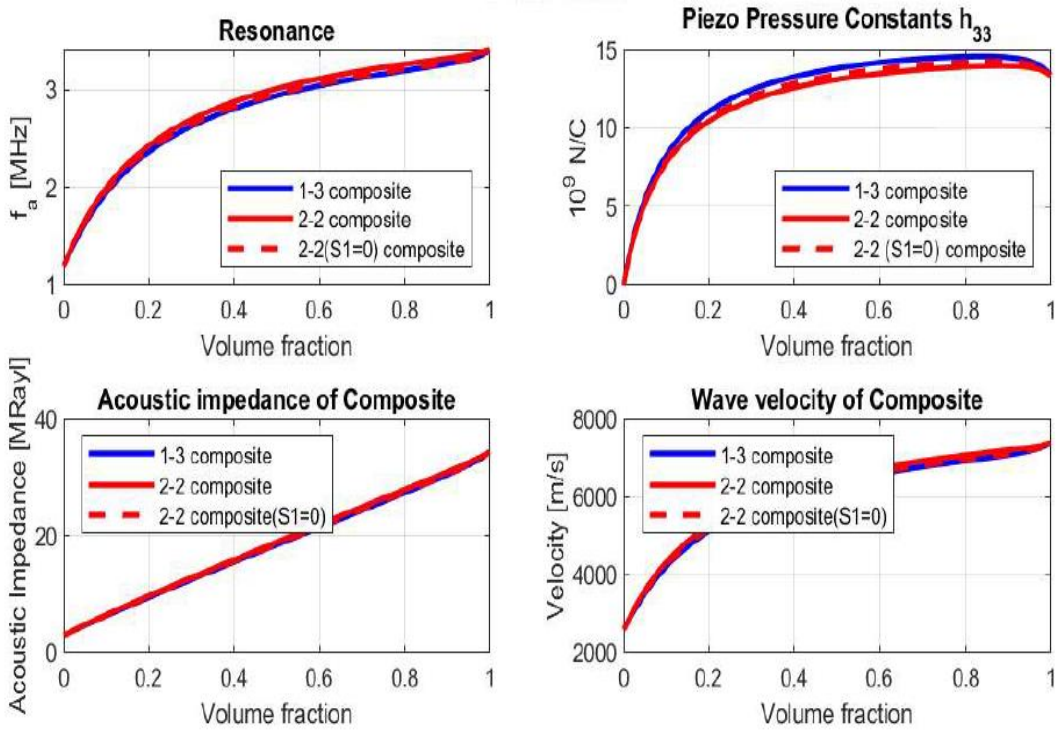

Figure 4.38 Variation with volume fraction of piezoelectric ceramic, v, of a composite's transducer parameters: specific acoustic impedance(Z); longitudinal-velocity (V_l); and thickness-mode electromechanical coupling constant (k_t), Material parameters are for $LiNbO_3$ ceramic and EpoTek 3012 polymer for 36 °Y-cut.

Figure of coupling coefficient (4.38a) demonstrates that the coupling coefficient reaches the thin plate coupling coefficient of k_t= 0.49 when the volume fraction equals 1 (representing a bulk piezoelectric plate). Conversely, when the volume fraction approaches zero, indicating a simple polymer without piezoelectric characteristics, k_t tends toward 0. The figure (4.38) illustrates the variations in material parameters for both 1-3 composite and two distinct 2-2 composites. These variations arise due to the strain being clamped in different directions, as detailed in the constitutive equations provided in the preceding chapter. For EpoTek 3012 epoxy material, the coupling coefficient peaks in 2-2 composite (S_1= 0) at around 0.553, in 2-2 composite (S_2= 0) at around 0.534 and in 1-3 composite has higher value at around 0.575 for a volume fraction of roughly 0.8, as indicated in Figure above.

The K_{33} that shows there is no stiffness in filler material (free pillars) is equal to 0.61.

For X-Trans simulation, the material parameters derived from acoustic impedance, wave velocity, and piezo pressure constant, as provided earlier, are listed. The table below presents the corresponding values for both composites, alongside the material properties of bulk $LiNbO_3$ for comparison with the composite plate.

We assumed that the area for both 1-3 and 2-2 composites is the same as bulk $LiNbO_3$.

To simulate the one-dimensional Mason model in Xtrans, we have used the material parameters related to Figure 4.38 to list the material parameters of 1-3 and two distinct 2-2 composites of $LiNbO_3$ with EpoTek 3012 filler in table 4.12 as below.

Table 4.12: Fitting of material parameters of the $LiNbO_3$, EpoTek 3012-filled piezocomposite for one-dimensional Mason modelling in Xtrans for 36°Y-cut.

Parameter	Bulk $LiNbO_3$	1-3 composite ($LiNbO_3$/ EpoTek3012)	2-2 composite (S_1=0) ($LiNbO_3$/EpoTek3012)	2-2 composite (S_2=0) ($LiNbO_3$/EpoTek301)
A [mm^2]	78.5	78.5	78.5	78.5
h_{33}[10^8V/m]	133	145.6	142.1	139.2
$\varepsilon^S / \varepsilon_0$	38.6	33.4	32.7	32.9
Z[MRayls]	33.7	27.3	27.4	27.9
c_l [m/s]	7340	6920.2	6959.3	7063

Upon comparing the values in the table, it becomes evident that the 1-3 composite exhibits the highest piezoelectric pressure constant (h_{33}) and the lowest acoustic impedance and wave velocity values. Consequently, it proves to be the most efficient ultrasonic transducer, offering greater sensitivity (a higher coupling factor tends to correlate with higher sensitivity because the transducer can detect smaller changes in the measured quantity) compared to both the plate and the 2-2 composite.

Table 4.13 illustrates the values corresponding to various layers of the 1-3 piezocomposite within the Mason model for this cut.

To enhance transmission, it is imperative to incorporate a single matching layer, as outlined by the Eq. (2.17) in which the load is chosen as water and steel. For determining the optimal matching layer within this acoustic impedance range, the selection is (EpoTek 3012 + 10% Al_2O_3) [22] for the load as water and silver when the load is steel [23].

Table 4-13: Material properties for different layers of the $LiNbO_3$, EpoTek 3012-filled 1-3piezocomposite in one dimensional Mason Model for36 ◦Y-cut.

Material	Z [MRayls]	C [m/s]	Q
Backing layer (Air)	0.000413	343	10
Matching layer [22]. Load (water)	3.95 1.5	2580.6 1540	10
Matching layer [23]. Load (Steel)	38.6 46	3600 5980	10

Figure 4.39 demonstrates the electrical impedance for 1-3 composite of $LiNbO_3$ and EpoTek- 3012 as polymer material in this cut that the water is used as load. The values for the composite and different layers 's parameters are listed in table 4.12 and 4.13, respectively.

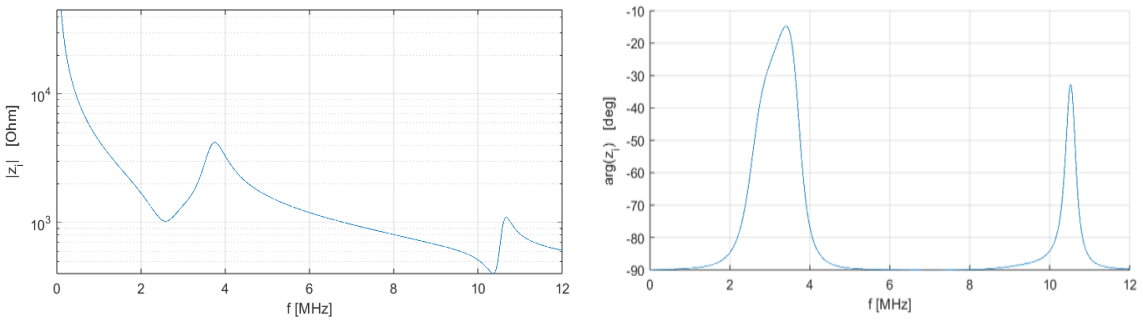

Figure 4.39 Electrical impedance of 1-3 composite of $LiNbO_3$ and EpoTek 3012-filler with water as load for 36 ◦Y-cut.

This part is shown the transfer function for different composites based on table 4.12 and steel as load with ideal matching layer with parameters based on table 4.13. The transfer function for different composites will be compared with lithium niobate plate.

Figure 4.40 shows the transfer function for plate, 1-3, 2-2 composite in different directions when the load is chosen as steel. It is expected that the 1-3 composite could have the higher bandwidth because of its higher coupling coefficient and piezo pressure constant. So, the next part will be compared the transfer function for this composite in different loads as water and steel with ideal matching layer and without matching layer for steel load based on parameters of table 4.13.

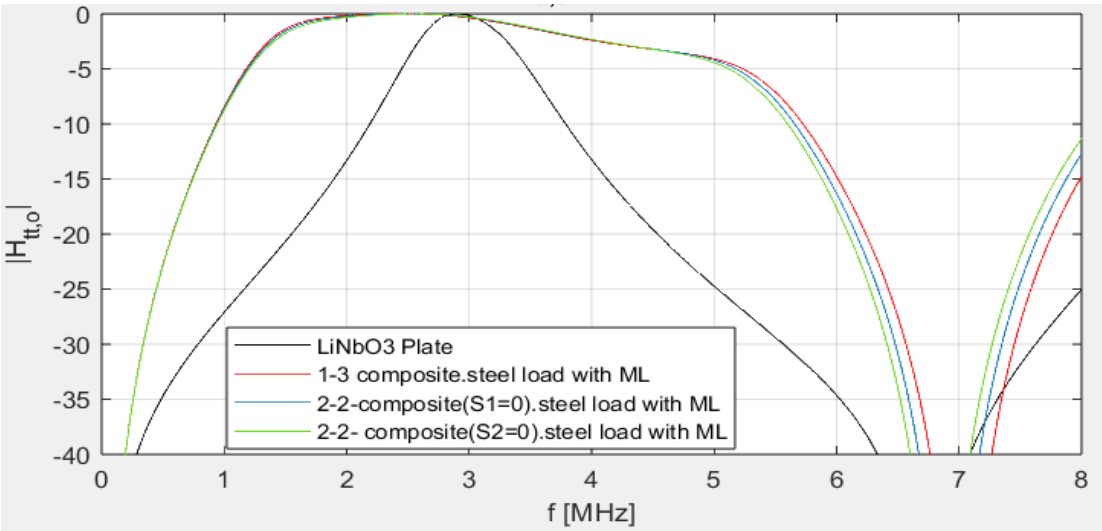

Figure 4.40 Transfer function of three types of composites of $LiNbO_3$ and EpoTek 3012-filler for 36˚Y-cut with the steel as load and ideal matching layer as Silver, Plate in black line, 1-3 composite in red one, 2-2 composite (S1=0) in blue one and 2-2 composite (S2=0) in green line.

This part is dedicated to compare the transfer function in different ways as plate with water loading and matching layer, 1-3 composite with water load and ideal matching layer, 1-3 composite with steel load and no matching layer, and 1-3 composite with steel and ideal matching layer based on table.4.13.

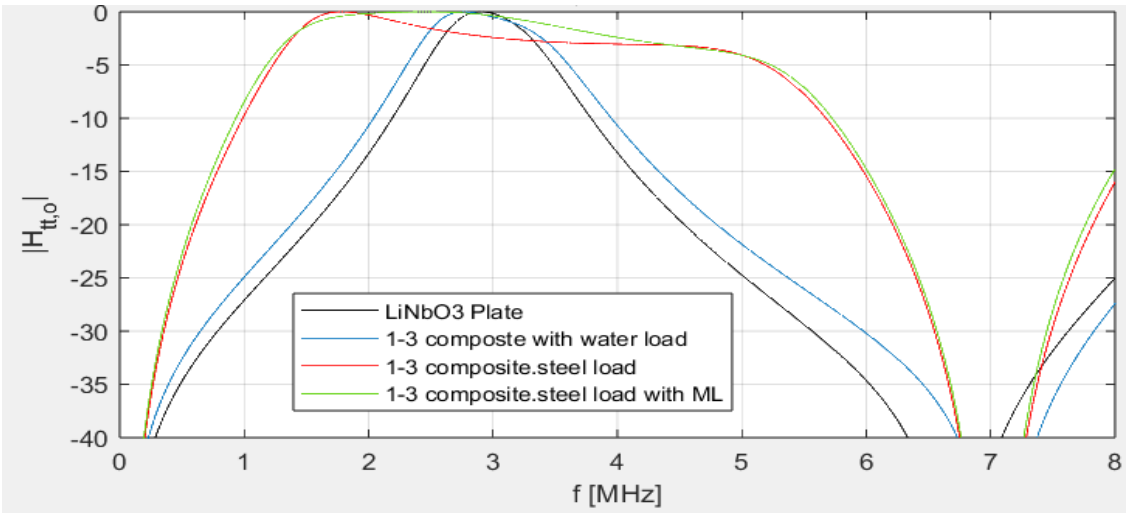

Figure 4.41 Transfer function of 1-3 composite of $LiNbO_3$ and EpoTek 3012-filler for 36 ˚Y-cut, Plate in black line, 1-3 composite with water load as blue line, composite with steel load without any matching layer as red line and composite with steel load and ideal matching layer in green line.

This result shows that by making the composite and choosing the ideal matching layer, the bandwidth of transmission will be increased.

The next composite is considered as 2-2 composite that is clamped in first direction and there is no strain in this direction. For simulation in X.Trans, the values refer to table 4.12 and 4.14 are used. The best matching layer for this range of acoustic impedance is chosen as EpoTek 3012 + 10% Al_2O_3.

Table 4-14 Material properties for different layers of the $LiNbO_3$, EpoTek 3012-filled 2-2 piezocomposite (S_1= 0) in one dimensional Mason Model for 36 ◦Y-cut.

Material	Z [MRayls]	C [m/s]	Q
Backing layer (Air)	0.000413	343	10
Matching layer [22]. Load (water)	3.95 1.5	2580.6 1540	10
Matching layer (Silver) [23]. Load (Steel)	38.7 46	3600 5980	10

The electrical impedance and transfer function for this composite by using water as load are shown below. The acoustic matching layer is the same as previously.

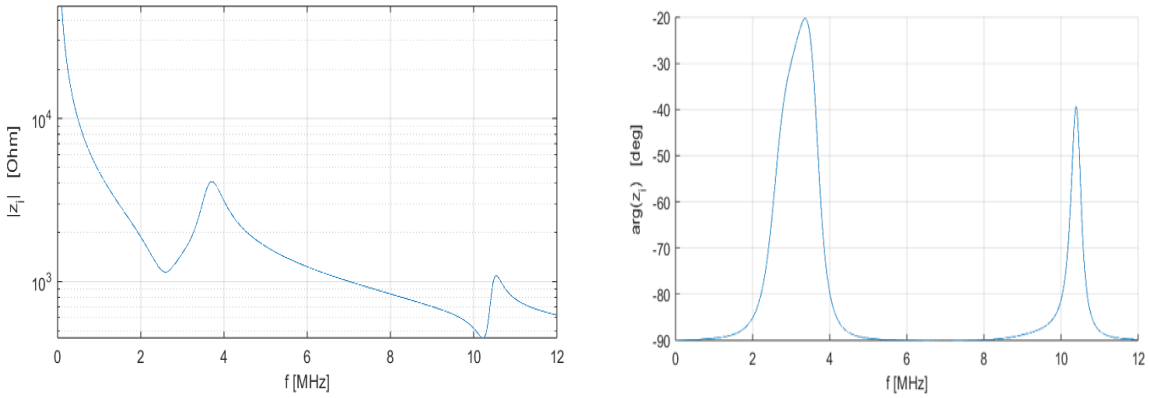

Figure 4.42 Electrical impedance of 2-2 composite (S_1=0) of $LiNbO_3$ and EpoTek 3012-filler with water as load for 36 ◦Y-cut

Next section illustrates the behavior of 2-2 composite of lithium niobate and EpoTek-3012 polymer that is clamped in 2nd direction and strain is zero *(S_2= 0)* in this direction which is different with previous direction. The value for this composite is listed in table 4.12 and table 4.15 shows the material parameters of different layers.

The load is chosen water for first step and the matching layer is the same as 1-3 composite as EpoTek 3012 + 10% Al_2O_3 [22].

When the load is selected as steel, the ideal matching can be achieved based on Eq.2.17.

Table 4-15Material properties for different layers of the $LiNbO_3$, EpoTek 3012-filled 2-2 piezocomposite (S_2= 0) in one dimensional Mason Model for 36 ◦Y-cut.

Material	Z [MRayls]	C [m/s]	Q
Backing layer (Air)	0.000413	343	10
Matching layer [22]. Load (water)	3.95 1.5	2580.6 1540	10
Matching layer (Silver) [23]. Load (Steel)	38.9 46	3600 5980	10

The electrical impedance for this composite refers to values of table 4.12 and 4.15 that is shown in figure 4.43 as below.

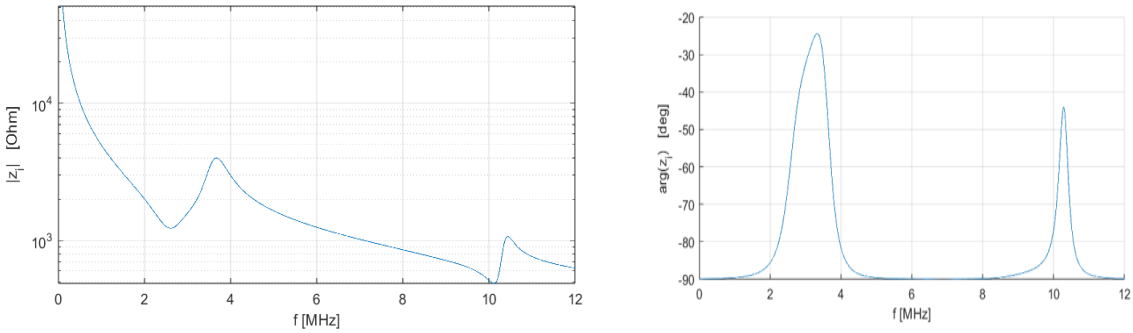

Figure 4.43 Electrical impedance of 2-2 composite (S_2=0) of $LiNbO_3$ and EpoTek 3012-filler with water as load for 36 ◦Y-cut.

4.6.2 Composite of LiNbO3 and RTV -3140 polymer for 36°/Y-cut

This section is considered as composite of $LiNbO_3$ with RTV-3140 filler material. Figure 4.44 demonstrates the material parameters with respect to volume fraction of ceramic phase.

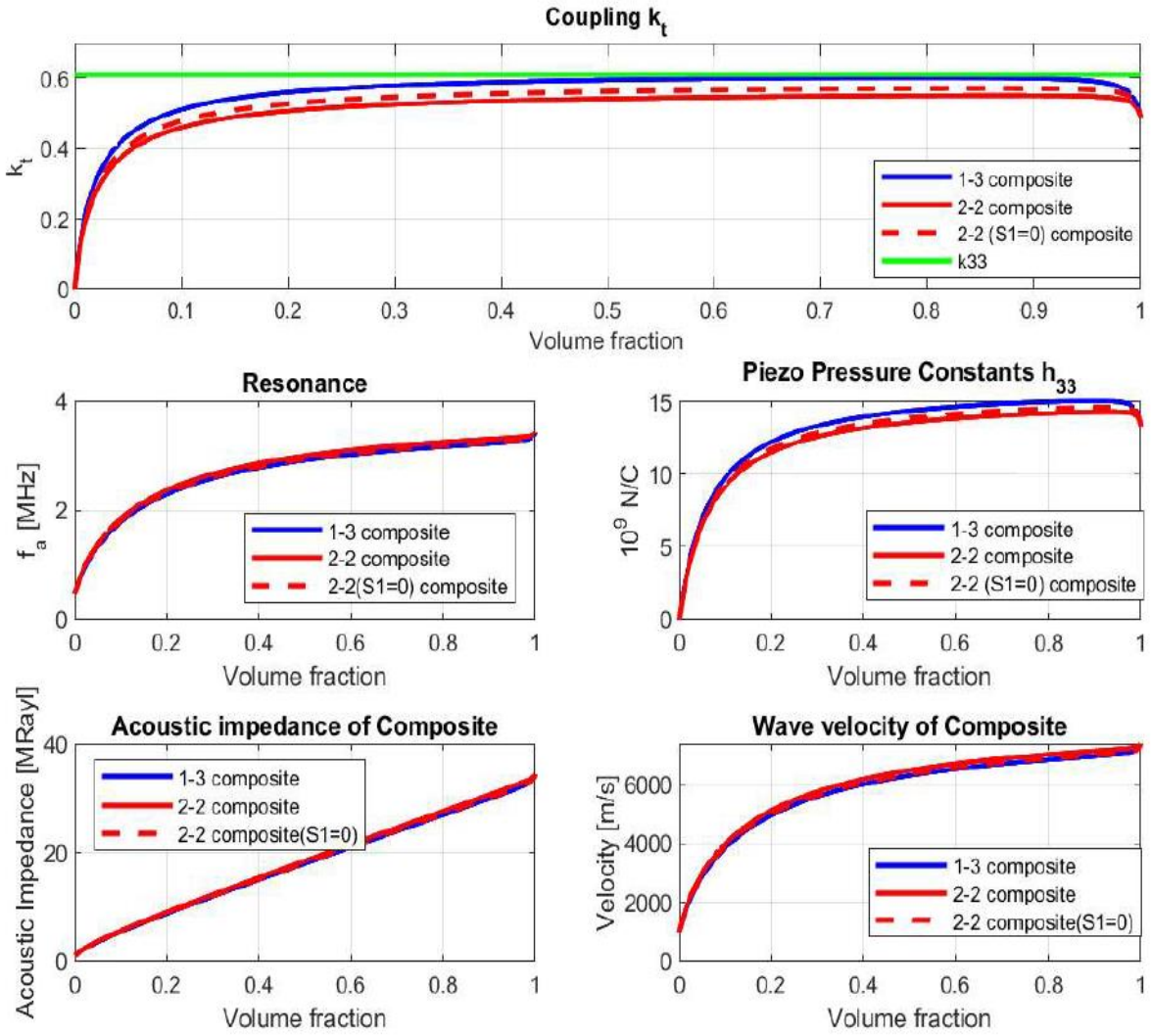

Figure 4.44 Variation with volume fraction of piezoelectric ceramic, v, of a composite's transducer parameters: specific acoustic impedance(Z); longitudinal-velocity (V_l); and thickness-mode electromechanical coupling constant (k_t), Material parameters are for $LiNbO_3$ ceramic and RTV 3140 polymer for 36°Y-cut.

Figure of coupling coefficient (4.44a) demonstrates that the coupling coefficient reaches the thin plate coupling coefficient of k_t= 0.49 when the volume fraction equals 1 (representing a bulk piezoelectric plate). Conversely, when the volume fraction approaches zero, indicating a simple polymer without piezoelectric characteristics, k_t

tends toward 0. The figure (4.44) illustrates the variations in material parameters for both 1-3 composite and two distinct 2-2 composites. These variations arise due to the strain being clamped in different directions, as detailed in the constitutive equations provided in the preceding chapter. For RTV 3140 epoxy material, the coupling coefficient peaks in 2-2 composite (S_1= 0) at around 0.57, in 2-2 composite (S_2= 0) at around 0.55 and in 1-3 composite has higher value at around 0.6 for a volume fraction of roughly 0.8, as indicated in Figure above.

The K_{33} that shows there is no stiffness in filler material (free pillars) is equal to 0.61.

For X-Trans simulation, it is employed the material parameters derived from acoustic impedance, wave velocity, and piezo pressure constant as previously provided. The table below presents the corresponding values for both composites, alongside the material properties of bulk $LiNbO_3$ for comparison with the composite plate.

We assumed that the area for both 1-3 and 2-2 composites is the same as bulk $LiNbO_3$.

To simulate the one-dimensional Mason model in Xtrans, we have used the material parameters related to Figure 4.44 to list the material parameters of 1-3 and two distinct 2-2 composites of $LiNbO_3$ with RTV 3140 filler in table 4.16 as below.

Table 4.16: Fitting of material parameters of the $LiNbO_3$, RTV 3140-filled piezocomposite for one-dimensional Mason modelling in Xtrans for 36°Y-cut.

Parameter	Bulk $LiNbO_3$	1-3 composite ($LiNbO_3$/ RTV)	2-2composite (S_1=0) ($LiNbO_3$/ RTV)	2-2composite (S_2=0) ($LiNbO_3$/ RTV)
A [mm^2]	78.5	78.5	78.5	78.5
h_{33} [10^8 V/m]	133	150	145.3	142
$\varepsilon^S / \varepsilon_0$	38.6	33.5	32.6	32.8
Z[MRayls]	33.7	26.9	27.2	27.7
c_l [m/s]	7340	6848.7	6901.8	7031

The initial section pertains to the composite of $LiNbO_3$ and RTV-3140 for a 36°/Y-cut, with the values for various layers provided in Table 4.16. When considering water as the load, the optimal single matching layer selected is Epotek 3012+ with 10% Al_2O_3 [22]. However, when steel is the load, there is no requirement for a matching layer due to the close

acoustic impedance between steel and lithium niobate, but for the ideal transmission of sound waves, silver is selected as matching layer[23].

Table 4-17 Material properties for different layers of the $LiNbO_3$, RTV 3140-filled 1-3 piezocomposite in one dimensional Mason Model for 36 ◦Y-cut.

Material	Z [MRayls]	C [m/s]	Q
Backing layer (Air)	0.000413	343	10
Matching layer [22]	3.93	2580.6	10
Load (water)	1.5	1540	
Matching layer (Silver) [23]	38.5	3600	10
Load (Steel)	46	5980	

The electrical impedance and for this composite related to above tables are shown in advance for water as load.

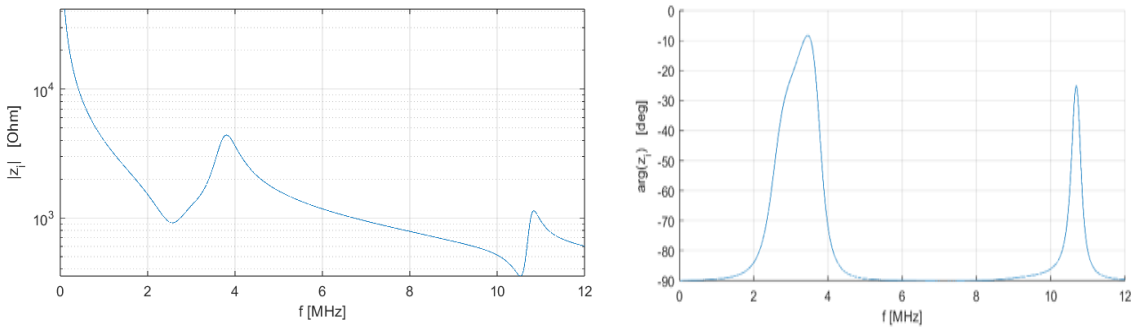

Figure 4.45 Electrical impedance of 1-3 composite of $LiNbO_3$ and RTV 3140-filler with water as load for 36 ◦Y-cut.

This part is dedicated to transfer function for different composites based on table 4.16 for composite of $LiNbO_3$ and RTV polymer for steel as load with ideal matching layer with parameters based on table 4.17. The transfer function for different composites will be compared with lithium niobate plate.

Figure 4.46 shows the transfer function for plate, 1-3, 2-2 composite in different directions when the strain is clamped for load as steel. The expectation is that the 1-3 composite would have the higher bandwidth because of its higher coupling coefficient and piezo pressure constant. So, the next part will be compared the transfer function for this composite in different loads as water and steel with ideal matching layer and without matching layer for steel load based on parameters of table 4.17.

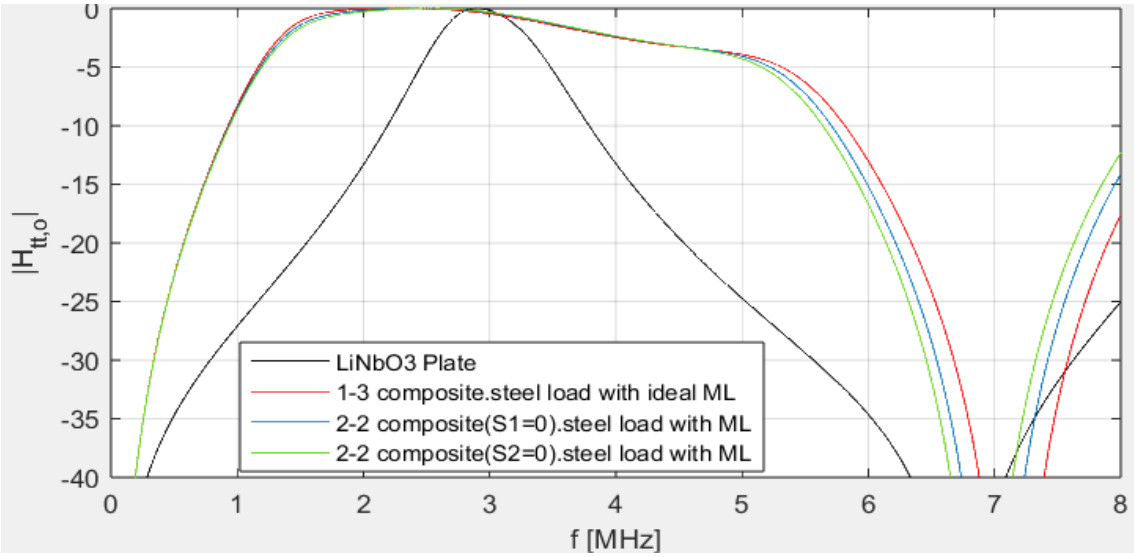

Figure 4.46 Transfer function of three types of composites of $LiNbO_3$ and RTV 3140-filler for 36°Y-cut with the steel as load and ideal matching layer as Silver, Plate in black line, 1-3 composite in red line, 2-2 composite (S1=0) in blue one and 2-2 composite (S2=0) in green line.

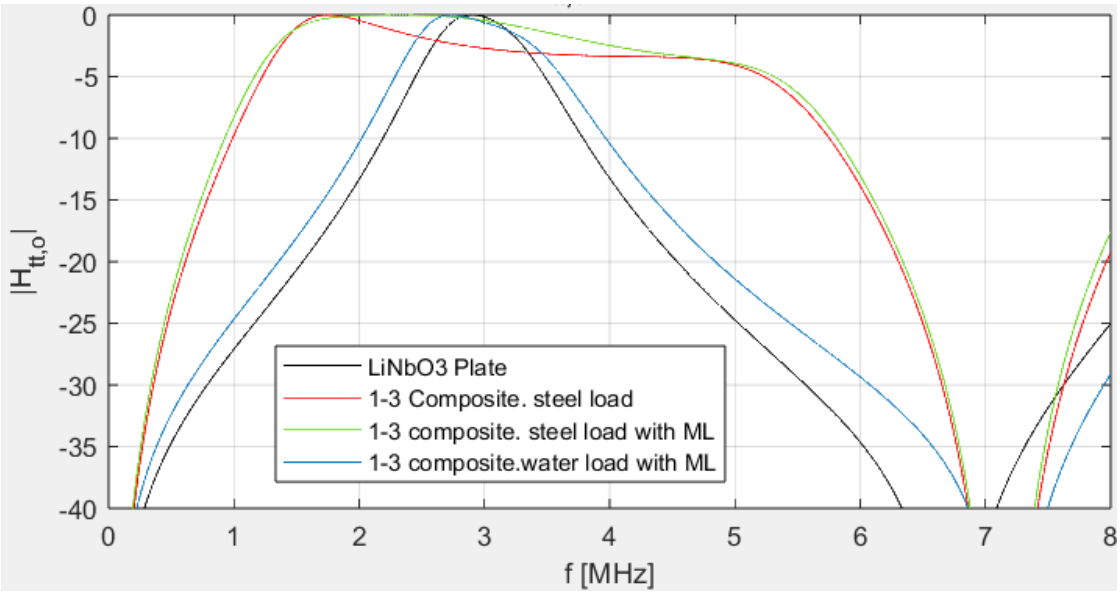

Figure 4.47 Transfer function of 1-3 composite of $LiNbO_3$ and RTV 3140-filler for 36°Y-cut, Plate in black line, 1-3 composite with water load as blue line, composite with steel load without any matching layer as red line and composite with steel load and ideal matching layer in green line.

This part is related to simulation of 2-2 composite when it is clamped in first direction and strain is equal zero(S_1=0). The values for these composite and different layers are listed in 4.16 and 4.18, respectively. The electrical impedance and transfer function for loading water and steel are shown in the figures below.

Table 4-18 Material properties for different layers of the $LiNbO_3$, RTV 3140-filled 2-2 piezocomposite(S_1=0) in one dimensional Mason Model for 36 ◦Y-cut.

Material	Z [MRayls]	C [m/s]	Q
Backing layer (Air)	0.000413	343	10
Matching layer [22]	3.93	2580.6	10
Load (water)	1.5	1540	
Matching layer (Silver) [23]	38.61	3600	10
Load (Steel)	46	5980	

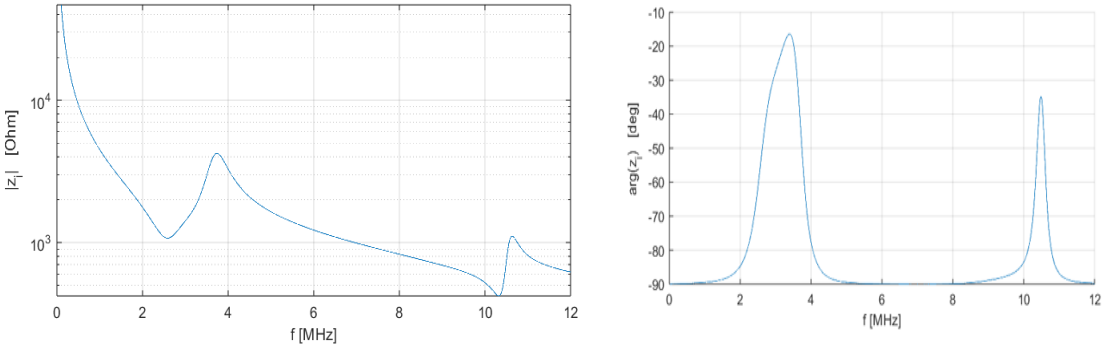

Figure 4.48 Electrical impedance of 2-2 composite (S_1=0) of $LiNbO_3$ and RTV 3140-filler with water as load for 36 ◦Y-cut.

The last part of this section is dedicated to 2-2 composite when it is clamped in 2nd direction (S_2=0). It will be simulated in X. Trans by values refer to tables 4.16 and 4.19.

Table 4-19 Material properties for different layers of the $LiNbO_3$, RTV 3140-filled 2-2 piezocomposite(S_2=0) in one dimensional Mason Model for 36 ◦Y-cut.

Material	Z [MRayls]	C [m/s]	Q
Backing layer (Air)	0.000413	343	10
Matching layer [22]	3.93	2580.6	10
Load (water)	1.5	1540	
Matching layer (Silver) [23]	38.8	3600	10
Load (Steel)	46	5980	

The electrical impedance and transfer function are illustrated in advance figures for water load.

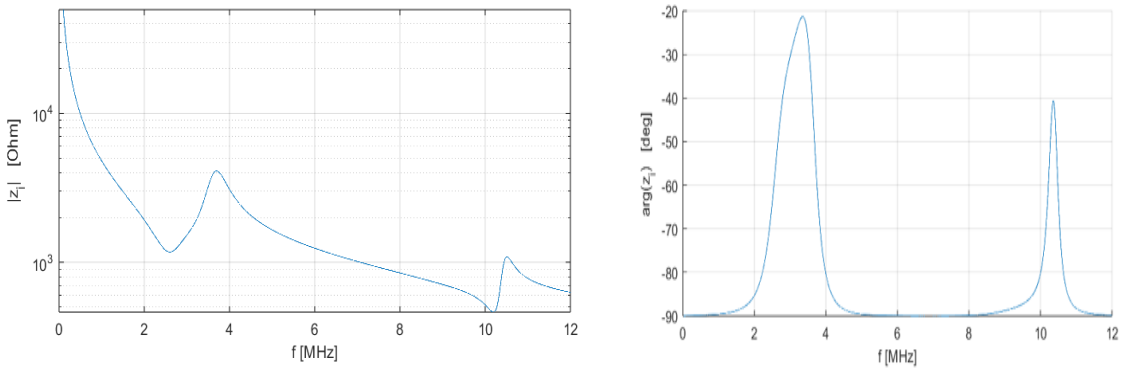

Figure 4.49 Electrical impedance of 2-2 composite (S_2=0) *of* $LiNbO_3$ *and RTV 3140-filler with* water as load for 36 *°Y-cut.*

4.6.3 Composite of LiNbO3 and Air polymer for 36 °/Y-cut

This part represents a composite comprised of $LiNbO_3$ and air filler material. Figure 4.50 illustrates the material parameters concerning the volume fraction of the ceramic phase.

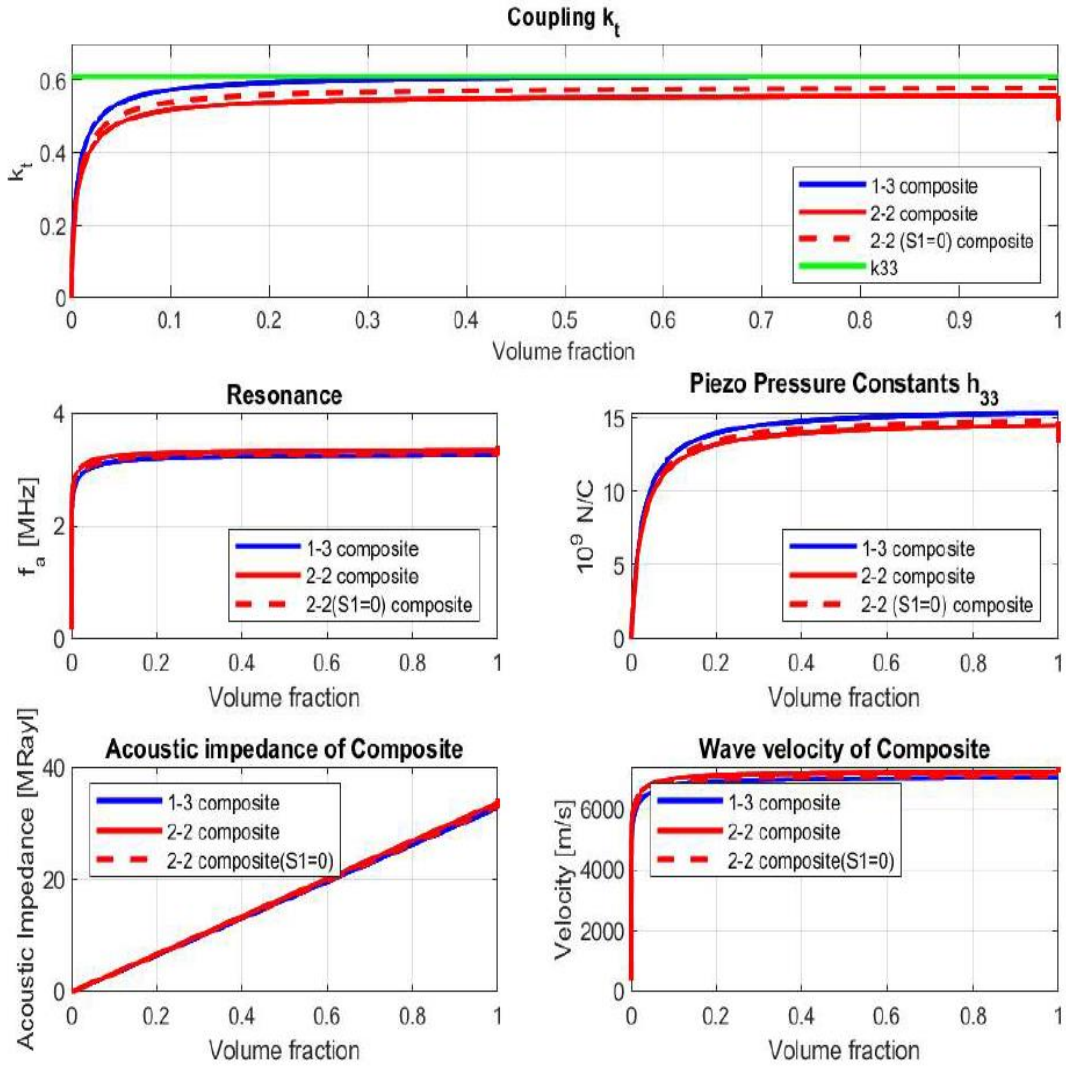

Figure 4.50 Variation with volume fraction of piezoelectric ceramic, v, of a composite's transducer parameters: specific acoustic impedance(Z); longitudinal-velocity (V_l); and thickness-mode electromechanical coupling constant (k_t), Material parameters are for $LiNbO_3$ ceramic and air polymer for 36 °Y-cut.

The figure illustrating the coupling coefficient (4. 50a) shows that the coupling coefficient reaches the thin plate coupling coefficient of k_t = 0.49 when the volume fraction equals 1, indicating a bulk piezoelectric plate. Conversely, as the volume fraction decreases towards zero, indicating the presence of a simple polymer without piezoelectric

properties, k_t tends toward 0. The figure (4. 50) illustrates the variations in material parameters for both 1-3 composite and two distinct 2-2 composites. According to the constitutive equations in the preceding chapter, these variations arise because strain is clamped in different directions. For air epoxy material, the coupling coefficient peaks in 2-2 composite (S_1= 0) at around 0.576, in 2-2 composite (S_2= 0) at around 0.554 and in 1-3 composite has higher value at around 0.609 for a volume fraction of roughly 0.8, as indicated in Figure above.

The K_{33} that shows there is no stiffness in filler material (free pillars) is equal to 0.61.

For X-Trans simulation, based on the previously provided acoustic impedance, wave velocity, and piezo pressure constant, the material parameters are used. The table below presents the corresponding values for both composites, alongside the material properties of bulk $LiNbO_3$ for comparison with the composite plate. It is assumed that the area for both 1-3 and 2-2 composites is the same as bulk $LiNbO_3$.

To simulate the one-dimensional Mason model in Xtrans, we have used the material parameters related to Figure 4. 50 to list the material parameters of 1-3 and two distinct 2-2 composites of $LiNbO_3$ with air filler in table 4.20 as below.

Table 4-20: Fitting of material parameters of the $LiNbO_3$, Air-filled piezocomposite for one-dimensional Mason modelling in Xtrans for 36°Y-cut.

Parameter	Bulk $LiNbO_3$	1-3 composite ($LiNbO_3$/ Air)	2-2 composite(S_1=0) ($LiNbO_3$/ *Air*)	2-2 composite(S_2=0) ($LiNbO_3$/ Air)
A [mm^2]	78.5	78.5	78.5	78.5
h_{33} [10^8 V/m]	133	152.4	147.2	144
$\varepsilon^S / \varepsilon_0$	38.6	33.2	32.4	32.6
Z[MRayls]	33.7	26.1	26.4	26.8
c_l [m/s]	7340	7025.7	7086.03	7220.8

Table 4-21 Material properties for different layers of the $LiNbO_3$, Air-filled 1-3 piezocomposite in one dimensional Mason Model for 36°Y-cut.

Material	Z [MRayls]	C [m/s]	Q
Backing layer (Air)	0.000413	343	10
Matching layer [22]	3.93	2580.6	10
Load (water)	1.5	1540	
Matching layer (Silver) [23]	38.08	3600	10
Load (Steel)	46	5980	

The electrical impedance for 1-3 composite of lithium niobate and air filler material are shown in figure 4.51. The load is taken as water and matching layer is calculated and is same as previous sections. (EpoTek 3012+ 10% Al_2O_3).

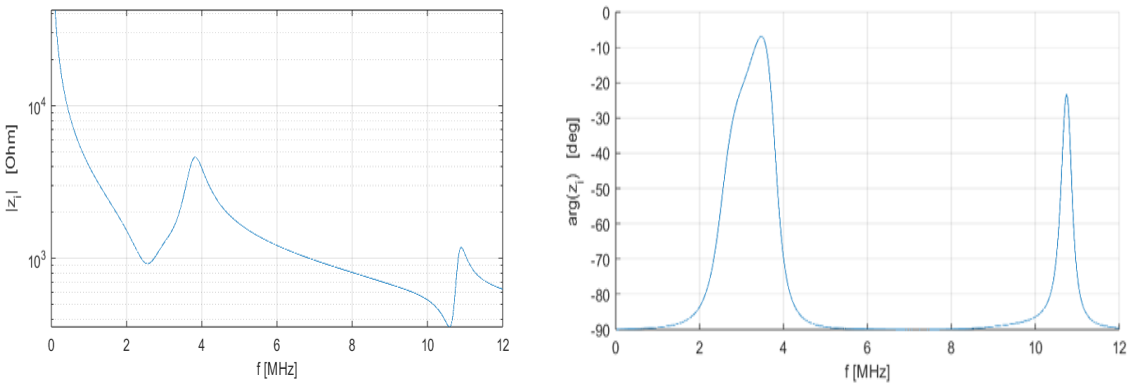

Figure 4.51 Electrical impedance of 1-3 composite of $LiNbO_3$ and Air-filler with water as load for 36°Y-cut.

This part is dedicated to transfer function for different composites based on table 4.20 for composite of $LiNbO_3$ and air for steel as load with ideal matching layer with parameters based on table 4.21. The transfer function for different composites will be compared with lithium niobate plate.

Figure 4.52 shows the transfer function for plate, 1-3, 2-2 composite in different directions when the strain is zero for load as steel. The expectation is that the 1-3 composite would have the higher bandwidth because of its higher coupling coefficient and piezo pressure constant. So, the next part (Figure 4.53) will be shown the transfer function for this composite in different loads as water and steel with ideal matching layer and without matching layer for steel load based on parameters of table 4.21.

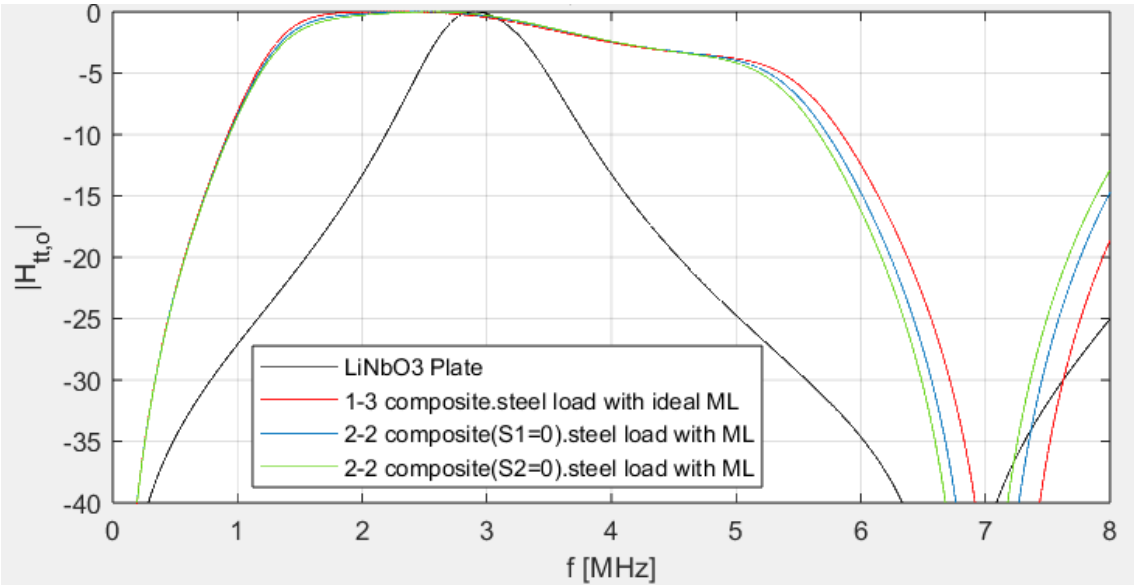

Figure 4.52 Transfer function for three types of composites of $LiNbO_3$ and air-filler for 36°Y-cut, plate as black line, 1-3 composite as red line, 2-2 composite(S1=0) as blue one and 2-2 composite(S2=0) as green line.

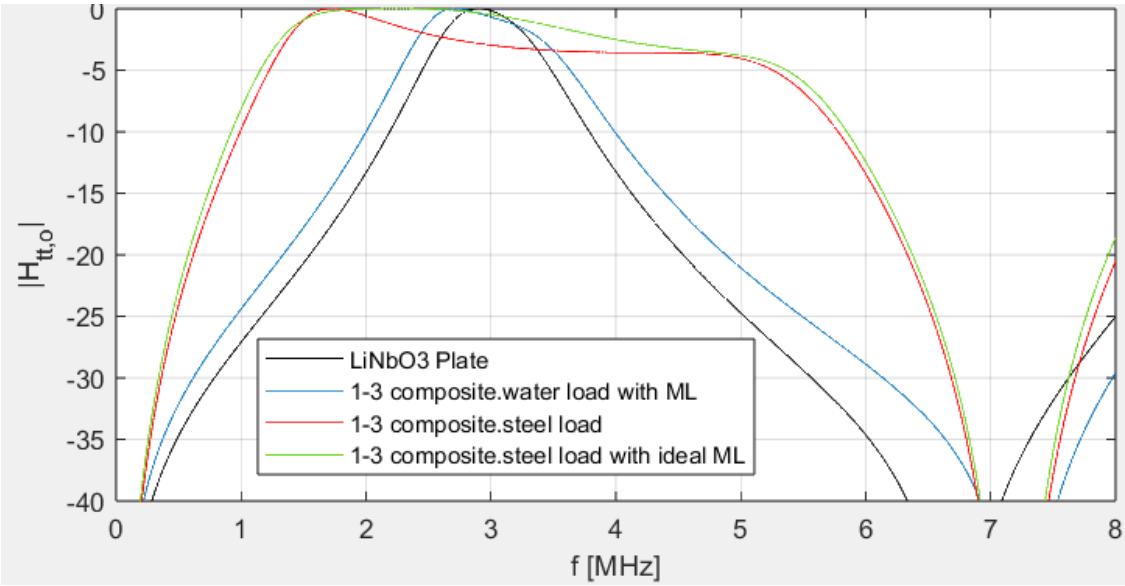

Figure 4.53 Transfer function of 1-3 composite of $LiNbO_3$ and air-filler for 36 °Y-cut, Plate in black line, 1-3 composite with water load as blue line, composite with steel load without any matching layer as red line and composite with steel load and ideal matching layer in green line.

This section pertains to the 2-2 composite comprising $LiNbO_3$ and air filler material acting as a polymer when the first direction is clamped, and strain is zero. Material parameters for these composite and various layers are presented in Table 4.20 and 4.22.

Table 4-22 Material properties for different layers of the $LiNbO_3$, Air-filled 2-2 piezocomposite(S_1=0) in one dimensional Mason Model for 36°Y-cut.

Material	Z [MRayls]	C [m/s]	Q
Backing layer (Air)	0.000413	343	10
Matching layer [22]	3.93	2580.6	10
Load (water)	1.5	1540	
Matching layer (Silver) [23]	38.23	3600	10
Load (Steel)	46	5980	

The electrical impedance is shown in further figures for water as load.

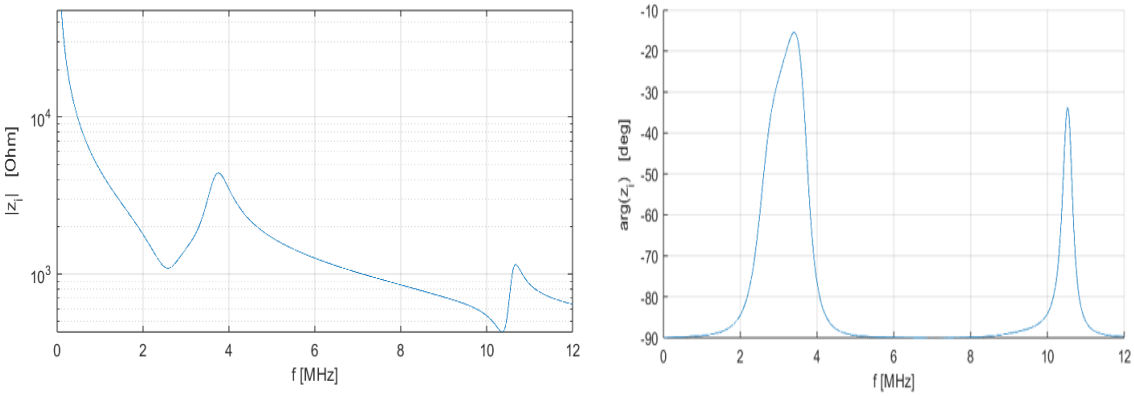

*Figure 4.54 Electrical impedance of 2-2 **(S_1)** composite of $LiNbO_3$ and Air-filler with water as load for 36°Y-cut.*

This section focuses on the 2-2 composite of lithium niobate and air filler, where the strain in the second direction is clamped to zero. Tables 4.20 and 4.23 present the material parameters for this composite.

Table 4-23 Material properties for different layers of the $LiNbO_3$, Air-filled 2-2 piezocomposite(S_2=0) in one dimensional Mason Model for 36°Y-cut.

Material	Z [MRayls]	C [m/s]	Q
Backing layer (Air)	0.000413	343	10
Matching layer [22]	3.93	2580.6	10
Load (water)	1.5	1540	
Matching layer (Silver) [23]	38.42	3600	10
Load (Steel)	46	5980	

The simulation of electrical impedance is done by X. Trans refer to table 4.20 when the load assumed to be water.

The load will be assumed to be water because of similarity to body tissues and it will be considered as steel for high temperature applications.

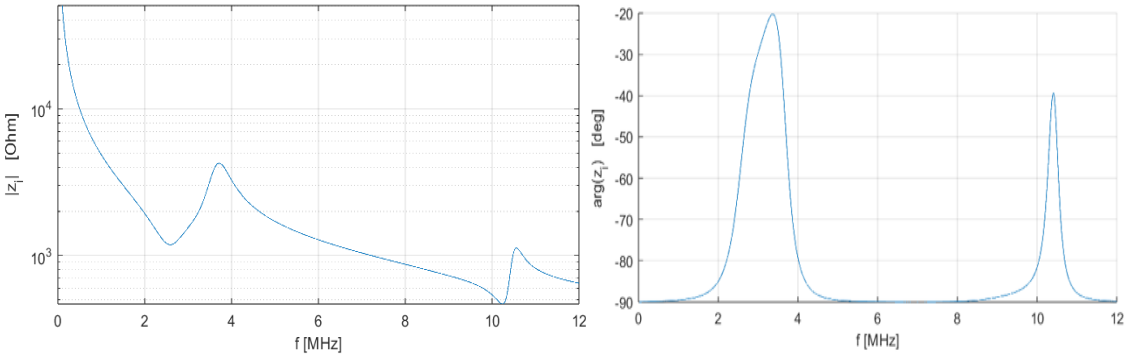

*Figure 4.55 Electrical impedance of 2-2 **(S_2)** composite of $LiNbO_3$ and Air-filler with water as load for 36 ̊Y-cut.*

4.7 Measurement in the Lab in USN

The material that we have used for measuring and evaluation is the circular $LiNbO_3$ (Lithium Niobate) with sputter gold (Gold is used to making electrode for PZT in general, with chromium on the crystal as the adhesion layer firstly then the gold layer is added. Usually, 20nm Cr then 200nm gold is used). The thickness of the sample is measured by cage device in the lab and the diameter of it is measured by ruler.

Table 4-24 Piezoceramic geometry

Diameter [mm]	Thickness [mm]
10	1.1

Initially, it is imperative to calibrate the device to facilitate the evaluation of electrical impedance, necessitating the removal of all cable-related artifacts. This calibration process commences with setting the device to an open mode, devoid of any connections. Subsequently, the short mode is established by connecting a wire atop the surface, while observing the resultant line on the screen. Finally, resistance is introduced, and a wire is connected atop the surface to observe the corresponding line as well.

Following the calibration process, the $LiNbO_3$ sample is placed onto the surface, and two cables are connected without applying additional force. Subsequently, the results for electrical impedance are obtained as outlined below.

Figure 4.56: Calibration of the device.

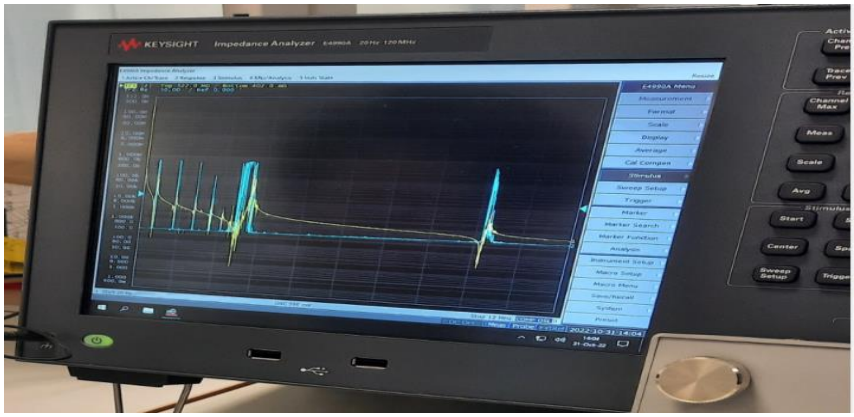

Figure 4.57 Measurement of electrical impedance for $LiNbO_3$.

The measurement result of electrical impedance for 36°/Y-cut $LiNbO_3$ is shown in figure 4.58.

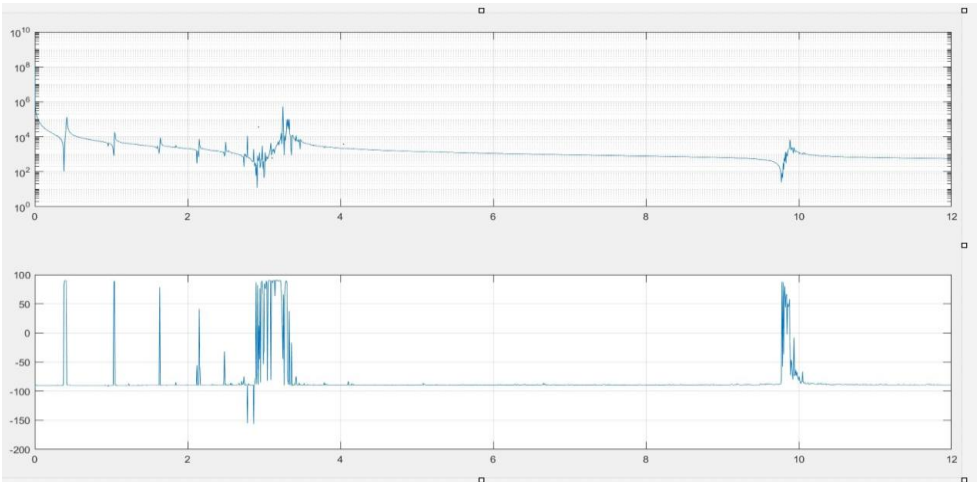

Figure 4.58: The measurement electrical impedance for 36°/Y-cut $LiNbO_3$.

As we can see in the above figure, there are lateral modes in measurement figure which it can be removed by using piezocomposite (specially Y/cut).

5 Discussion

5.1 1-3 composite of $LiNbO_3$ with EpoTek 3012 filler for 36° / Y-cut

This part is dedicated to discussing about composite of $LiNbO_3$ with EpoTek-3012 as polymer material in 36° / Y-cut refer to section 4.5.1. It seems that the 1-3 composite is more efficient in comparison to 2-2 composites in both directions because of higher h_{33} value (piezoelectric constant), higher electromechanical coupling coefficient and lower acoustic impedance based on Figure 4.38. So, higher coupling factor results higher energy conversion, meaning that less input energy is required to achieve the desired mechanical or electrical output.

For this 1-3 composite, the different types of transfer function are shown and compared in Figure 4.38, the relative bandwidth can be calculated by considering the maximum and minimum points at -3dB. These values are listed in table 5.1.

Table 5-1 Fitting of material parameters of the $LiNbO_3$, EpoTek 3012-filled piezocomposite bandwidth for 36°Y-cut.

Material	F_r [MHz]	F_a [MHz]	Relative bandwidth
Plate	2.55	3.34	0.26
composite/water load	2.4	3.44	0.35
composite/steel load	1.34	3.99	0.88
composite/steel load+ ML	1.32	4.34	1.01

To calculate the relative bandwidth [22], the maximum and minimum values of frequency in -3dB for transmitting the sound waves are considered and listed as table (5.1).

$$BW = \frac{f_{max} - f_{min}}{f_0} \quad (5.1)$$

In the Eq. (5.1), the f_0 is the center frequency that is equal to 3 MHZ. When the load was water, the ideal matching layer was selected as EpoTek3012+ 10% Al_2O_3.

When the load is steel, the first part is done without any matching layer which is simple for fabrication and second part is done with ideal matching layer like Silver with 0.3 mm

thickness which is more complex for fabrication but has some advantages. Silver is chosen as matching layer because it is a good conductor of electricity and has excellent thermal conductivity, also it forms strong bonds with many materials, which can enhance the adhesion between layers in the composite structure. The drawback of this material is that it is expensive and may oxidize at high temperatures.

Comparing the values of relative bandwidth related to table 5.1, the composite with using steel as load and ideal matching layer has the most bandwidth compared to other types of composites. So, using the steel as load and silver as matching layer is more efficient to fabricate the ultrasound transducer for transmitting and receiving the sound waves with higher coupling between the electrical and mechanical parts.

5.2 1-3 composite of $LiNbO_3$ with RTV 3140 filler for 36° / Y-cut

This part is dedicated to discussing about composite of $LiNbO_3$ with RTV-3140 as polymer material in 36° / Y-cut refer to section 4.5.2.

When the different types of transfer function are shown and compared, the relative bandwidth can be calculated by considering the resonance and anti-resonance as maximum and minimum point at -3db. These values are listed in table 5.2.

Table 5-2: Fitting of material parameters of the $LiNbO_3$, RTV 3140-filled piezocomposite bandwidth for 36°Y-cut.

Material	F_r [MHz]	F_a [MHz]	Relative bandwidth
Plate	2.55	3.34	0. 26
composite/water load	2.39	3.45	0.35
composite/steel load	1.34	3.27	0.64
composite/steel load+ ML	1.29	4.32	1.01

The calculation of relative bandwidth and choosing the ideal matching layers for both loads as water and steel are the same as previous section (5.1). When the load was selected as water, the thickness of matching layer is 0.215 [mm]. When the load was steel, thickness of matching layer is 0.3 [mm]. The load is selected as steel material with acoustic impedance close to Lithium niobate material which is suitable for high temperature applications. Even though choosing steel as load does not have more bandwidth for softer polymer material like RTV 3140 compared to hard polymer like EpoTek 3012, but it is more suitable for high temperature applications.

5.3 1-3 composite of $LiNbO_3$ with air filler for 36° / Y-cut

This part is dedicated to discussing about composite of $LiNbO_3$ with air as polymer material in 36° / Y-cut refer to section 4.5.2.

Comparing the transfer function for different types of composites of Lithium niobate and air filler based on figure 4.50, it is shown that the bandwidth for 1-3 composite is higher than both 2-2 composites.

When the different types of transfer function are shown and compared in figure 4.50, the relative bandwidth can be calculated by considering the resonance and anti-resonance as maximum and minimum point at -3dB. These values are listed in table 5.3.

Table 5-3: Fitting of material parameters of the $LiNbO_3$, air-filled piezocomposite bandwidth for 36°Y-cut.

Material	F_r [MHz]	F_a [MHz]	Relative bandwidth
Plate	2.55	3.34	0. 26
composite/water load	2.37	3.458	0.36
composite/steel load	1.335	3.001	0.56
composite/steel load+ ML	1.277	4.309	1.011

The calculation of relative bandwidth and choosing the ideal matching layers for both loads as water and steel are the same as previous section (5.1).

When the load was selected as water, the thickness of matching layer is 0.215 [mm]. When the load was steel, thickness of matching layer is 0.3 [mm].

The bandwidth for the composite with applied load as steel without any matching layer is less than harder polymer material, but steel is suitable for high temperature applications.

The bandwidth for this type of composite with steel as load and ideal matching layer has the most value.

6 Conclusion

By rotating the system and using the 36° Y-cut $LiNbO_3$ compared to Z-cut, the piezo pressure constant will be higher than Z-cut and exhibits a higher electromechanical coupling coefficient (k) than the Z-cut. This results in more efficient conversion of energy, enhancing the sensitivity and efficiency of the transducer. In addition, using 36°/Y-cut crystals often have broader bandwidth, as the transducer can operate effectively over a wider range of frequencies.

As a result of creating composite for ultrasound transducers, it has several benefits which enhance the performance of transducers. The first one is about improved acoustic matching because of lower value of acoustic impedance for composite of $LiNbO_3$ and polymer filler compared to pure $LiNbO_3$ ceramic material. The second is related to electromechanical coupling coefficient which will be higher by creating composite. So, leading to more efficient energy conversion. Higher value for coupling coefficient makes the broader bandwidth and more sensitive transducer.

By making the composite (especially 1-3 composite) with softer material, the electromechanical coupling factor(k) will be higher than hard material. So, using the air is the most efficient polymer material which makes the most value for k factor and lowest acoustic impedance (Z).

By using the steel material as load, even though it has not higher bandwidth compared to water as load, but it is more suitable for high temperature applications, and it can withstand harsh environmental conditions.

References

[1] W. Smith and B. Auld, “Modeling 1-3 composite piezoelectrics: Thickness-mode oscillations”, IEEE Transactions on Ultrasonics, Ferroelectrics, and Frequency Control, vol. 38, no. 1, pp. 40–47, 1991. DOI: 10.1109/58.67833.

[2] W. Qi and W. Cao, “Finite element analysis and experimental studies on the thickness resonance of piezocomposite transducers”, Ultrasonic Imaging, vol. 18, no. 1, pp. 1–9, 1996, issn:0161-7346. DOI: https://doi.org/10.1006/uimg.1996.0001.

[3] C. Desilets, J. Fraser, and G. Kino, “The design of efficient broad-band piezoelectric transducers”, IEEE Transactions on Sonics and Ultrasonics, vol. 25, no. 3, pp. 115–125, 1978. DOI:10.1109/T-SU.1978.31001.

[4] Determination of Elastic and Piezoelectric Constants for Crystals in Class (3m) A. W. WAsNra, M. 0Nor, * ANt) G. A. COQUIN.

[5] Lithium niobate piezocomposite phased arrays operating at high temperatures, K J Kirk, N Schmarje and S Cochran), DOI: 10.1784/insi.46.11.662.52284

[6] K. K. Shung, Diagnostic Ultrasound: Imaging and Blood Flow Measurements. CRC Press, 39-55, 2005.

[7] Epotek 301-2 technical data sheet, Rev. XVII, EPOXY TECHNOLOGY, Nov. 2019.

[8] Dowsil™ 3140 rtv coating technical data sheet, 11-3214-01 D, DOWSIL™, 2018.

[9] S. Sherrit and B. K. Mukherjee, “Characterization of piezoelectric materials for transducers”, Dielectric and Ferroelectric Reviews, 2007.

[10] Q. Zhou, K. H. Lam, H. Zheng, W. Qiu, and K. K. Shung, “Piezoelectric single crystals for ultrasonic transducers in biomedical applications,” Prog Mater Sci, vol. 66, pp. 87–111, Oct. 2014.

[11] Lawrence E. Kinsler, Austin R. Frey, Alan B. Coppens, and James V. Sanders, Fundamentals of Acoustics. New York: John Wiley & Sons, 1982.

[12] Investigation of high-temperature ultrasonic transducer design using lithium niobate Piezocomposite Kirk, Katherine; Hou, Ruozhou ; Schmarj, Nicole ; Pragada, Naga Mahesh ; Torbay, Louis; Hutson, David

[13] Comparison of y/36°-cut and z-cut lithium niobate composites for high temperature ultrasonic applications N. SCHMARJE*, K. J. KIRK and S. COCHRAN

[14] Piezoelectricity, Matrix representation of tensors EH, Voigt notation

[15] H. J. Lee, S. Zhang, Y. Bar-Cohen, and S. Sherrit, “High temperature, high power piezoelectric composite transducers”, Sensors (Basel, Switzerland), vol. 14, pp. 14 526–14 552, Aug. 2014. DOI: 10.3390/s140814526.

[16] https://www.bostonpiezooptics.com/lithium-niobate

[17] D. Folds, “Speed of sound and transmission loss in silicone rubbers at ultrasonic frequencies”, Journal of the Acoustical Society of America, vol. 56, pp. 1295–1296, 1974.

[18] P. G. Johnson, in Performance of exterior building walls. ASTM International, 2003, p. 138.

[19] J. Cannata, J. Williams, Q. Zhou, T. Ritter, and K. Shung, “Development of a 35-mhz piezocomposite ultrasound array for medical imaging”, IEEE Transactions on Ultrasonics, Ferroelectrics, and Frequency Control, vol. 53, no. 1, pp. 224–236, 2006. doi:10.1109/TUFFC.2006.1588408.

[20] Design manual for potting electronic assemblies, Sep. 1976. [Online]. Available: https://www.osti.gov/servlets/purl/12042152.

[21] A. E. Brown, “Rationale and summary of methods for determining ultrasonic properties of materials at lawrence livermore national laboratory”, vol. 1, no. 3, Feb. 1995. DOI: 10.2172/45628. [Online]. Available: https://www.osti.gov/biblio/45628.

[22] Md Ebne Al Ashad, “Manufacturing and Characterization of acoustic matching layers for ultrasound transducers”, 2019.

[23] https://www.ondacorp.com/images/Solids.

List of Tables and Figures

Appendix

This section is explanation of MATLAB Code for rotational system that is needed for computing the material constants of 36°/Y-cut.

```
C= [2.030e11 5.73e10 7.52e10 8.5e9 0 0;5.73e10 2.030e11 7.52e10 -8.5e9 0
0;7.52e10 7.52e10 2.424e11 0 0 0;8.5e9 -8.5e9 0 5.95e10 0 0; 0 0 0 0
5.95e10 8.5e9;0 0 0 0 8.5e9 7.28e10]

e= [0 0 0 0 3.83 -2.37; -2.37 2.37 0 3.83 0 0;0.23 0.23 1.3 0 0 0]

Ep= [44.3 0 0;0 44.3 0;0 0 27.9]
```

Euler angle

Z–X–Z scheme.

$$R_{\varphi_1,\Phi,\varphi_2} =$$

$$\begin{bmatrix} \cos\varphi_1\cos\varphi_2 - \cos\Phi\sin\varphi_1\sin\varphi_2 & \cos\Phi\cos\varphi_1\sin\varphi_2 + \sin\varphi_1\cos\varphi_2 & \sin\Phi\sin\varphi_2 \\ -\cos\varphi_1\sin\varphi_2 - \cos\Phi\sin\varphi_1\cos\varphi_2 & \cos\Phi\cos\varphi_1\cos\varphi_2 - \sin\varphi_1\sin\varphi_2 & \sin\Phi\cos\varphi_2 \\ \sin\Phi\sin\varphi_1 & -\sin\Phi\cos\varphi_1 & \cos\Phi \end{bmatrix}$$

$$C_{EBSP_0} = T_\sigma^{-1}\, C\, T_\varepsilon$$

$T_\sigma =$

$$\begin{bmatrix} R_{11}^2 & R_{21}^2 & R_{31}^2 & 2R_{11}R_{21} & 2R_{21}R_{31} & 2R_{31}R_{11} \\ R_{12}^2 & R_{22}^2 & R_{32}^2 & 2R_{12}R_{22} & 2R_{22}R_{32} & 2R_{32}R_{12} \\ R_{13}^2 & R_{23}^2 & R_{33}^2 & 2R_{13}R_{23} & 2R_{23}R_{33} & 2R_{33}R_{13} \\ R_{11}R_{12} & R_{21}R_{22} & R_{31}R_{32} & R_{11}R_{22}+R_{12}R_{21} & R_{21}R_{32}+R_{31}R_{22} & R_{31}R_{12}+R_{32}R_{11} \\ R_{12}R_{13} & R_{22}R_{23} & R_{33}R_{32} & R_{23}R_{12}+R_{13}R_{22} & R_{22}R_{33}+R_{32}R_{23} & R_{32}R_{13}+R_{12}R_{33} \\ R_{11}R_{13} & R_{23}R_{21} & R_{33}R_{31} & R_{13}R_{21}+R_{11}R_{23} & R_{23}R_{31}+R_{21}R_{33} & R_{33}R_{11}+R_{31}R_{13} \end{bmatrix}$$

$T_\varepsilon =$

$$\begin{bmatrix} R_{11}^2 & R_{21}^2 & R_{31}^2 & R_{11}R_{21} & R_{21}R_{31} & R_{31}R_{11} \\ R_{12}^2 & R_{22}^2 & R_{32}^2 & R_{12}R_{22} & R_{22}R_{32} & R_{32}R_{12} \\ R_{13}^2 & R_{23}^2 & R_{33}^2 & R_{13}R_{23} & R_{23}R_{33} & R_{33}R_{13} \\ 2R_{11}R_{12} & 2R_{21}R_{22} & 2R_{31}R_{32} & R_{11}R_{22}+R_{12}R_{21} & R_{21}R_{32}+R_{31}R_{22} & R_{31}R_{12}+R_{32}R_{11} \\ 2R_{12}R_{13} & 2R_{22}R_{23} & 2R_{33}R_{32} & R_{23}R_{12}+R_{13}R_{22} & R_{22}R_{33}+R_{32}R_{23} & R_{32}R_{13}+R_{12}R_{33} \\ 2R_{11}R_{13} & 2R_{23}R_{21} & 2R_{33}R_{31} & R_{13}R_{21}+R_{11}R_{23} & R_{23}R_{31}+R_{21}R_{33} & R_{33}R_{11}+R_{31}R_{13} \end{bmatrix}$$

Auld

$$[c'] = [M][c][N]^{-1}$$

nds that the transfor

$$[s'] = [N][s][M]^{-1}$$

```
a=0;
b=36-90;
g=0;
phi_1=a*pi/180;
Phi=b*pi/180;
phi_2=g*pi/180;
Rz=[cos(phi_1) -sin(phi_1) 0; sin(phi_1) cos(phi_1) 0;0 0 1];
Rx= [1 0 0;0 cos (Phi) -sin(Phi);0 sin(Phi) cos(Phi)];
Rz1=[cos(phi_2) -sin(phi_2) 0; sin(phi_2) cos(phi_2) 0;0 0 1];


R1=Rz*Rx*Rz1;
R=transpose(R1)
```

```
%R=sym('R', [3,3])
```

```
M1=R.^2;
for i=1:3

    for j=1:3
        JJ=[1 2 3];
        JJ1=JJ;
JJ1(:,j)=[];
        M2(i,j)=2*R(i,JJ1(1))*R(i,JJ1(2));
    end
end


for i=1:3

    for j=1:3
        JJ=[1 2 3];
        JJ1=JJ;
JJ1(:,i)=[];
        M3(i,j)=R(JJ1(1),j)*R(JJ1(2),j);
    end
end


for i=1:3

    for j=1:3

 JJ=[1 2 3];
        JJ1=JJ;
        JJ2=JJ;
JJ1(:,i)=[];
JJ2(:,j)=[];
M4(i,j)=R(JJ1(1),JJ2(1))*R(JJ1(2),JJ2(2))+R(JJ1(1),JJ2(2))*R(JJ1(2),JJ2(1
));
    end
end




N1=R.^2;
for i=1:3

    for j=1:3
        JJ=[1 2 3];
        JJ1=JJ;
JJ1(:,j)=[];
        N2(i,j)=R(i,JJ1(1))*R(i,JJ1(2));
    end
end


for i=1:3

    for j=1:3
```

```
        JJ=[1 2 3];
        JJ1=JJ;
JJ1(:,i)=[];
        N3(i,j)=2*R(JJ1(1),j)*R(JJ1(2),j);
    end
end


for i=1:3

    for j=1:3

 JJ=[1 2 3];
        JJ1=JJ;
        JJ2=JJ;
JJ1(:,i)=[];
JJ2(:,j)=[];
N4(i,j)=R(JJ1(1),JJ2(1))*R(JJ1(2),JJ2(2))+R(JJ1(1),JJ2(2))*R(JJ1(2),JJ2(1
));
    end
end


M=[M1 M2;M3 M4];
N=[N1 N2;N3 N4];
```

Transformed

```
CT=M*C*inv(N)
```

```
CT = 6×6
10^11 ×
    2.0300       0.6093       0.7157      -0.1114            0            0
    0.6093       2.2148       0.9059      -0.0880            0            0
    0.7157       0.9059       1.9314      -0.0730            0            0
   -0.1114      -0.0880      -0.0730       0.7489            0            0
         0            0            0            0       0.7629       0.0370
         0            0            0            0       0.0370       0.5601
```

```
eT=R*e*transpose(M)
```

```
eT = 3×6
         0              0              0              0       0.3338      -4.4916
   -1.5791        -2.4124         2.5677         0.3784            0            0
   -1.7822        -1.7376         4.5543        -0.3448            0            0
```

```
EpT=R*Ep*transpose(R)
```

```
EpT = 3×3
   44.30                  0                  0
         0            33.5661            7.7987
         0            7.7987            38.6339
```